PART I

ISOLATION OF OREXIN RECEPTOR REGULTORS VIA A MICROARRAY-BASED, TWO-COLOR, CELL-BINDING SCREEN

PART II

TARGETED INACTIVATION OF PROTEINS TRIGGERED BY VISIBLE LIGHT

APPROVED BY SUPERVISORY COMMITTEE

Thomas Kodadek, Ph.D. (Mentor)
Michael Rosen, Ph.D. (Chair)
A. Dean Sherry, Ph.D.
Cheng-Ming Chiang, Ph.D.

ACKNOWLEDGMENTS

There are many people that I would like to thank for their support during my years as a graduate student at UT Southwestern. I would like to thank my advisor Dr. Thomas Kodadek for being a constant source of support, advice, encouragement, and guidance. You have taught me to become independent scientist who can do important and exciting research. I would also like to thank my committee members Drs. Michael Rosen (Chair), A. Dean Sherry and Cheng-Ming Chiang for their insight, valuable advice, constructive criticism, and guidance. I would also like to thank all of the members of the Kodadek lab, past and present, especially Peng Yu, Xiangshu Xiao, Hyun-Suk Lim, Young-Chan Kim, Gomika Udugamasooriya, Devanjan Sikder, Niclas Tan, and Anne Gocke, for all of their technical support, intellectual discussion, collaboration, and friendship.

I would like to give special thanks to my family, especially my parents, Kihum Lee and Kisoon Jeon. You have given me endless love, support, motivation, and understanding throughout these many educational years. I would also like to thank my brother and sisters, Jihong, Seonae, and Donghee, for their encouragement and understanding, especially when I decided to study abroad. Thank you also to

my mother in-law, Okee Min, my sisters in law, Jeonghyun. You are responsible for all the God's blessings I have experience so far and I owe a great deal to you.

I would like to thank my wife, Eul Hyun. You are my true inspiration. I could not have made it this far without you. Thank you for always being there to listen, to talk about science with me, and for making me laugh when I am discouraged. I truly believe your prayers for my successful Ph.D. study granted at last. I admire you and love you very much. Thank you also to my daughter Yehwon for bringing joy and happiness into my life everyday.

Finally, thank you God for all the blessings I have, and all the blessings I am receiving.

PART I

ISOLATION OF OREXIN RECEPTOR REGULTORS VIA A MICROARRAY-BASED, TWO-COLOR, CELL-BINDING SCREEN

PART II

TARGETED INACTIVATION OF PROTEINS TRIGGERED BY VISIBLE LIGHT

by

JIYONG LEE

DISSERTATION

Presented to the Faculty of the Graduate School of Biomedical Sciences

The University of Texas Southwestern Medical Center at Dallas

In Partial Fulfillment of the Requirements

For the Degree of

DOCTOR OF PHILOSOPHY

The University of Texas Southwestern Medical Center at Dallas

Dallas, Texas

July, 2009

PART I

ISOLATION OF OREXIN RECEPTOR REGULTORS VIA A MICROARRAY-BASED, TWO-COLOR, CELL-BINDING SCREEN

PART II

TARGETED INACTIVATION OF PROTEINS TRIGGERED BY VISIBLE LIGHT

PUBLICATION NO. _____

JIYONG LEE, Ph.D.

THE UNIVERSITY OF TEXAS SOUTHWESTERN MEDICAL CENTER AT DALLAS, 2009

SUPERVISING PROFESSOR: THOMAS KODADEK, Ph.D.

Part I. Isolation of orexin receptor regulators via a microarray-based, two-color, cell-binding screen

We have developed a novel two-color, cell-binding peptoid microarray screening approach with which we discovered new orexin receptor ligands. We found that peptoids on microarray, which showed preferential binding to receptor-expressing cells, indeed regulate the function of the receptor in living cells. Although cell-adhesion peptide

microarrays have been used to isolate peptides that bind to cell surface receptors, this is the first time that a non-peptide, small molecule microarray has been used to do so. We also demonstrated that the pharmacophore of a hit peptoid can be rapidly identified through sarcosine scanning. Subsequent modifications of the pharmacophore yielded a potent antagonist (IC_{50} = 1.7 μM) and an allosteric potentiator (EC_{50} = 120 nM) of the orexin receptor.

Part II. Targeted inactivation of proteins triggered by visible light

Advances in genomics and proteomics have helped to provide thousands of potential drug targets and thus target validation strategies are more important than ever. Among target validation technologies, we are interested in chromophore-assisted light inactivation of proteins (CALI) since it allows for time-resolved protein knock-out in living cells. However, the practical use of this technology is limited, partially because of the low CALI efficiency of chromophores that are currently in use. To solve this problem, we developed a convenient system to compare different chromophores for their CALI efficiency, from which we found that Ru(II) complex is a photo-stable and unusually efficient CALI "warhead". This finding led us to develop "photo-chemical protein knock-out reagents" in which Ru(II) complex was conjugated to small molecule ligands targeting VEGFR2 or the 26S proteasome. When irradiated with visible light, these reagents showed significantly increased potencies in inhibiting VEGF-induced VEGFR2 activation or proteolytic activity of the 26S proteasome.

TABLE OF CONTENTS

Abstract	vi
Table of contents	viii
Publications	xiv
List of figures	xviii
List of table	xxi
List of scheme	xxi
Abbreviations	xxii
Part I	1
Chapter 1: Introduction	2
1.1. G-protein coupled receptors	2
1.2. Orexins and Orexin receptors	3
1.3. Orexin system-related diseases	4
1.3.1. Sleep disorder	4
1.3.2. Cancer	5
1.3.3. Metabolic disorders	6
1.3.4. Addiction	7
1.4. Screening ligands using small molecule microarray	8
1.4.1. Small molecule microarray (SMM)	8
1.4.2. Peptoid microarray	9
1.5 References	11

Chapter 2: Isolation of an orexin receptor antagonist via a microarray-based, two-color, cell-based screen. 13

2.1. Introduction: 13

2.2. Results 15

- A microarray-based, two-color, cell-based screen to isolate peptoids that bind specifically to orexin receptor. 15
- Hit validation 17
- Hit optimization: Identification of minimal pharmacophore 19
- Hit optimization: rational design 22
- Hit optimization: combinatorial chemistry 24
- Specificity of OBPt-5 26

2.3. Discussion 28

2.4. Experimental section 30

- General remarks 30
- Peptoid microarrays 30
- A microarray-based, two-color, cell-binding screen and ratio-metric image analysis. 31
- Peptoid synthesis 31
- Preparation of OBPt-3, OBPt-5, and OBPt-6 32
- Cell culture 32
- cAMP production assay 32
- ERK phosphorylation assay 33
- MS/MS sequence analysis 34

- References for experimental section 38

2.5. References 39

Chapter 3: A small molecule allosteric potentiator of orexin receptors 41

3.1. Introduction 41

3.2. Results 43

3.3. Discussion 47

3.4. Experimental section 48

- General remarks 48

- Peptoid synthesis 48

- Cell culture 49

- cAMP production assay 49

- References for experimental section 50

3.5. References 51

Part II 53

Chapter 1: Introduction 54

1.1. Identification of protein function via ‘loss of function’ approaches 54

1.1.1. Genetic methods targeting mRNA 54

- Gene knockouts 55

- Antisense 55

- Ribozymes 56

- RNAi 56

- Limitations of genetic methods 56

1.1.2. Non-genetic methods targeting proteins directly 57

- Function-blocking antibody 57

- Aptamer 58

- Small molecules 58

- Chromophore-assisted light inactivation 58

- Limitation of CALI 60

1.2. Singlet oxygen-mediated protein inactivation 60

1.2.1. Singlet oxygen chemistry 60

1.2.2. Singlet oxygen generation 61

1.2.3. Singlet oxygen-mediated oxidative modification of proteins 63

1.3 References 65

Chapter 2: A general system for evaluating the efficiency of chromophore-assisted light inactivation (CALI) of proteins reveals Ru(II) tris-bipyridyl as an unusually efficient "warhead" 67

2.1. Introduction 67

2.2. Results 70

- Covalent attachment of small molecules to the target protein in complex biological mixtures 70

- Delivery of fluorescein and Ru(II) tris(bipyridyl) dication derivatives

to the Luc- HTP fusion protein and comparison of their efficacy in CALI 73

- Evidence that singlet oxygen is the protein-damaging agent in Ru-HT-mediated CALI 76

- Ru-HT inactivates target protein inside living cells 77

2.3. Discussion 79

2.4. Experimental Section 82

- Materials and Instruments 82

- Syntheses HaloTag reagents 82

- Plasmid 83

- Cell culture, transfection, and preparation of cell lysate 84

- Measurement of luciferase activities 84

- Labeling of target protein with HaloTag reagents 85

- Immunoprecipitation 85

- In vitro CALI 86

- In vivo CALI 86

2.5. References 87

Chapter 3: Facile transformation of low-potency small molecules into photochemical protein knock-out reagents 90

3.1. Introduction 90

3.2. Results 92

- Ru(II)-conjugated VEGFR2 antagonist showed a significant increase in potency

with visible light 92

- Specificity of VEGFR2 inactivation by RuGU40C 97

- A Super-potent photo-antagonist of VEGFR2 98

- A photo-antagonist of the 26S proteasome 100

- Inhibition of the 26S proteasome inside living cells 104

- Photo-stability of Ru(II)-conjugates 105

3.3. Discussion 107

3.4. Experimental section 109

- General remarks 109

- Cell culture 109

- Peptoid synthesis 109

- Preparation of Ruthenium-peptoids 110

- Cell viability assay 114

- MS spectrometry for photostability measurement of Ruthenium-peptoids 114

- Visible light irradiation 115

- Autophosphorylation assay 115

- Tube formation assay 115

- 26S proteasome peptidase assay 116

- Cell-based proteasomal peptidase assay 116

- References for experimental section 117

3.5. References 118

PUBLICATIONS

1. **Lee, J**., Udugamasooriya, D. G., Lim, H-S., Kodadek, T. "Facile transformation of low-potency small molecules into photochemical protein knock-out reagents" manuscript under revision.
2. Gocke, A. R., Archer, C. T., Udugamasooriya, D. G., **Lee, J**., Kodadek, T. "Synthetic antagonists of autoimmune T cell proliferation" submitted.
3. **Lee, J**., Kodadek, T. "Isolation of an orexin receptor antagonist via a microarray-based, two-color, cell-binding screen." Manuscript under revision.
4. **Lee, J**., Kodadek, T. "A small-molecule allosteric potentiator of orexin receptor" manuscript in preparation.
5. Jung, H. J., Shim, J. S., **Lee, J**., Song, Y. M., Park, K. C., Choi, S. H., Mungai, P. T., Schumacker, P. T., Kwon, H. J. "Terpestacin, a small molecule inhibitor of angiogenesis, binds to the QP-C protein in mitochondrial complex III and blocks hypoxia-induced ROS and HIF-1α stabilization" submitted.
6. Shim, J. S.*, **Lee, J**.*, Huh, T-L., Kwon, H. J. "Inhibition of zebrafish neovascularization by a synthetic homoisoflavanone" manuscript in preparation. **(*equal contribution)**
7. **Lee, J**., Yu, P., Xiao, X., Kodadek, T. "A general system for evaluating the efficiency of chromophore-assisted light inactivation (CALI) of proteins reveals Ru(II) tris-bipyridyl as an unusually efficient warhead" *Mol.BioSyst*. **2008**, *4*, 59-65. (Selected as a "Hot article" in *Molecular BioSytems*. Highlighted in *Chemical Biology*, Dec. **2007**, *2*(12*)*, B90.

8. Shim, J. S., Park, H. M., **Lee, J**., Kwon, H. J. "Global and focused transcriptional profiling of small molecule aminopeptidase N inhibitor reveals its mechanism of angiogenesis inhibition" *Biochem. Biophys. Res. Commun*. **2008**, *371*(1), 99-103.

9. Shim, J. S., **Lee, J**., Kim, K. N., Kwon, H. J. "Development of a new Ca^{2+}/calmodulin antagonist and its anti-proliferative activity against colorectal cancer cells" *Biochem. Biophys. Res. Commun*. **2007**, *359*(3), 747-751.

10. Kim, D. H.*, **Lee, J**.*, Kwon. H. J. "Anti-tumor activity of N-hydroxy-7-(2-naphthylthio)heptanomide, a novel histone deacetylase inhibitor" *Biochem. Biophys. Res. Commun.* **2007**, *356*(1), 233-238.

(* equal contribution)

11. **Lee, J**., Shim, J. S., Jung, S-A., Lee, S-T., Kwon, H. J. "N-Hydroxy-2-(naphthalene-2-ylsulfanyl)-acetamide, a novel hydroxamate inhibitor of aminopeptidase *N* and its anti-angiogenic activity" *Bioorg. Med. Chem. Lett.* **2005**, *15*(1), 181-183.

12. Yoo, H., Kim, S. H., **Lee, J**., Kim H. J., Seo, S. H., Chung, B. Y., Jin, C., Lee, Y. S. "Synthesis and antioxidant activity of 3-methoxyflavones" *Bull. Kor. Chem. Soc*. **2005**, *26*(12), 2057-2060

13. Kim, K. N., **Lee, J**., Kim, D. H., Yoo, J-S., Kwon, H. J. "A new synthetic analogue of thymidine, 7-(3-bromo-phenoxy)-tymidine, inhibits the proliferation of tumor cells" *Bioorg. Med. Chem. Lett*. **2005**, *15*(1), 77-79.

14. Shim, J. S., **Lee, J**., Park, H-J., Park, S-J., Kwon, H. J. "A new curcumin derivatives, HBC, interferes with the cell cycle progression of colon cancer cells

via antagonization of the $Ca2^{+}$/calmodulin function" *Chemistry & Biology* **2004**, *11*, 1455-1463.

15. Shim, J. S., Kim, J. H., **Lee, J**., Kim, S. N., Kwon, H. J. "Anti-angiogenic activity of the homoisoflavanone from *Cremastra appendiculata*" *Planta Medica* **2004**, *70*(2), 171-173.
16. Cho, M-K., Kim, S-S., Lee, M. R., Shin, J., **Lee, J**., Lim, S-K., Baik, J-H., Yoon, C-J., Shin, I., Lee, W. "NMR studies on turn mimetic analogs derived from melanocyte stimulating hormones" *J. Biochem. Mol. Biol*. **2003**, *36*, 552-557.
17. Lee, M. R., **Lee, J**., Baek, B-H., Shin, I. "The first solid-phase synthesis of oligomeric α-aminooxy peptides" *Synlett* 2003, 3, 325.
18. Dok-Go, H., Lee, K. H., Kim, H. J., Lee, E. H., **Lee, J**., Song, Y. S., Lee, Y., Jin, C., Lee, Y. S., Cho, J. "Neuroprotective effects of antioxidative flavonoids, quercetin, (+)-dihydroquercetin and quercetin 3-methyl ether, isolated from *opuntia ficus-indica var saboten*" *Brain Research* **200**2, *965*, 130-136
19. Lee, M. R., **Lee, J**., Shin, I. "Synthesis of novel glycopeptidomimetics containing *O*- and *N*-glycosylated α-aminooxy acids by fragment coupling on solid support" *Synlett* **2002**, No.9, 1463.
20. Shin, I., Lee, M, R., **Lee, J**., Jung, M., Lee, W., Yoon, J. "Synthesis of optically active phthaloyl D-aminooxy acids from L-amino acids or L-hydroxy acids as building blocks for the preparation of aminooxy peptides" *J. Org. Chem.* **2000,** *65*(22), 7667-7675.

21. Shin, I., **Lee, J**. "Facile synthesis of N-and O-glycosylated α-aminooxy acids as building blocks for the structural studies of glycosylated pseudopeptides" *Synlett* **2000**, No.9, 1297-1299.

LIST OF FIGURES

PART I

Figure 1.Representative structure of a generic GPCR 3

Figure 2. Orexins are produced in the lateral hypothalamus (LH) 4

Figure 3. Preparation and screening of SMMs 8

Figure 4. Chemical structures of peptide and peptoid 10

Figure 5. Protein profiling using peptoid microarray 10

Figure 6. A two-color, cell-binding peptoid microarray to isolate ligands for hOXR1 16

Figure 7. Chemical structures of hit peptoids (OBPs) 17

Figure 8. A reporter gene assay monitoring OX1R activation by orexin A. 18

Figure 9. Regulation of hOXR1 function by hit peptoids 19

Figure 10. Pharmacophore identification using the sarcosine scanning strategy 20

Figure 11. Chemical structures of OBP1-N, sarcosine derivatives 21

Figure 12 Introduction of hydrophobic moiety at N-terminal of OBPt 23

Figure 13. Chemical structure of CON 24

Figure 14. Chemical structures of OBPt-1 derivatives 24

Figure 15. Antagonist activities of OBPt-3 and OBPt-4 25

Figure 16. Antagonist activities of OBPt-5 and OBPt-6 25

Figure 17. Agonist activity of OBPt-5 26

Figure 18 Effect of OBPt-5 on orexin A or orexin B-induced OXR2 activation 27

Figure 19. Chemical structure of Bis-amide 27

Figure 20. Effect of OBPt-5 on forskolin (fsk)-induced cAMP production in HEK293 cells 27

Figure 21. The peptoid library used in this study 30

Figure 22. 44

Figure 23. Concentration-response curves of orexin A on cAMP elevation of OXR1 expressing cells in the presence or absence of OBPt-9 45

Figure 24 Concentration-response curves of orexin A on cAMP elevation of OXR2 expressing cells in the presence or absence of OBPt-9 46

Figure 25. Effect of OBPt-9 in the absence of orexin A on cAMP level of OXR1 expressing cells 46

PART II

Figure 26. Identification of protein functions via 'loss of function' approaches 54

Figure 27. Illustration of chromophore-assisted light inactivation (CALI) 59

Figure 28. Molecular orbitals of Triplet (left) and Singlet oxygen (right) 61

Figure 29. Photochemical generation of singlet oxygen 62

Figure 30. Singlet oxygen-mediated oxidative modification of histidine 64

Figure 31. A system to evaluate CALI efficiencies of different chromophores 70

Figure 32. Chemical structures of the HaloTag reagents used in this study 71

Figure 33. Labeling of target protein with the HaloTag reagent 72

Figure 34. Comparison of the 3xFlag-Luc-HTP-Myc labeling efficiencies

of Ru-HT and F-HT 74

Figure 35. Comparison of Ru-HT and F-HT as CALI “warheads” 76

Figure 36. Ru-HT-mediated protein inactivation involves singlet oxygen 77

Figure 37. Ru-HT-mediated CALI in living cells 79

Figure 38. Visible light-triggered inactivation of the Vascular Endothelial Growth Factor Receptor 2 (VEGFR2) by a ruthenium-peptoid conjugate 94

Figure 39. Competitive binding assay of RuGU40 95

Figure 40. Structures of RuCON and FGU40C 95

Figure 41. Effect of RuGU40C on VEGF-induced tube formation by HUVECs 96

Figure 42. Effect of RuGU40C on recombinant Luciferase activity 97

Figure 43. Effect of RuGU40C on the cell viability of PAE/KDR cells 98

Figure 44. 99

Figure 45. Competitive binding assay of RuGU40C4 100

Figure 46. 101

Figure 47. Visible light-triggered inactivation of the 26S proteasome by a ruthenium-peptoid conjugate 102

Figure 48. 103

Figure 49. Effect of RuRIP1 on recombinant Luciferase activity 104

Figure 50. Effect of RuRIP1 on activity of Renilla Luciferase activity in HeLa cells 105

Figure 51. 106

LIST OF TABLE

Table 1. MALDI-TOF/MS data 37

LIST OF SCHEMES

Scheme 1. Synthesis of azide-functionalized Ru(II) complex (1) 110

Scheme 2. Synthesis of RuRIP1 or RuGU40C via click chemistry 111

Scheme 3. Synthesis of RuGU40C 112

Scheme 4. Synthesis of RuCON 113

ABBREVIATIONS

AC	Adenyl cyclase
AMC	Aaminomethyl cumarin
AMPA	α-amino-3-hydroxyl-5-methyl-4-isoxazole-propionate
BAP	Borane-pyridine complex
BBB	Blood-brain barrier
BMI	Body mass index
BSA	Bovine serum albumin
CALI	Chromophore-assisted light inactivation
cAMP	Cyclic adenosine monophosphate
CHO	Chinese hamster ovary cell
CP	Core particle
DIC	Diisopropylcarbodiimde
DIPEA	Diisopropylethylamine
DMF	Dimethyl formamide
DMEM	Dulbecco's Modification of Eagle's Medium
DMSO	Dimethylsulfoxide
dsRNA	double-stranded RNA
EC50	Half maximal effective concentration
ECM	Endothelial cell medium
EGF	Epidermal growth factor
EGFR	Epidermal growth factor receptor
EGFP	Enhanced green fluorescent protein

ERK	Extracellular Signal-related kinase
Ex	Excitation
Em	Emission
FALI	Fluorophore-assisted light inactivation
FlAsH	Fluorescein arsenic helix binder
FBS	Fetal bovine serum
GPCR	G-protein-coupled receptor
HBTU	2-(1H-Benzotriazole-1-yl)-1,1,3,3-tetramethyluronium hexafluorophosphate
HOBT	Hydroxybenzotriazole
HEK	Human embryonic kidney
HeLa	Human cervical adenocarcinoma
HPLC	High performance liquid chromatography
HT	HaloTag ligand
HTP	HaloTag protein
HTS	High-throughput screening
HUVEC	Human Umbilical Vein Endothelial Cells
IC_{50}	Half maximal inhibitory concentration
KDR	Kinase insert domain receptor (VEGFR2)
LH	Lateral hypothalamus
MALDI	Matrix-assisted laser desorption/ionization
MLCT	Metal to ligand charge transfer
MS	Mass spectra

mRNA	messenger RNA
NHS	N-hydroxysucciimide
NMDA	N-methyl-D-aspartic acid
NMR	Nuclear magnetic resonance
OBOC	One bead one compound
OXR1	Orexin recptor 1
OXR2	Orexin receptor 2
PAE	Porcine aortic endothelial
PBS	Phosphate buffered saline
PCR	Polymerase chain reaction
RISC	RNA-induced silencing complex
RNAi	RNA interference
RP	Regulatory particle
SDS	Sodium dodecyl sulfate
Sen	Sensitizer
SELEX	Systematic evolution of ligand by exponential enrichment
SMM	Small molecule microarray
TFA	Trifluoroacetic acid
THF	Tetrahydrofuran
TOF	Time of flight
VEGF	Vascular Endothelial Growth Factor
VEGFR2	Vascular Endothelial Growth Factor Receptor 2
VTA	Ventral tegmental area

Part I

Isolation of orexin receptor regulators via a microarray-based, two-color, cell-binding screen

Chapter 1: Introduction

1.1. G-protein coupled receptors

G-protein-coupled receptors (GPCRs) are the largest class of cell-surface receptors and play crucial roles in virtually every organ system. GPCRs are responsible for conveying extracellular signals to the inside of the cell via interaction with intracellular heterotrimeric G proteins. These signals include hormones, neurotransmitters, ions, odorants and photons (Figure 1)[1-3]. GPCRs have been implicated in a multitude of human disorders and numerous diseases have been linked to mutations and polymorphisms in GPCRs. GPCRs are the target of many therapeutic agents that are currently in use. It is estimated that nearly 50% of all modern drugs regulate GPCR activity in some way [4, 5].

All GPCRs contain three extracellular loops, seven transmembrane helices, and three intracellular loops, with an extracellular N-terminal tail and an intracellular C-terminal tail. The transmembrane domain is largely hydrophobic, whereas the extracellular and intracellular segments, or loops, are generally hydrophilic, as would be anticipated from amino acids exposed to the phospholipid-rich membrane and the water-rich environments, respectively. The seven transmembrane helices are each ~24 amino acid long, while the C- and N-terminal tails as well as loops can vary widely in length with up to hundreds of amino acids[2].

The specific effectors influenced by a given GPCR depend on the type of G-protein that the receptor couples and activates [6]. There are many types of Gα, Gβ, and Gγ subunits, allowing for diverse combinations, although the most commonly used simple categorization of GPCRs is by designation of coupling to either Gαq, Gαi, and Gαs. The mutual effector for both Gαi and Gαs is adenylyl cyclase (AC), which is located on the inner leaflet of the plasma membrane and generates cyclic-AMP in response to stimulation or inhibition by Gαs

and Gαi, respectively. By contrast, the primary effector for Gαq is phospholipase Cβ, a membrane-bound enzyme that converts phophatidylinositol-1,4,5-triphosphate.

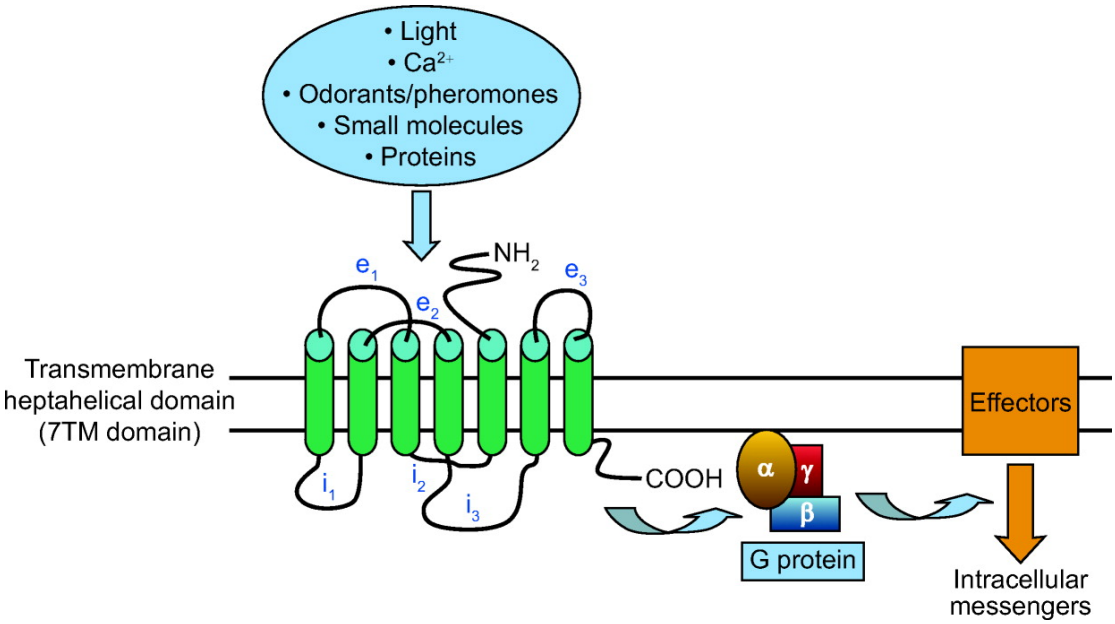

Figure 1. Representative structure of a generic GPCR. GPCRs all have a common core composed of seven transmembrane helices (the 7TM domain composed of TM-I-TM-VII) with an extracellular N-terminal domain and an intracellular C-terminal domain.

1.2. Orexins and Orexin receptors

Orexins A and B (also named hypocretins 1 and 2) are neuropeptides discovered by two groups in 1998 via orphan GPCR technologies or subtractive cDNA cloning [7, 8]. The two peptides are derived from a common precursor peptide, prepro-orexin. As GPCRs of orexins, two orexin receptor subtypes OXR1 (HCRT1) and OXR2 (HCRT2) have been cloned. In humans, OXR1 and OXR2 show 65% amino acid identity in transmembrane domains. Orexin receptors have been described in the central nervous systems as well as peripheral organs. OXR1s have preferential affinity for orexin-A, while OXR2s do not discriminate between

both peptides in vitro. In the brain, orexins produced by the neuronal cell body located in the lateral hypothalamus (LH) (Figure 2) and are important regulators of wakefulness, autonomic nervous system tone, neuroendocrinal secretion, feeding behavior and energy expenditure[9, 10]. Orexin systems have been a target of therapeutic interventions due to their roles in various diseases described below.

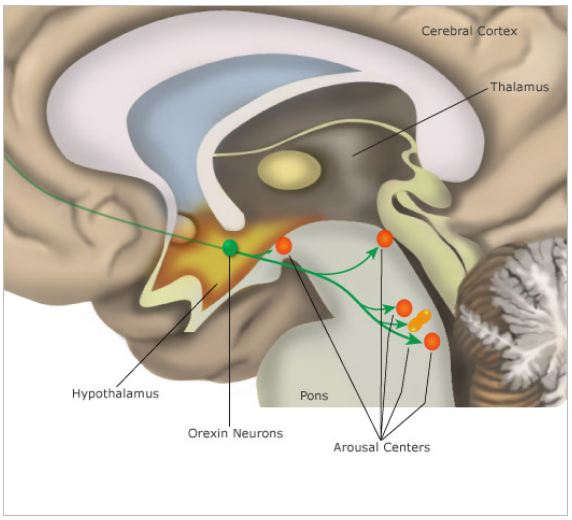

Figure 2. Orexins are produced in the lateral hypothalamus (LH). Orexin neurons keep the arousal centers active, helping stabilize wakefulness.
* Figure from http://healthysleep.med.harvard.edu/

1.3. Orexin system-related diseases

1.3.1. Sleep disorder

It has been observed that an orexin deficiency plays a role in the pathogenesis of narcolepsy[11]. Narcolepsy is the neurological disease, characterized by excessive daytime sleepiness, catalepsy, hypnagogic hallucinations and sleep paralysis. Deficiencies of orexins neurotransmission may be the cause of narcolepsy. Mutation in OXR2 in canine models and murine models with a targeted deletion of preproorexin gene (orexin knock-out animals) display a phenotype similar to the human narcoleptic condition[12]. Through genetic analysis

of narcolepsy in dogs, it's been suggested that deficits in OXR2 are sufficient to induce the syndrome. In patients with narcolepsy, orexin neurotransmission is altered and orexin A level is low or undetectable up to 95% patients examined. These findings suggest that replacement therapies based on administration of oreixn receptor agonists might be beneficial. Indeed, Yanagisawa et al. showed that symptoms of murine narcolepsy-cataplexy could be reversed either by ectopic production of orexin peptides from a prepro-orexin transgene or by pharmacological administration of synthetic orexin A.

On the contrary, blocking the orexin system has been proven beneficial for the treatment of chronic insomnia[13]. Transient and reversible reduction of brain orexin function can be induced by dual orexin receptor antagonists that effectively pass the blood-brain barrier (BBB). Such compounds under development for insomnia include SB-649,868 (by GlaxoSmithKline) and ACT-078573 (Almorexant by Actelion).

1.3.2. Cancer

Orexins induce dramatic apoptosis in human colon cancer cell lines, resulting in massive reduction of cell growth. The effect was also observed in human neuroblastoma cells and rat pancreatic tumor cells[14]. Orexin-stimulated apoptosis is associated with mitochondrial cytochrome c release into cytosol and activation of caspase-3 and caspase-7. The apoptosis appears to be mediated by the OXR1 in colon cancer cells and neuroblastoma cells and by the OXR2 in pancreatic tumor cells. Promotion of apoptosis by orexins is an intrinsic property of orexin receptors since transfection of OXR1 and OXR2 cDNAs in Chinese hamster ovary (CHO) cells deficient of endogenous receptors is sufficient to confer the ability of orexin to promote apoptosis. A recent study suggests that that orexin-induced apoptosis is driven by an immunoreceptor tyrosine-based inhibitory motif (ITIM) (IIY^{358}NFL) present in the OXR1[15]. This effect is mediated by SHP-2 phosphatase recruitment *via* a mechanism that requires Gq

protein but is independent of phospholipase C activation. These recent findings add a new dimension to the biological role of orexins and also suggest that a small molecule orexin receptor agonist will have a potential to be developed as anti-cancer drugs.

1.3.3. Metabolic disorders

Recent findings suggest that orexin neurons act as direct sensors of metabolic signals. Yamanaka et al. showed that the electrical properties of anatomically or functionally isolated orexin neurons are directly sensitive to changes in the extracellular concentration of glucose and the appetite-regulating hormones leptin and ghrelin[16]. Leptin and glucose inhibited the electrical activity of orexin neurons, while ghrelin was stimulatory. These finding provide a cellular explanation for how orexin neurons may become activated by body energy depletion.

It's been suggested that orexin neurons are also involved in the pathogenesis of metabolic disorders such as obesity. Narcoleptic patients (the majority of which are orexin deficient) have higher body mass index (BMI) than population controls and higher incidence of metabolic disorder such as obesity [17]. It is also reported that mice with genetically ablated orexin neurons become obese. Together, these results indicate that the activity of orexin neurons may stimulate more energy expenditure (vial increasing metabolism) than energy intake (via increased feeding). The link between the orexin systems and obesity was also investigated in studies of the Prader-Willi syndrome, a complex genetic disorder which leads to hypogonadism, appetite dysregulation, and hyperphagia associated with early childhood obesity. Some patients also present with excessive daytime sleepiness. Nevsimalova et al. looked at the levels of orexin in cerebrospinal fluid in four patients with confirmed Prader-Willi syndrome, and found decreased levels compared to controls[18].

The Yanagisawa lab recently described that orexin signaling also has the capacity to primarily promote energy expenditure via leptin sensitization. Activation of OXR2 signaling

or its downstream targets beneficially alters hypothalamic set points controlling metabolic rate, food intake, and leptin and insulin sensitivity. They suggested that, while OXR1 may influence circulating insulin levels, orexin overexpression improves insulin sensitivity by a predominantly OXR2-dependent mechanism.

1.3.4. Addiction

There have been indications that orexins might have an important role in addiction. Narcoleptic patients are often treated with highly addictive amphetamine-like drugs but they rarely become addicted to these drugs. Furthermore, orexin knockout mice are less susceptible than wild-type animals to develop morphine dependence. Harris et al. showed that orexin neurons in the lateral hypothalamus (LH) are activated by cues associated with rewards such as food or drugs, and that exogenous stimulation of LH orexin neurons reinstates extinguished drug-seeking behavior in rodents[19]. Recently, Borgland *et al*. identify a link between orexin and the neuronal changes induced by chronic exposure to cocaine in dopamine cells in the ventral tegmental area (VTA), a 'hot spot' in the brain for developing behaviors associated with drug addiction. They showed that release of orexin into the VTA promotes the insertion of NMDA receptors into the excitatory postsynaptic membrane of dopamine cells. This insertion eventually results in a delayed and more enduring increase in AMPA signaling mediated by both pre- and postsynaptic changes. This sequence of orexin-induced changes in NMDA and AMPA signaling are necessary for the induction of neuroplasticity and behavioral sensitization by chronic cocaine. Together, these data indicate that orexin-containing neurons in the lateral hypothalamus are necessary to induce neuroplasticity at glutamatergic synapses within the VTA by drugs of abuse [20]. A Recent study also indicated that orexin A plays role in nicotine addiction of human smokers.

Blocking orexin-1 receptors not only decreased the motivation to continue nicotine use in rats, it also abolished the stimulatory effects of nicotine on their brain reward circuitries [21].

1.4. Screening ligands using small molecule microarray

1.4.1. Small molecule microarray (SMM)

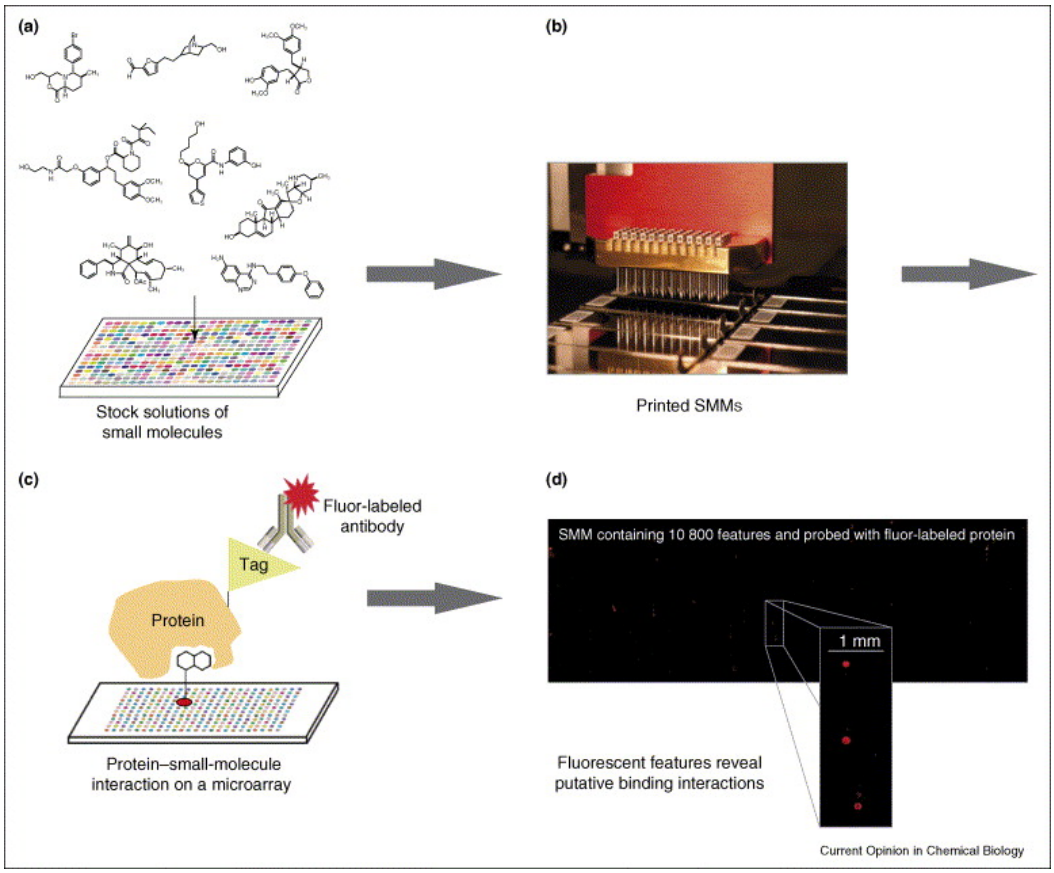

Figure 3. Preparation and screening of SMMs. (a) Stock solutions of small molecules are arrayed onto functionalized microscope slides. Microarrays are typically screened by **(b)** incubation with a protein of interest followed by **(c)** incubation with a fluorescently labeled antibody, either against the protein or an epitope tag. **(d)** Fluorescent images indicate putative protein–small-molecule interactions.

Small molecules are used as tools to study functions of proteins and cellular processes. Specific small-molecule probes might uncover novel therapeutic targets for human disease as well as serve as leads molecules for drug discovery. With increasing numbers of target proteins are available for drug discovery, high-throughput methods for ligand discovery is needed. Microarray technology has been advancing biomedical research by allowing high-throughput analysis of tens of thousands of samples and by examining low nanomolar to picomolar amounts of materials. Schreiber *et al.* initially reported a high-throughput protein-binding assay involving microarrays of small molecules [22]. Collections of small molecules are immobilized, typically covalently, onto glass microscope slides. The small-molecule microarrays (SMMs) are probed with a protein of interest and binding events are detected using a fluorescence-based readout with a standard microarray scanner (Figure 3). Since the initial discovery, there have been extensive efforts of developing several novel attachment chemistries for the preparation of SMMs, as well as novel screening and profiling applications [23].

1.4.2. Peptoid microarray

Peptoids (N-substituted glycines) closely resemble peptides except that the side chains are attached to the main chain nitrogen rather than the α-carbon (Figure 4). Peptoid oligomers are protease resistant and non-immunogenic. Peptoids contain better diversity in functionality than peptides. Because of ease of their synthesis via submonomer approach using thousands of commercially available primary amines, peptoids have been a choice of peptidomimetic libarary. Recent data suggest that peptoids are generally cell permeable and have been proven to have excellent protein capturing property.

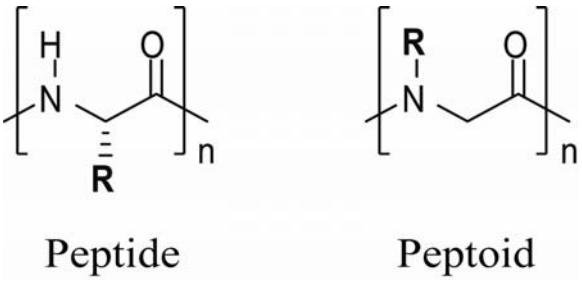

Figure 4. Chemical structures of peptide and peptoid.

Previously, Kodadek's lab developed methods to detect proteins using peptoid microarrays. With this method, they were able to transform lead compounds of low affinity into specific and efficient capture reagents for target proteins in the presence of complex mixtures [24]. Recently, they also showed that different proteins exhibit a different pattern of binding ("fingerprint") to the peptoids on the array (Figure 5) [25]. Together, these results suggest that peptoid microarray can be useful tools of high-throughput ligand discovery and protein profiling for diagnostic purposes.

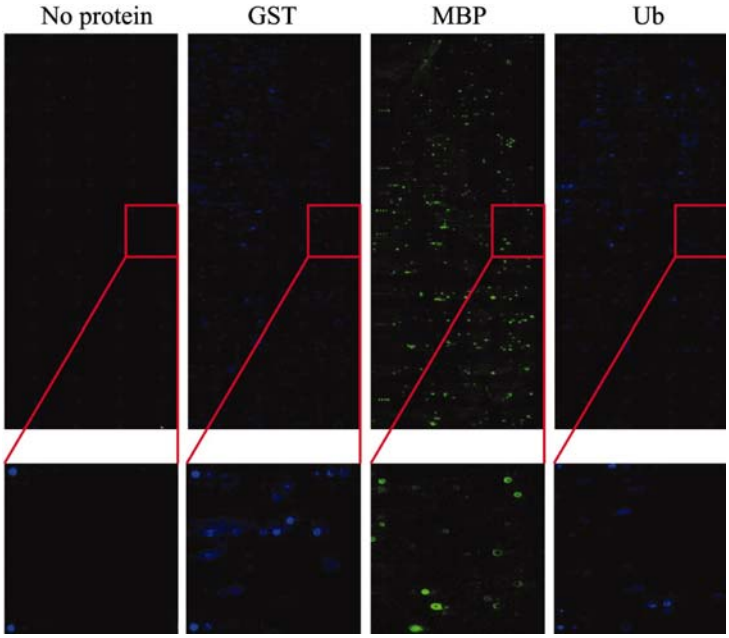

Figure 5. Protein profiling using peptoid microarray. Images of microarrays were obtained after incubating fluorescently labeled GST, MBP, or Ub on a peptoid microarray. Each protein showed different binding pattern to peptoids on microarray.

1.5. References

[1] G. Milligan, *Drug Discov Today* **2006**, *11*, 541.

[2] E. Jacoby, R. Bouhelal, M. Gerspacher, K. Seuwen, *ChemMedChem* **2006**, *1*, 761.

[3] T. M. Bridges, C. W. Lindsley, *ACS Chem Biol* **2008**, *3*, 530.

[4] *Nat Rev Drug Discov* **2004**, *3*, 575.

[5] S. M. Gopalakrishnan, R. B. Moreland, J. L. Kofron, R. J. Helfrich, E. Gubbins, J. McGowen, J. N. Masters, D. Donnelly-Roberts, J. D. Brioni, D. J. Burns, U. Warrior, *Anal Biochem* **2003**, *321*, 192.

[6] W. M. Oldham, H. E. Hamm, *Q Rev Biophys* **2006**, *39*, 117.

[7] T. Sakurai, A. Amemiya, M. Ishii, I. Matsuzaki, R. M. Chemelli, H. Tanaka, S. C. Williams, J. A. Richarson, G. P. Kozlowski, S. Wilson, J. R. Arch, R. E. Buckingham, A. C. Haynes, S. A. Carr, R. S. Annan, D. E. McNulty, W. S. Liu, J. A. Terrett, N. A. Elshourbagy, D. J. Bergsma, M. Yanagisawa, *Cell* **1998**, *92*, 1 page following 696.

[8] L. de Lecea, T. S. Kilduff, C. Peyron, X. Gao, P. E. Foye, P. E. Danielson, C. Fukuhara, E. L. Battenberg, V. T. Gautvik, F. S. Bartlett, 2nd, W. N. Frankel, A. N. van den Pol, F. E. Bloom, K. M. Gautvik, J. G. Sutcliffe, *Proc Natl Acad Sci U S A* **1998**, *95*, 322.

[9] M. Mieda, M. Yanagisawa, *Curr Opin Neurobiol* **2002**, *12*, 339.

[10] T. Sakurai, *Curr Opin Clin Nutr Metab Care* **2003**, *6*, 353.

[11] J. M. Siegel, *Cell* **1999**, *98*, 409.

[12] R. M. Chemelli, J. T. Willie, C. M. Sinton, J. K. Elmquist, T. Scammell, C. Lee, J. A. Richardson, S. C. Williams, Y. Xiong, Y. Kisanuki, T. E. Fitch, M. Nakazato, R. E. Hammer, C. B. Saper, M. Yanagisawa, *Cell* **1999**, *98*, 437.

[13] C. Brisbare-Roch, J. Dingemanse, R. Koberstein, P. Hoever, H. Aissaoui, S. Flores, C. Mueller, O. Nayler, J. van Gerven, S. L. de Haas, P. Hess, C. Qiu, S. Buchmann, M.

Scherz, T. Weller, W. Fischli, M. Clozel, F. Jenck, *Nat Med* **2007**, *13*, 150.

[14] P. Rouet-Benzineb, C. Rouyer-Fessard, A. Jarry, V. Avondo, C. Pouzet, M. Yanagisawa, C. Laboisse, M. Laburthe, T. Voisin, *J Biol Chem* **2004**, *279*, 45875.

[15] T. Voisin, A. El Firar, C. Rouyer-Fessard, V. Gratio, M. Laburthe, *FASEB J* **2008**, *22*, 1993.

[16] J. T. Willie, R. M. Chemelli, C. M. Sinton, M. Yanagisawa, *Annu Rev Neurosci* **2001**, *24*, 429.

[17] S. Nishino, B. Ripley, S. Overeem, S. Nevsimalova, G. J. Lammers, J. Vankova, M. Okun, W. Rogers, S. Brooks, E. Mignot, *Ann Neurol* **2001**, *50*, 381.

[18] S. Nevsimalova, J. Vankova, I. Stepanova, E. Seemanova, E. Mignot, S. Nishino, *Eur J Neurol* **2005**, *12*, 70.

[19] G. C. Harris, M. Wimmer, G. Aston-Jones, *Nature* **2005**, *437*, 556.

[20] S. L. Borgland, S. A. Taha, F. Sarti, H. L. Fields, A. Bonci, *Neuron* **2006**, *49*, 589.

[21] J. A. Hollander, Q. Lu, M. D. Cameron, T. M. Kamenecka, P. J. Kenny, *Proc Natl Acad Sci U S A* **2008**, *105*, 19480.

[22] G. MacBeath, A. N. Koehler, S. L. Schreiber, *J. Amer. Chem. Soc.* **1999**, *121*, 7967.

[23] A. J. Vegas, J. H. Fuller, A. N. Koehler, *Chem Soc Rev* **2008**, *37*, 1385.

[24] M. M. Reddy, K. Bachhawat-Sikder, T. Kodadek, *Chem Biol* **2004**, *11*, 1127.

[25] M. M. Reddy, T. Kodadek, *Proc Natl Acad Sci U S A* **2005**, *102*, 12672.

Chapter 2: Isolation of an orexin receptor antagonist via a microarray-based, two-color, cell-based screen.

2.1. Introduction:

G-protein coupled receptors (GPCRs) are perhaps the single most important class of drug targets today, with about 30% of current drugs either agonizing or antagonizing the activities of these receptor.[1] In addition to ~ 200 GPCRs that are already under investigation for drug development, an additional 500 or so GPCRs are predicted from the human genome sequence.[2] Therefore, there is a great interest in developing improved and more economical high-throughput screening (HTS) methods to isolate GPCR-modulating compounds. One commonly used approach is the radioligand binding assays, in which GPCR-binding compounds are identified based on their ability to compete with radiolabeled natural ligands. Recently, functional assays, such as triggering activation of a receptor-coupled reporter gene, have emerged as a favored approach that can be easily applied to cell surface receptors especially whose ligands are unknown (ex. orphan GPCRs).[3, 4] Functional assays have the advantage of not requiring the use of radioactive compounds. However, they are quite expensive and require a highly specialized robotic infrastructure, at least if large numbers of compounds are to be screened. Moreover, the "hits" that one obtains from functional HTS screens are of unknown quality, for example the degree to which they might cause off target effects.

An alternative approach, first developed by Lam and co-workers, [5, 6] is to employ one bead one compound (OBOC) synthetic libraries displayed on hydrophilic beads and expose these to cells that express the target receptor. Hits are identified by microscopic observation of cells "sticking" to beads that display receptor-binding compounds. We recently reported an

important elaboration of this type of screening technology with the development of a two-color assay that demands extremely high specificity in order for a compound to be scored as a hit.[7] In this assay, cells lacking the target receptor were labeled with a green quantum dot. The target receptor was then introduced into exactly the same cell type and these cells were labeled with red quantum dots. The cells were then mixed and exposed to an OBOC library. Only beads that bound red-labeled cells, but not green-labeled cells, were scored as hits. Thus, a bead-displayed compound must largely ignore all of the other molecules on the surface of the cell in order to be scored as a hit, ensuring high specificity for the target receptor. Using the Vascular Endothelial Growth Factor Receptor 2 (VEGFR2) as a model system and a library of ≈ 260,000 peptoids[8] as the source of potential ligands, we demonstrated that this process indeed provides highly specific receptor ligands. One of these was further developed into a potent antagonist of the receptor with the ability to inhibit angiogenesis in vivo.[7] In this part, we report an alternative platform for carrying out two-color, cell-based screens that employs microarrays[9, 10] comprised of several thousand peptoids.[11] As described below, this assay format has some advantages over the bead-based approach, including more facile identification of hits and more economical use of the combinatorial library.

For this study, we employed as a target the orexin receptor 1 (OXR1). OXR1 and the homologous orexin receptor 2 (OXR2), are GPCRs that are activated by the neuropeptide hormones orexin A and B. The orexin receptors are involved in the regulation of sleep and wakefulness [12, 13] as well as appetite control,[14] obesity and diabetes[15] and addictive behavior.[16] Antagonists of OXRs have been investigated as treatments for insomnia[17, 18, 19] and agonists of the receptor are predicted to be useful for the treatment of narcolepsy,[20] which in most humans results from the absence of orexin-producing neurons.[21]

2.2. Results

A microarray-based, two-color, cell-based screen to isolate peptoids that bind specifically to orexin receptor.

First, we examined if microarray-displayed peptoids are capable of binding to cells stably expressing human OXR1 (HEK293/hOXR1). The cells were incubated with the array, constructed as described previously,[11] for 1hr after first pre-blocking the array with 3% BSA in DMEM to inhibit non-specific binding. The slide was then washed with PBS, and the binding of the cells to the array was examined under a microscope. As shown in Figure 6A, circular patterns of cell monolayers were observed at certain points on the array and the diameters of the monolayers were similar to those of the printed peptoid spots (200 – 300 μm), suggesting a cell-peptoid interaction at these features. This experiment suggested that the hybridization conditions were appropriate for assay peptoid-receptor interactions.

Next, to identify peptoids that bind specifically to human OXR1 expressing cells, HEK293 cells, which lack orexin receptors, were stained with SYTO85 (green), and HEK293 cells expressing human OXR1 from a transgene were labeled with SYTO60 (red). After mixing the cells in an approximately 1:1 ratio, they were applied to a peptoid microarray displaying 5760 different 9-mers and incubated for 1hr at 37˚C. After washing followed by fixation, the slide was scanned at 635-nm (to visualize HEK293/hOXR1 binding) and 532-nm (to visualize HEK293 binding) and the two images were superimposed (Figure 6B). We hypothesized that spots showing a high ratio of red over green fluorescence display peptoids that bind to OXR1 specifically. After quantification of the level of fluorescence in each channel (532 nm and 635 nm, respectively) using a standard microarray scanner, we identified 99 spots displaying above background fluorescence in one or both channels. Some representative images of these spots are shown in Figure 6C. Calculated ratios of the

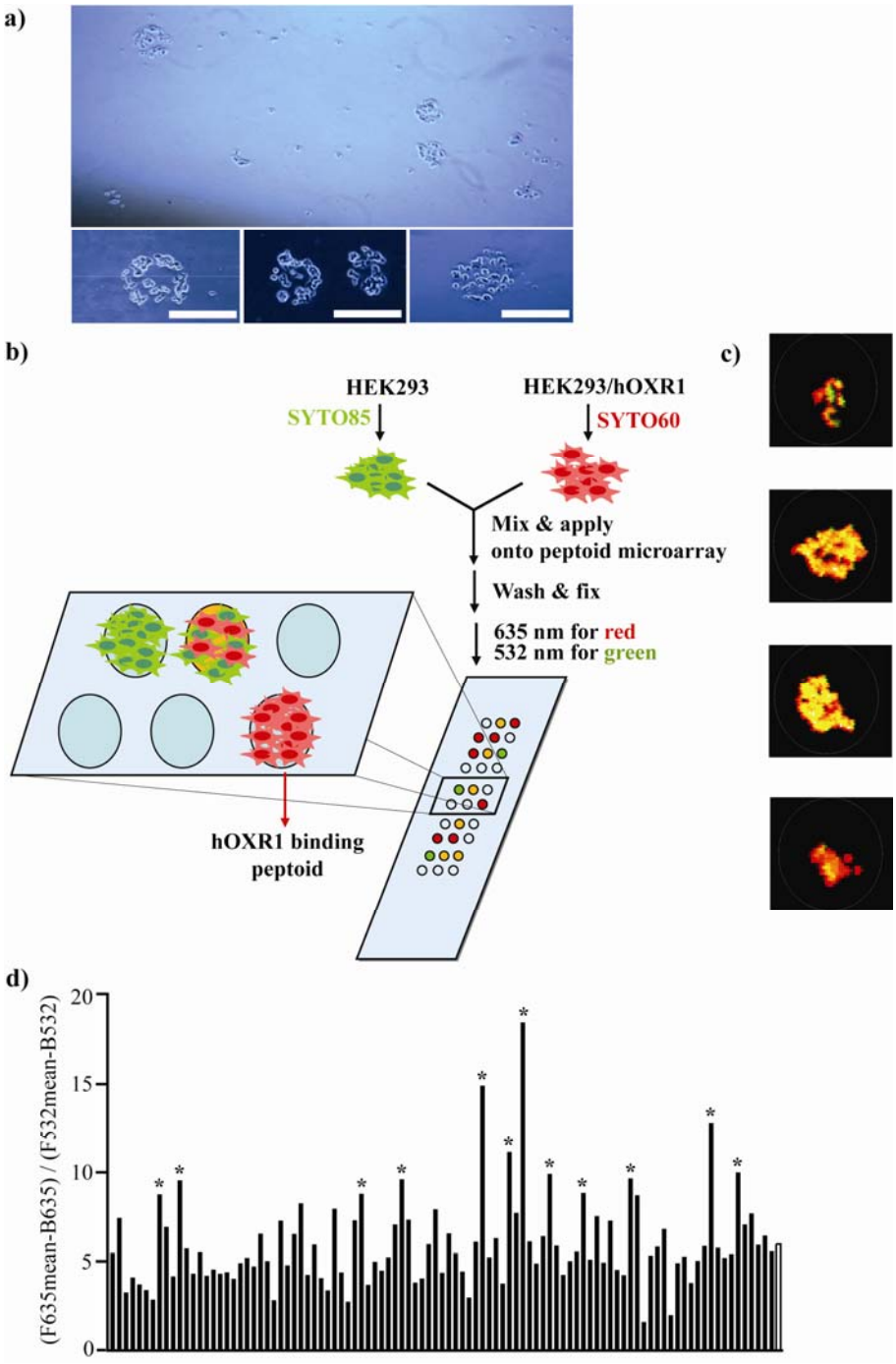

Figure 6. A two-color, cell-binding peptoid microarray to isolate ligands for hOXR1. A) light microscopic images of cells on peptoid microarray. Scale bar = 250 μm B) Schematic illustration of the screening procedure. C) Representative superimposed images (red and green) of cells on a microarray after washing. Variation of red fluorescence over green was observed. D) Ratiometric analysis of microarray images. Ratios of red over green fluorescence of 99 spots were shown. The unfilled bar represents the mean of the 99 spots. *-ed bars represent peptoids which were attempted for sequence analysis. F635 and F532 are mean fluorescence intensities of spots at 635-nm and 532-nm, respectively. B635 and B532 mean background fluorescence intensities at 635-nm and 532-nm, respectively.

fluorescence intensities in the red and green channels are illustrated in Figure 6D. The 12 peptoid features displaying the highest red/green ratio above the mean were chosen as possible OXR1 ligands and we attempted to sequence these molecules by tandem MALDI mass spectrometry by going back to the corresponding peptoid solutions used to spot onto the microarray. Sequencing provided unambiguous structures for five of these peptoids (see supporting information), which we named orexin receptor binding peptoids, OBPs (Figure 7).

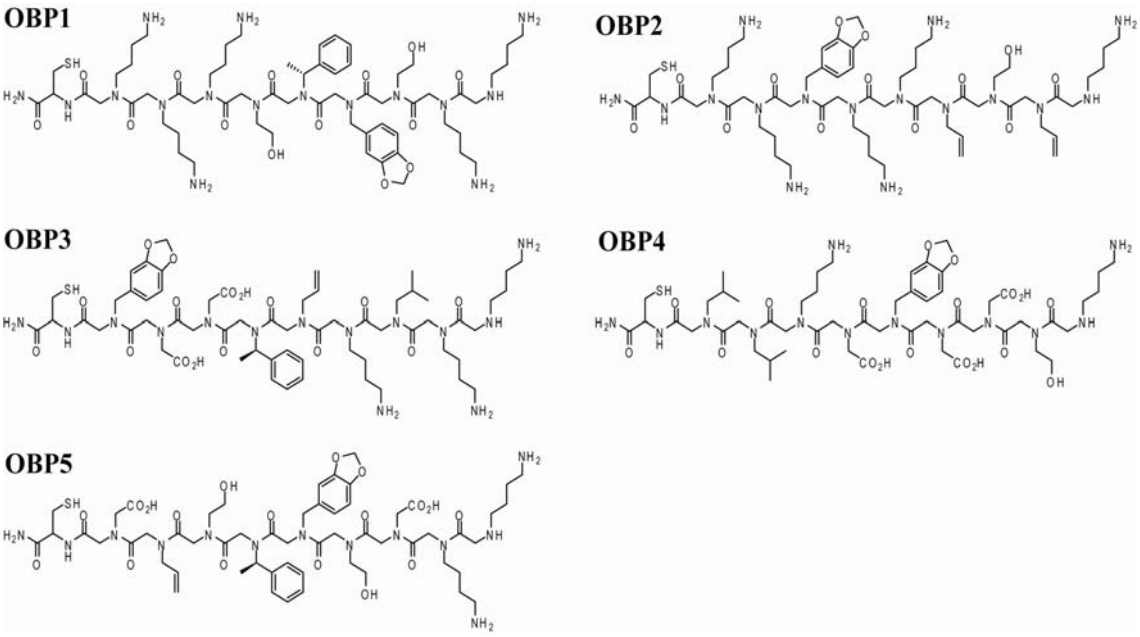

Figure 7. Chemical structures of hit peptoids (OBPs)

Hit validation

Of course, a binding screen does not provide information on whether a particular ligand might modulate the activity of the target receptor. Therefore, the five OBPs were re-synthesized, purified by HPLC and employed in functional assays. OXR1 receptor activation by orexin-A up-regulates adenyl cyclase, which subsequently increases cAMP production in

OXR1-expressing cells.[22] To quantify orexin-A induced cAMP elevation in HEK293/hOXR1 cells, we employed a reporter gene (3xCRE-Luc) assay in which the promoter of the reporter gene contains a cAMP responsive element upstream of the firefly luciferase gene. After co-transfection with this reporter plasmid and a cAMP-unresponsive *Renilla* luciferase-encoding plasmid, cells were serum-starved (4hr) and increasing concentrations of orexin-A were added. After six hours, cells were lysed and the luciferase activities were measured. As shown in Figure 8A, orexin-A stimulates cAMP elevation in a dose-dependent fashion (EC_{50} = 43 nM). This stimulation was blocked by the commercially available OXR1-selective antagonist SB408124 (Figure 8B), validating that this assay measures orexin-triggered receptor activity.

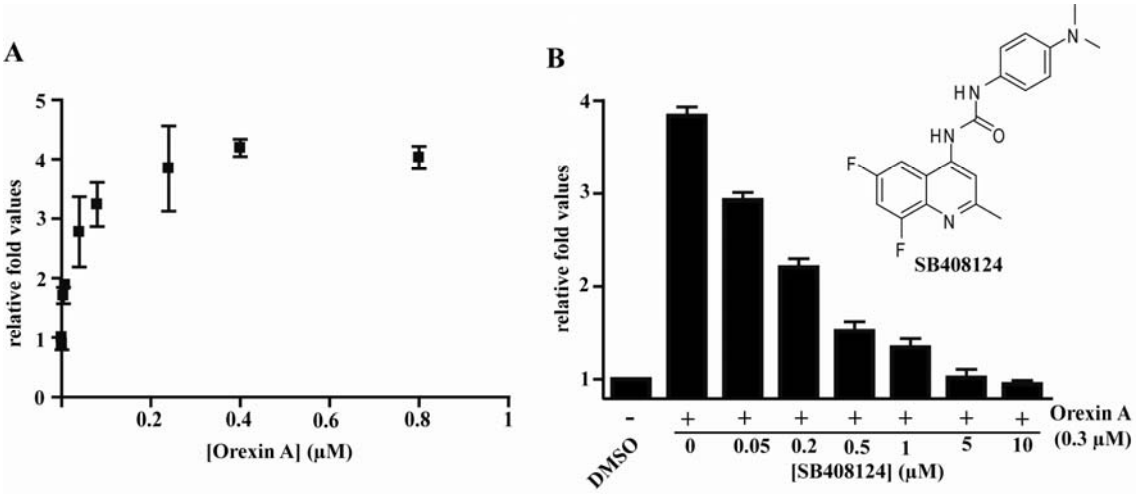

Figure 8. A reporter gene assay monitoring OX1R activation by orexin A. a) Orexin A induced a dose-dependent increase of cAMP production. b) The OX1R selective antagonist, SB408124 blocks orexin-induced cAMP production.

.

As shown in Figure 9A, none of the OBPs showed agonist activity in this assay at a concentration of 300 μM, but some weak antagonist activity was observed (Figure 9B). For example, OBP1 showed an approximately 30% inhibition of orexin A-induced cAMP elevation at 300 μM. OBP2 was not tested since it was cytotoxic to both HEK293 and

HEK293/hOXR1 cell lines. The weak activity of OBP1 as an antagonist shows that the microarray-based binding assay is capable of registering even low potency receptor-binding molecules, probably because of avidity effects (i.e., the ability of multiple array-immobilized peptoids to engage multiple receptors on the cell surface simultaneously).

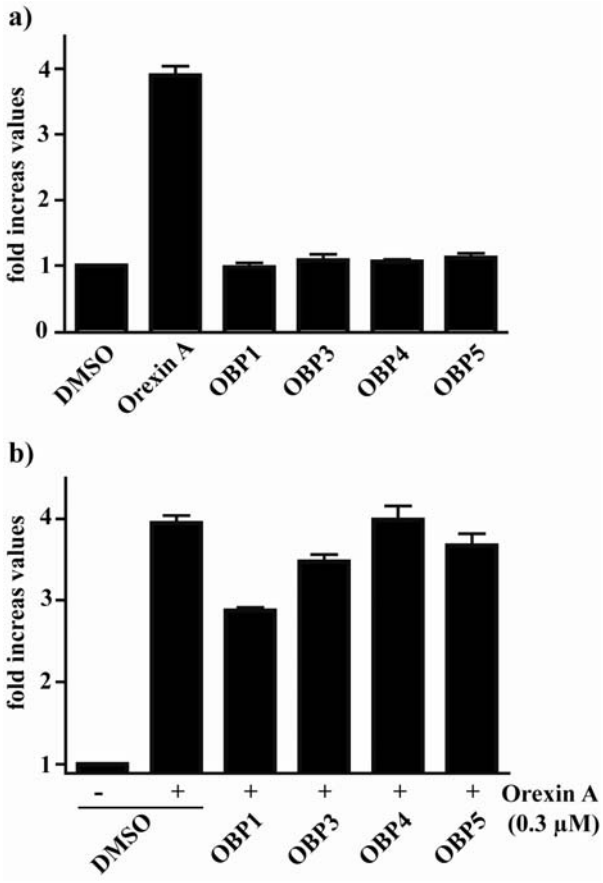

Figure 9. Regulation of hOXR1 function by hit peptoids. Hit peptoids (OBPs) were tested for their agonist (A) or antagonist (B) activities. Error bars represent the standard deviation of the mean from triplicate experiments.

Hit optimization: Identification of minimal pharmacophore

We are interested in the development of novel orexin receptor antagonists in connection with some of our own biological work.[23] Thus, we attempted to improve the low activity of OBP1. As a first step, we sought to identify the minimal pharmacophore of OBP1.

Derivatives were synthesized in which each side chain (R) of OBP1 was replaced, in turn, with a methyl group (Figure 10A and Figure 11). This "sarcosine scanning" strategy is similar to the "alanine scanning" experiment that is often used to determine the residues in peptides that are important for their biological activities.[24]

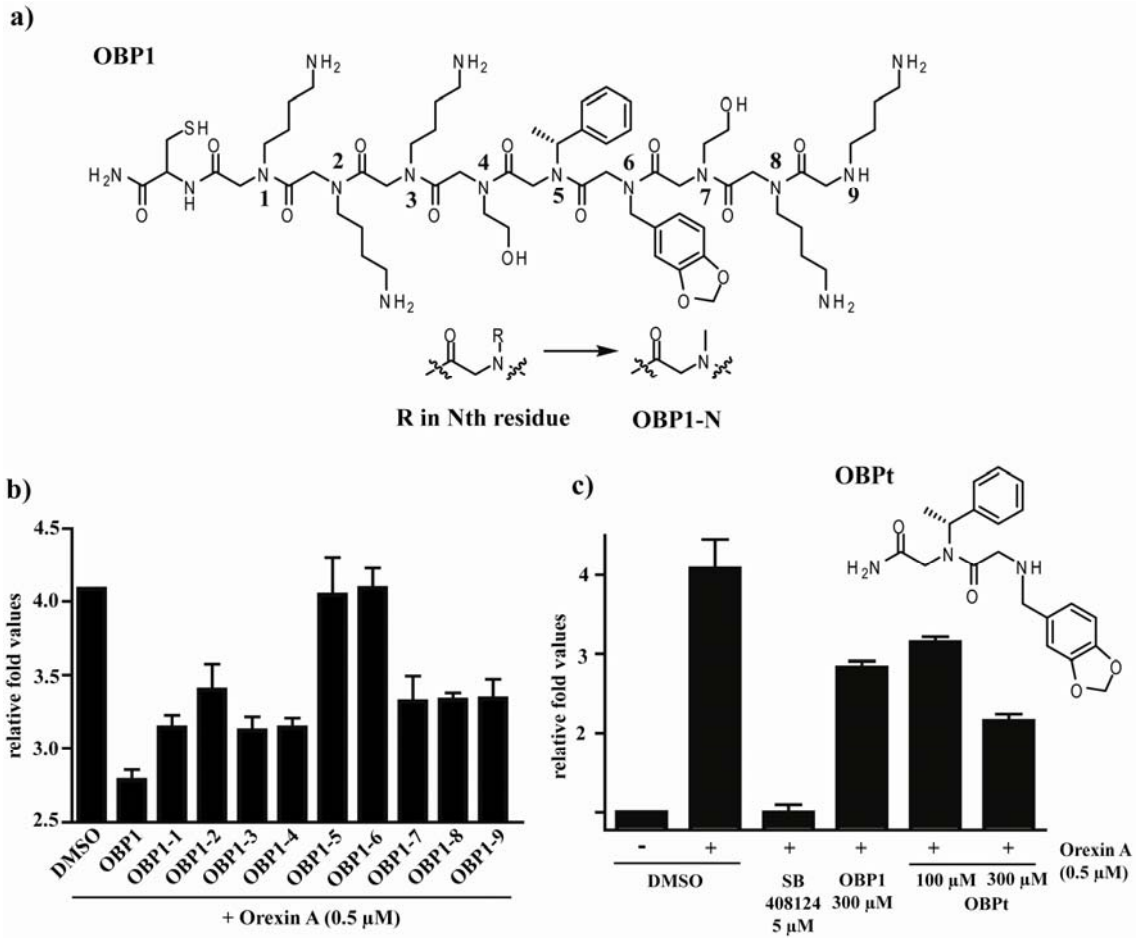

Figure 10. Pharmacophore identification using the sarcosine scanning strategy. A) Each side chain (R) of the Nth residue was replaced with a methyl group to afford OBP1-N, sarcosine containing peptoids. B) Effects of sarcosine replacements in antagonist activity of OBP1 ([OBP1-N] = 300 μM). C) Chemical structure of truncated OBP1 (OBPt) and its antagonist activity. Error bars represent the standard deviation of the mean from triplicate experiments.

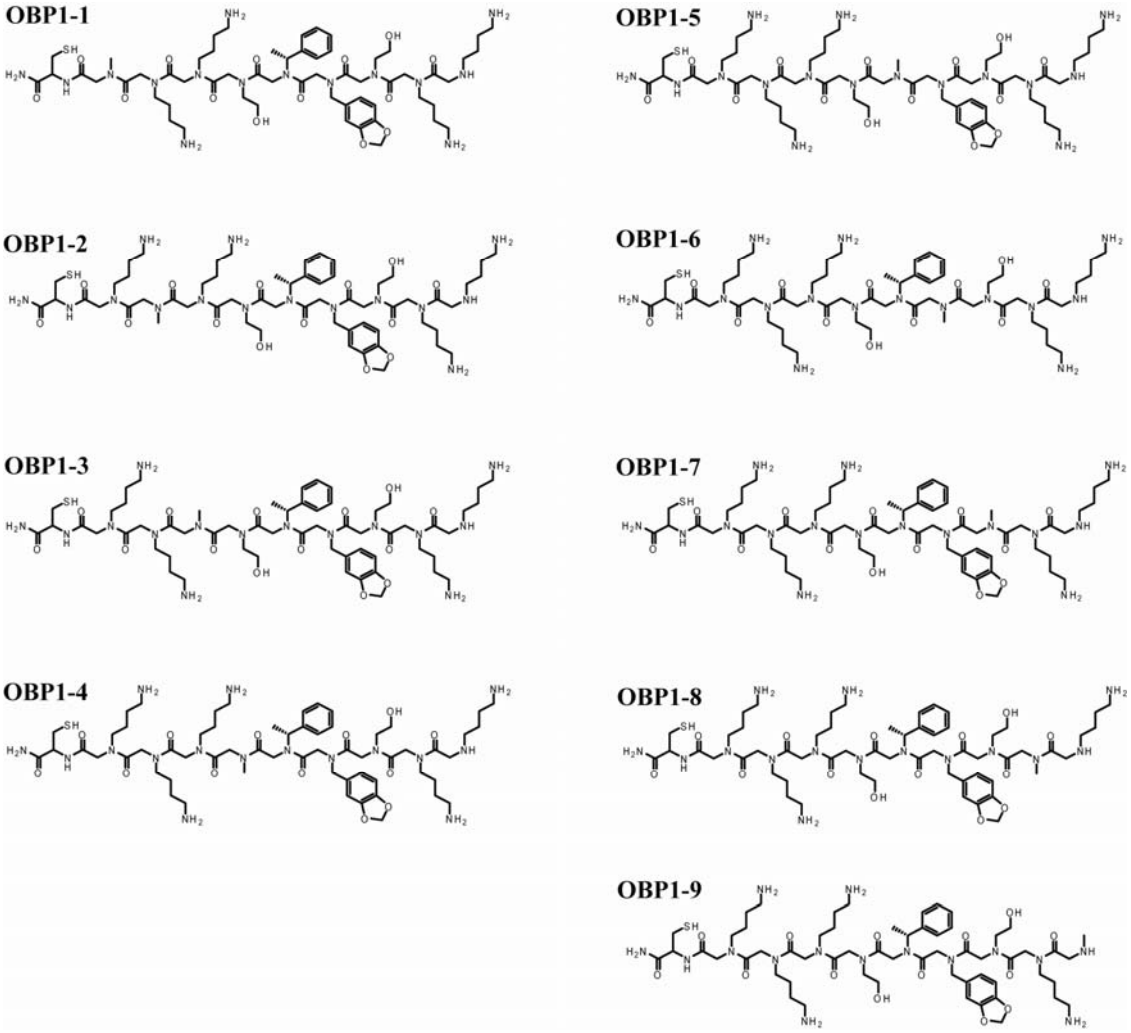

Figure 11. Chemical structures of OBP1-N, sarcosine derivatives

As shown in Figure 10B, all of the methyl-substituted derivatives exhibited lower activity than the parent OBP1 peptoid in this single point assay (300 μM peptoid). However, while some of the effects were modest, substitution of the side chains at the fifth and sixth positions of the peptoid (compounds OBP1-5 and OBP1-6) resulted in a complete loss of antagonist activity. Moreover, a truncated form of OBP1 (OBPt) containing only these two residue was synthesized and found to exhibit antagonist activity equal to or even slightly better than the parent OBP1 peptoid (Figure 10C). These results argue that the Nmba and

Npip residues in the OBP1 hit comprise the minimal pharmacophore.

Hit optimization: rational design

The realization that the dimeric peptoid OBPt is the core pharmacophore immediately suggested a possible route to improved compounds. As shown in Figure 4A, there appears to be significant structural similarity between OBPt and ACT-078573, an orexin receptor antagonist under investigation at Actelion Pharmaceuticals for the treatment of insomnia.[17] We hypothesized that appending a hydrophobic unit to Npip nitrogen would place this group in approximately the same region of space as the CF_3-substituted aryl ring in ACT-078573. The N-terminal secondary amine of OBPt was benzylated or benzoylated to afford OBPt-1 and OBPt-2, respectively (Figure 12a). OBPt-1 indeed was found to block orexin-A-induced cAMP elevation much more efficiently (IC_{50} = 20 μM; Figure 12b) than OBPt in the reporter gene assay. OBPt-2 showed a weaker, but still substantially improved, activity (IC_{50} = 55 μM; Figure 12b), implying that our structural model is valid.

To validate this result using a different assay, we examined the effect of these compounds on orexin-mediated stimulation of ERK phosphorylation. In CHO/OXR1 cells, it is known that orexin-A induced activation of OXR1 leads to a rapid, strong, and long-lasting increase in phosphorylated ERK (pERK), which is the active form of this signaling protein.[25] As depicted in Figure 12c, orexin-A strongly elevated ERK phosphorylation and this was inhibited by OBPt-1 in a dose-dependent fashion. The same effect was observed with SB408124, an OXR1 selective antagonist. We conclude that OBPt-1 is indeed an improved OXR1 antagonist.

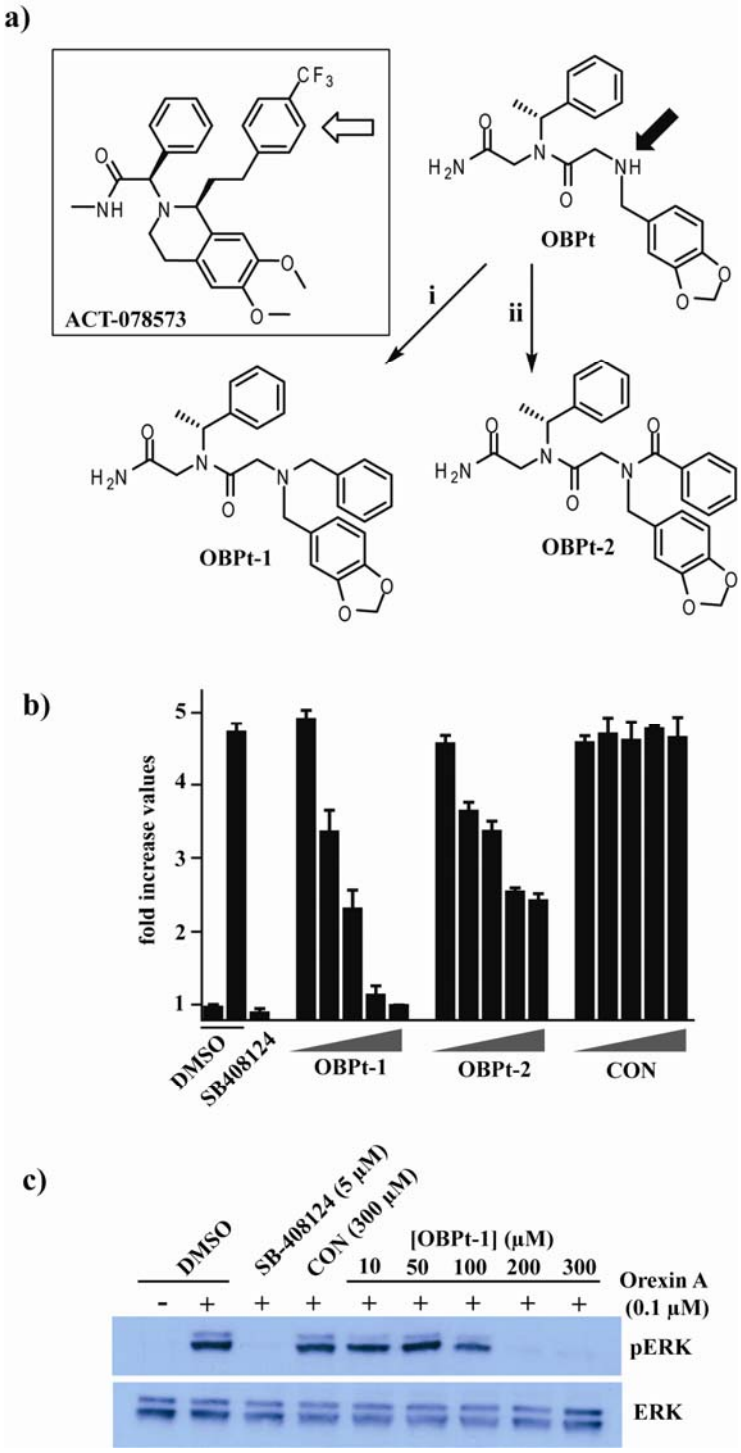

Figure 12 Introduction of hydrophobic moiety at N-terminal of OBPt. A) Scheme of N-terminal modification. i) BnBr, DIPEA ii) BzOH, DIC, HOAt B) Antagonist activities of OBPt-1 and OBPt-2. Increasing concentrations (2, 20, 30, 50, and 75 μM) of peptoids were used. CON is N-benzylated control peptoid (Figure 13). Error bars represent the standard deviation of the mean from triplicate experiments. C) Inhibition of orexin-mediated phosphorylation of ERK by OBPt-1. A representative figure from three different experiments is shown.

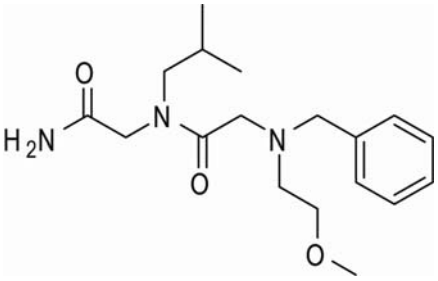

Figure 13. Chemical structure of CON.

Hit optimization: combinatorial chemistry

In an attempt to further improve the activity of the compound a small library of additional derivatives were synthesized in which the substituents at positions R1-R4 (Figure 14) were varied.

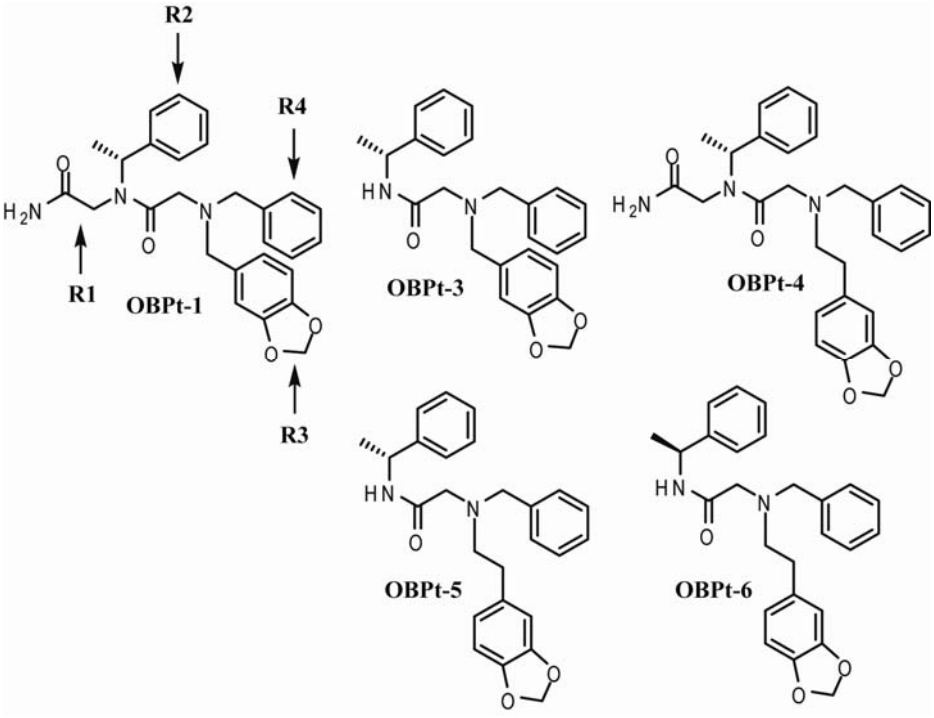

Figure 14. Chemical structures of OBPt-1 derivatives.

From the library, we found that OBPt-3 and OBPt-4 were more potent OXR1 antagonists than OBPt-1 with IC_{50}s of 4.5 μM and 15.1 μM, respectively (Figure 15). We then synthesized a derivative by combining the two substitutions in OBPt-3 and OBPt-4 that distinguished them from OBPt-1 to afford OBPt-5. In addition, to examine if the absolute configuration of the chiral center can affect activity, we also synthesized OBPt-6. As shown in Figure 16, OBPt-5 showed increased potency (IC_{50} = 1.7 μM). The potency of OBPt-6 was quite similar (IC_{50} = 2.9 μM) to OBPt-5. OBPt-5 itself did not show any agonist activity suggesting truncation and modification of the initial hit (OBP1) did not affect its regulatory property (Figure 17)

.

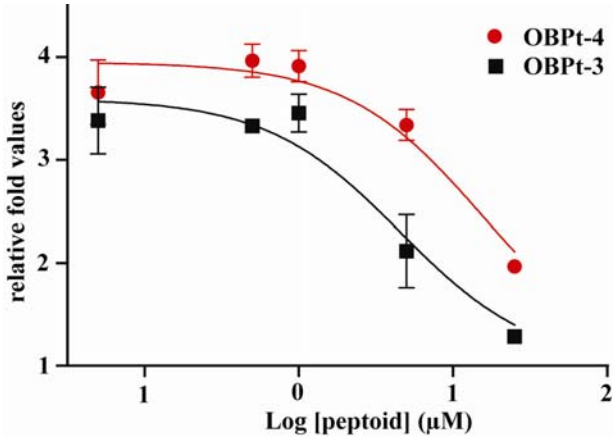

Figure 15. Antagonist activities of OBPt-3 and OBPt-4.

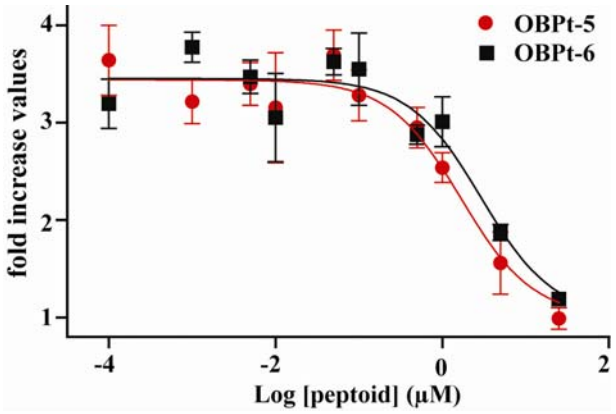

Figure 16. Antagonist activities of OBPt-5 and OBPt-6.

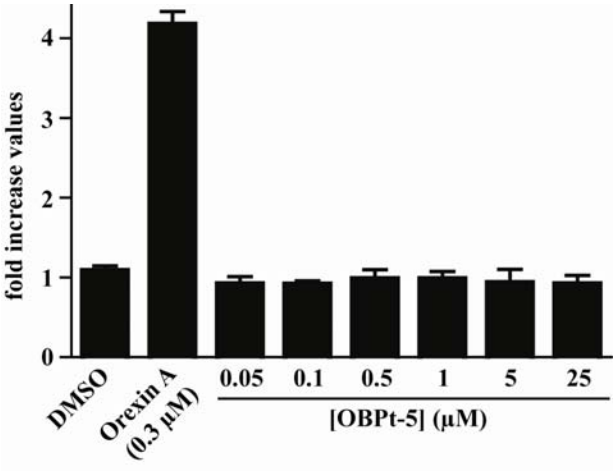

Figure 17. Agonist activity of OBPt-5

Specificity of OBPt-5

To examine the receptor sub-type specificity of OBPt-5, we tested the activity of OBPt-5 against OXR2. After transient expression of human OXR2, HEK293 cells were treated with OBPt-5 before the addition of orexins. As shown in Figure 18, both orexin A and B activated OXR2 and increased cAMP production and this activity was antagonized by OBPt-5 (IC_{50} = 1.6 μM for orexin A and 1.4 μM for orexin B). This was not surprising, since OXR1 and OXR2 display 64% amino acid sequence identity. Note that an OXR1 selective antagonist, SB408124, showed a little inhibition while an OXR1/R2 dual antagonist, Bis-amide (Figure 19) showed significant inhibition. Again, to ensure that the antagonistic effect observed in the presence of OBPt-5 is not due to some receptor-independent activity, we examined if OBPt-5 can directly interfere with the cAMP signaling pathway by assessing its effect on forskolin (adenyl cyclase activator)-induced cAMP production,[26] which does not depend on orexin signaling. As shown in Figure 20, OBPt-5 did not show any inhibition of cAMP production in this assay.

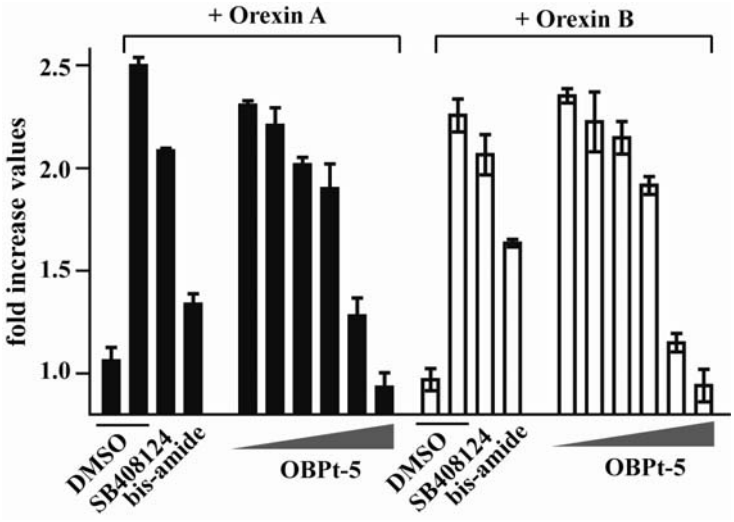

Figure 18 Effect of OBPt-5 on orexin A or orexin B-induced OXR2 activation. SB408124 is OX1R selective antagonist. Bis-amide is OX1R/2R dual antagonist.

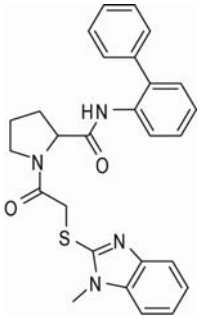

Figure 19. Chemical structure of Bis-amide.

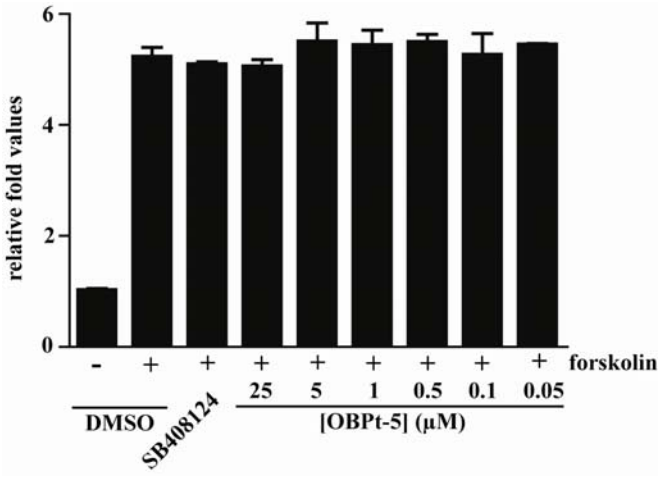

Figure 20. Effect of OBPt-5 on forskolin (fsk)-induced cAMP production in HEK293 cells.

2.3. Discussion

In summary, we have developed a novel microarray-based, two-color, cell-binding screen with which we discovered a new orexin receptor antagonist. We demonstrated that a peptoid on the microarray that showed preferential binding to receptor-expressing cells indeed regulates the function of the receptor in living cells, though this need not have been the case. We also demonstrated a rapid and efficient route to a preliminary optimization (≈ 180-fold improvement) of the hit that took advantage of a resemblance to a known receptor antagonist. This microarray-based screening method is, we believe, complementary to the bead-based approach that we have reported previously.[7] The disadvantage is that it is difficult to screen as many compounds as one can do with bead-based libraries. However, since at least several hundred can be constructed form a single OBOC library, the microarray format should allow for large numbers of such screens to be conducted without the need for constant library re-synthesis. Moreover, the microarray format facilitates quantitative comparisons of different compounds in the library with respect to both their apparent affinity for the receptor-displaying cells and their specificity for the target receptor. Finally, the bead-based method requires a rather tedious visual analysis of the beads under a fluorescence microscope to identify the best hits, whereas this is far more straightforward using a common microarray scanner in the present assay. The array-based screening assay appears to be capable of identifying even modest affinity receptor ligands, as evidenced by the >300 μM IC_{50} of OBP1, so it is clearly applicable to screening completely naïve libraries that are unlikely to contain extremely high affinity ligands. Moreover, it should also be useful for screening for “expanded” derivatives of minimized hits, such as OBPt-5, with higher affinity. In this approach, an alkyne- or azide-derivatized version of OBPt-5 would be coupled to all of the Azide- or alkyne-modified molecules on a new library arrayed on the glass slide. The process described in this paper could then be repeated to identify improved receptor ligands,

perhaps by including soluble OBPt-5 as a competitor during the cell-array hybridization step. This work is underway. We anticipate that this methodology will be of significant utility for the discovery of high affinity and specificity ligands for cell surface receptors.

2.4. Experimental section

General remarks. All chemicals and solvents were purchased from commercial suppliers and used without further purification. Mass spectra were obtained with a Voyager-DE^{TM} PRO (Applied Biosystems) for MALDI-TOF with α-cyano-4-hydroxycinnamic acid matrix. MS/MS spectra were obtained on a 4700 Proteomics Analyser (Applied Biosystems).

Peptoid microarrays. Peptoid microarrays featuring 5760 different 9-mer peptoids were prepared as described before [1] using the peptoid library shown below.

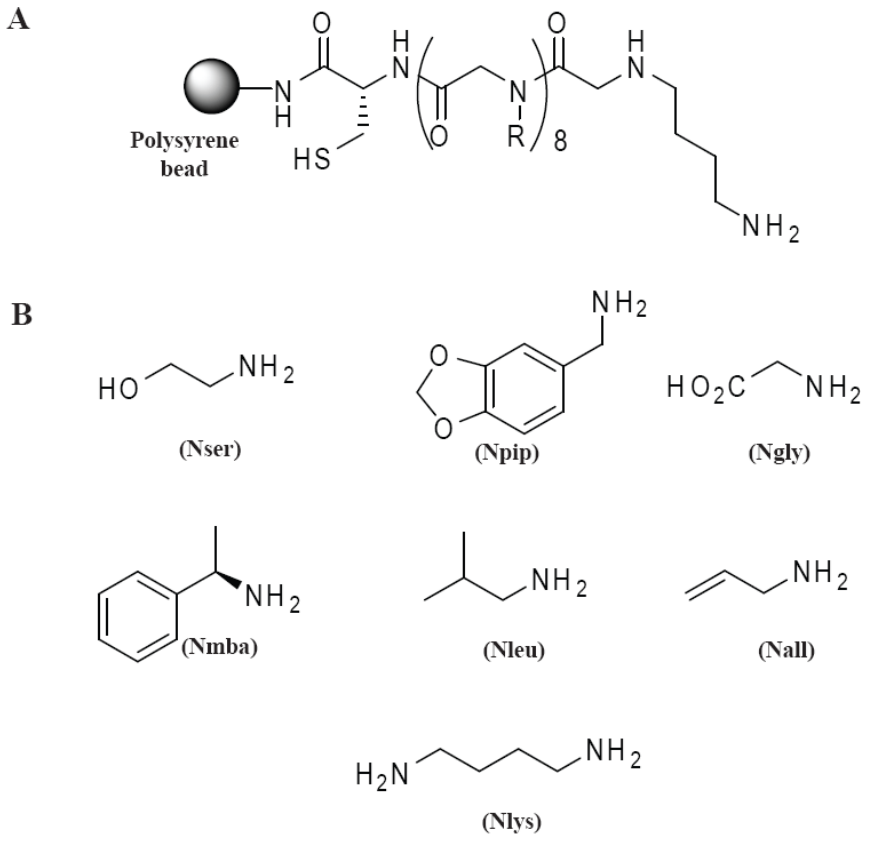

Figure 21. The peptoid library used in this study. a) General structure of peptoid library. b) Amines used for the preparation of the library. In brackets included the corresponding nomenclature of the peptoid residues.

A microarray-based, two-color, cell-binding screen and ratio-metric image analysis. Cells were grown in culture plates to 95% confluency. The medium was replaced with a Syto dye staining solution (5μM in PBS) and incubated for 10 min at 37˚C. Syto85 was used for HEK293 and Syto60 was used for HEK293/hOXR1. Cells were washed with PBS (pH = 7.4) three times and re-suspended with an incubation medium (3% BSA in DMEM). The two differentially stained cells were mixed at a 1:1 ratio in incubation media (10 mL), using $1x10^6$ cells from each cell type. The cell suspension was added onto a microarray slide which had been washed with PBS and equilibrated with an incubation medium for 1hr. The Super PAP Pen (The Binding Sites, Inc.) was used to make a boundary along the edge of the microarray to hold cell suspension. After incubation for 1hr at 37˚C, the cell suspension was removed by suction and the microarray slide was placed on a Petri dish. PBS was added to cover the slide and the plate was gently shaken to wash off cells that bind nonspecifically to the microarray surface (30 sec x 5 times). The microarray slide was then fixed (3% formaldehyde in PBS) for 10 min at room temperature and washed with PBS (10 sec x 2 times). After brief washing with ddH_2O, excess water was decanted and the microarray slide was dried with reduced exposure to light. The microarray slide was scanned with a ScanArray ExpressHT microarray scanner (PerkinElmer) using 532-nm (Syto 85) and 635-nm (Syto 60) lasers at 100% power and 300 PMT with pixel size of 5. All the scanned images were analyzed by using the GENEPIX PRO 5.0 software (Axon Instruments, Union City, CA). Fluorescence intensities (F) of each spot at 635-nm or 532-nm after subtraction of mean local background intensity (B) were used for ratio-metric analysis in which ratio = (F635-B635) / (F532-B532).

Peptoid synthesis. All peptoids (except OBPt-3, OBPt-5, and OBPt-6) were synthesized by on Rink Amide AM resin (NovaBiochem) using the sub-monomer approach by a microwave-assisted protocol [(2)] and purified by preparative RP-HPLC (Waters) and confirmed with

MALDI-TOF/MS (Table S1). Amines used for peptoid synthesis are shown in Figure S1. For the preparation of sarcosine derivatives, methyl amine (2.0 M in THF) was used. For the preparation of CON, 2-methoxyeethylamine was used. For OBPt-5, after addition of second amine, N-terminal secondary amine was benzylated under reductive alkylation condition using benzaldehyde (10 eq.) and BAP (10 eq) [3]. Peptoids were cleaved from resins with cleavage cocktail (95% TFA, 2.5% water, 2.5 % TIS) and purified by preparative RP-HPLC.

Preparation of OBPt-3, OBPt-5, and OBPt-6. TentaGel Macrobeads NH_2 resin (RAPP Polymere) was reacted with 4-(bromomethyl)-3-nitrobenzoic acid (5 eq) in the presence of DIC (5 eq) and HOBt (5 eq) for 3 hr. After washing with DMF, the resin was reacted with (R) or (S)-α-methylbenzylamine in DMF (2 M) for 3 hr. The resin was washed with DMF and then reacted with DIC (2 M) and bromoacetic acid (2 M) for 3 hr. After washing with DMF, the resin was reacted with second amine for 3 hr to afford secondary amine. The resin was washed with DMF and then reacted with benzaldehyde (10 eq) and BAP (10 eq) for reductive alkylation. After washing, peptoids were cleaved from the resin by exposing to UV (365 nm, 6W) for 12 hr in 2% v/v TFA/MeOH.

Cell culture. HEK293 cells were maintained in DMEM (Dulbecco's modified Eagle's medium, Invitrogen) supplemented with 110 mg/L sodium pyruvate, 2mM L-glutamine and 10% (v/v) fetal calf serum at 37˚C in a 5% CO_2 environment. For HEK293/hOXR1 cells [4], G418 (500μg/mL, Gibco) was included in the medium.

cAMP production assay. HEK293/hOXR1 Cells were grown to ~60% confluency in 48-well plates and transfected with the luciferase reporter plasmid, pGL3-3xCRE-TATA (100 ng/well) [5]. 24 hr after transfection, the cells were serum-starved for 4hr and treated with the

indicated concentrations of orexins. In the case of evaluating antagonists, cells were pre-treated with indicated concentrations of SB408124 or peptoids for 20 min. 6 hr after orexin addition, cells were lysed with passive lysis buffer (Promega) for 10 min at room temperature. The luciferase activity of the cell lysate was measured using the dual-luciferase assay kit (Promga) following the manufacture's protocol and normalized to Renilla luciferase activity from the co-transfected Renilla luciferase expression plasmid (pRLuc, 2 ng/well). Fold increase values of the normalized luciferase activities were presented in data. When HEK293 cells were used, indicated concentration of forskolin was used instead of orexin. To examine the effect of OBPt-5 on OXR2 expressing cells, HEK293 cells were transfected with phOXR2 (OriGene Technology Inc., 50 ng/well), pGL3-3xCRE-TATA (50 ng/well), and pRLuc (1 ng/well).

ERK phosphorylation assay. HEK/hOXR1 cells were grown (~75% confluency) in 6-well plates and serum-starved overnight prior to stimulation with orexin A for 12 min. For the antagonist evaluation, cells were treated with antagonists (SB408124 or peptoids) 20 min before the addition of orexin A. Cells were lysed with reporter lysis buffer (Promega) for 15 min at 4˚C. The collected lysates were mixed with 2x SDS sample buffer and heated for 5min at 95˚C. The samples were separated by SDS-PAGE and transferred to PDVF membranes (Immobilon, Millipore). The membranes were probed with anti-phospho ERK(1/2) or anti-ERK(1/2) primary antibodies (Santa Cruz) and subsequently developed with appropriate HRP-conjugated secondary antibody (BioRad) followed by chemiluminescence detection using SuperSignal® West Pico substrate (PIERCE). Quantifications of blot bands were performed using "Image J" software.

MS/MS sequence analysis

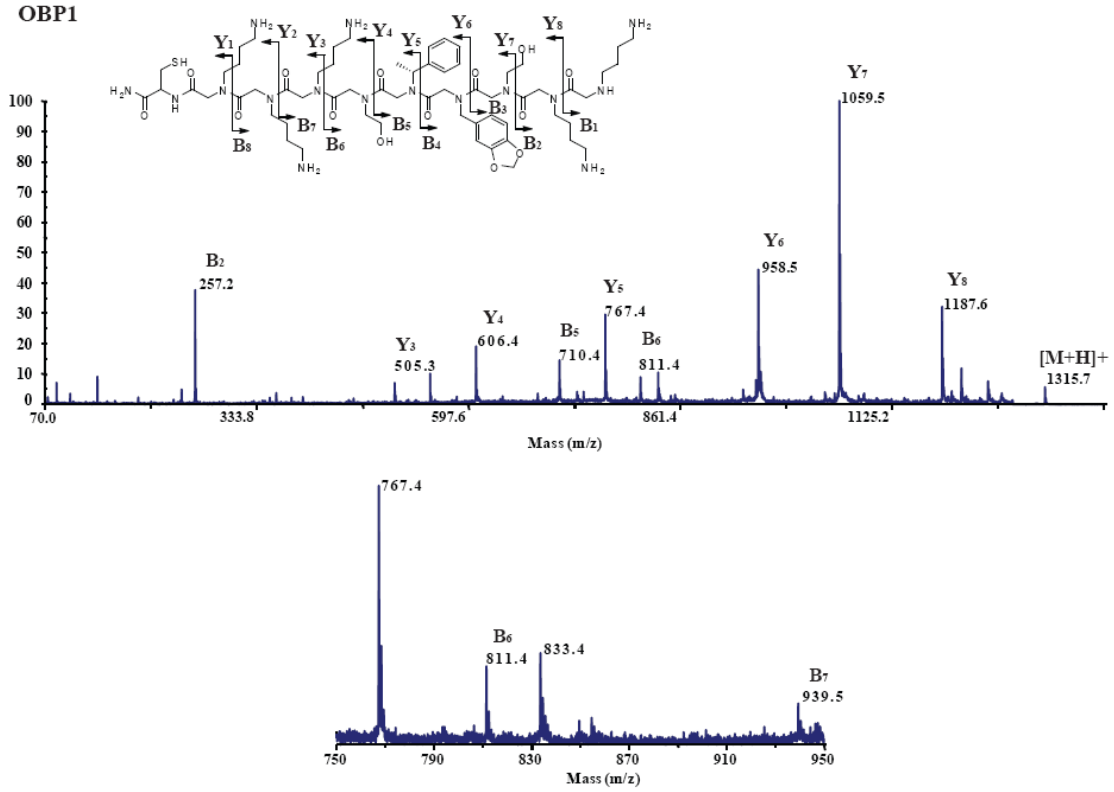

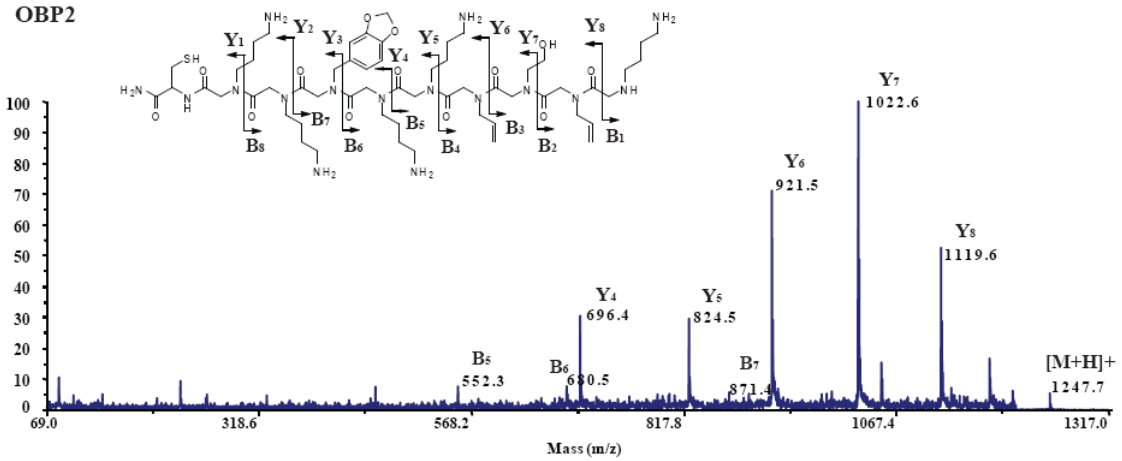

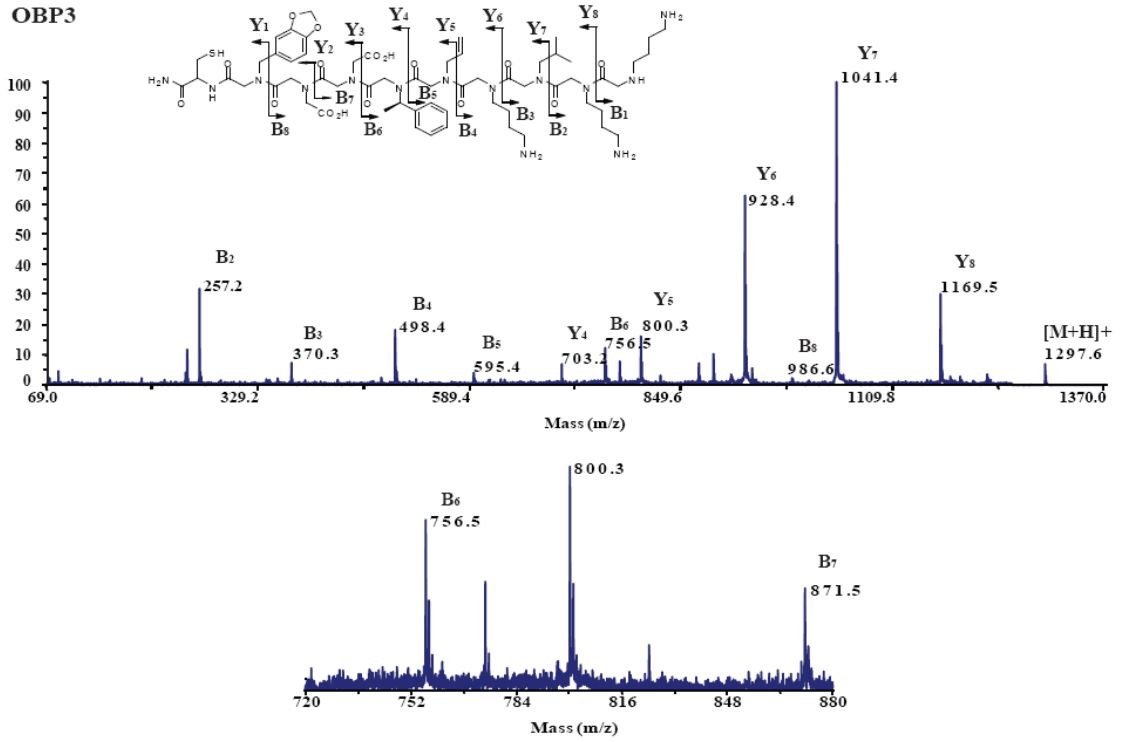
OBP3
Y1
Y2
Y3
Y4
Y5
Y6
Y7
Y8
B1
B2
B3
B4
B5
B6
B7
B8
Y7 1041.4
Y6 928.4
B2 257.2
Y8 1169.5
B4 498.4
Y5 800.3
B3 370.3
B6 756.5
Y4 703.2
B5 595.4
B8 986.6
[M+H]+ 1297.6
100
90
80
70
60
50
40
30
20
10
0
69.0
329.2
589.4
849.6
1109.8
1370.0
Mass (m/z)
800.3
B6 756.5
B7 871.5
720
752
784
816
848
880
Mass (m/z)

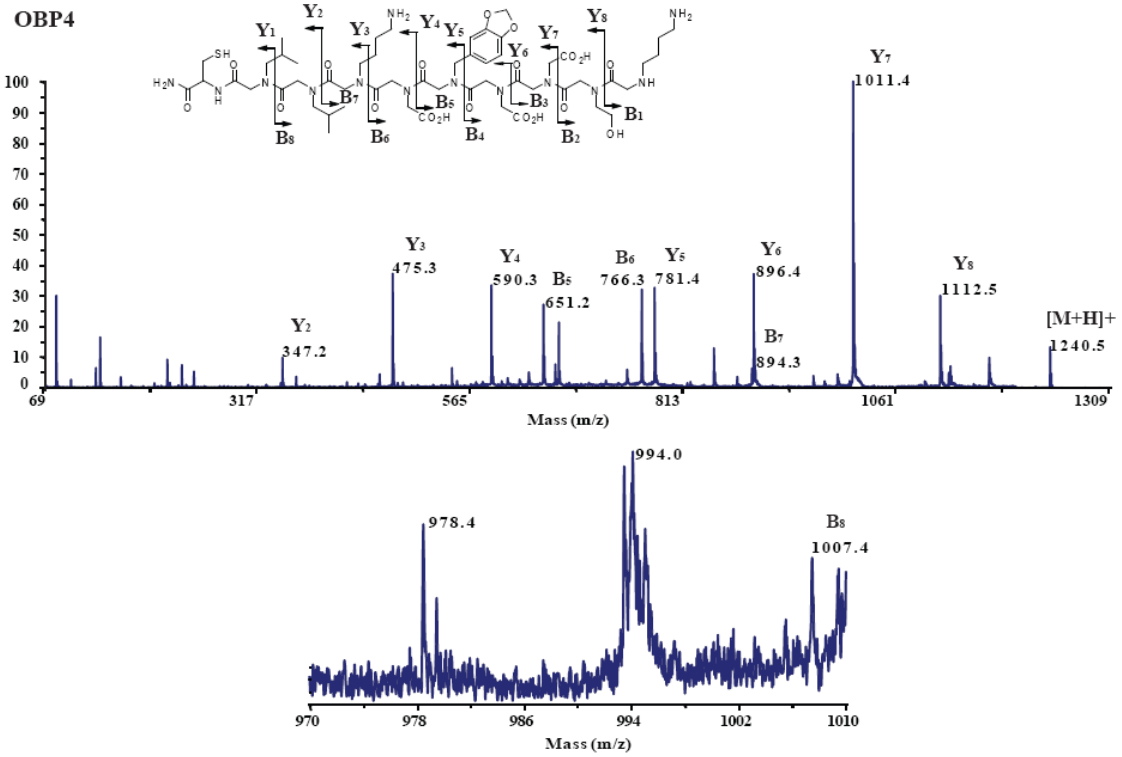
OBP4
Y1
Y2
Y3
Y4
Y5
Y6
Y7
Y8
B1
B2
B3
B4
B5
B6
B7
B8
Y7 1011.4
Y3 475.3
Y4 590.3
B5 651.2
B6 766.3
Y5 781.4
Y6 896.4
Y8 1112.5
Y2 347.2
B7 894.3
[M+H]+ 1240.5
100
90
80
70
60
50
40
30
20
10
0
69
317
565
813
1061
1309
Mass (m/z)
994.0
978.4
B8 1007.4
970
978
986
994
1002
1010
Mass (m/z)

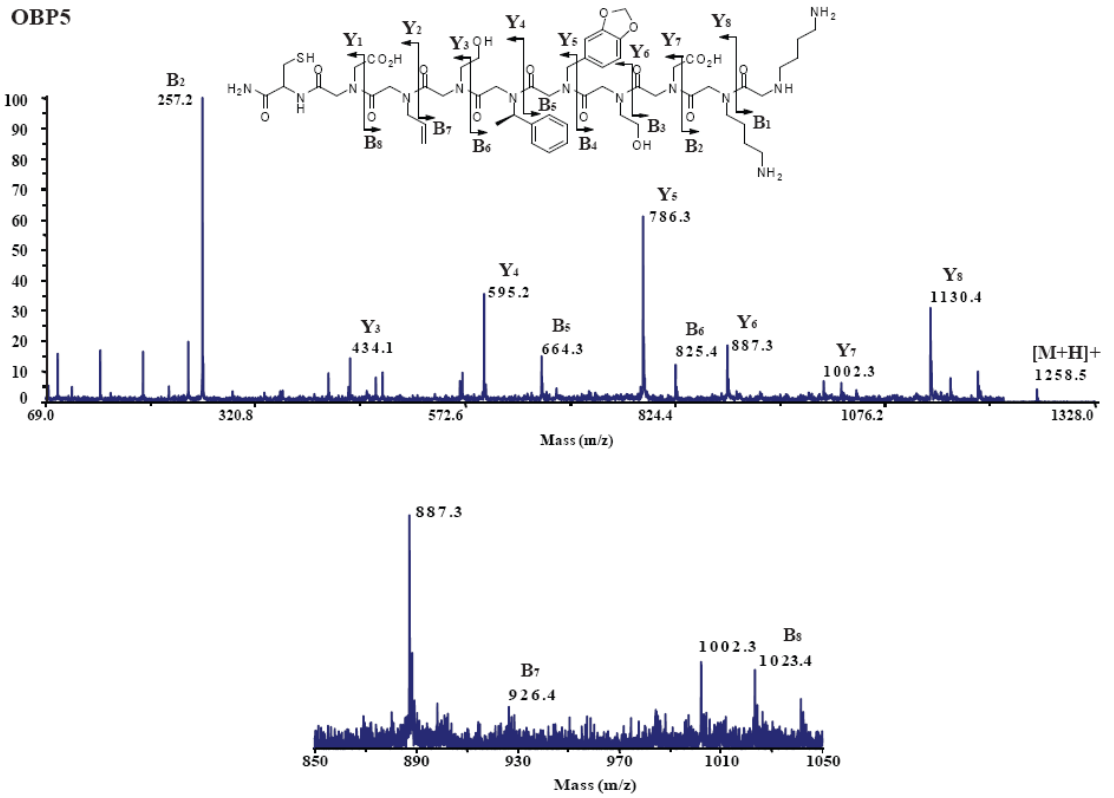
OBP5
B2
257.2
Y5
786.3
Y4
595.2
Y8
1130.4
Y3
434.1
B5
664.3
B6
825.4
Y6
887.3
Y7
1002.3
[M+H]+
1258.5
100
90
80
70
60
50
40
30
20
10
0
69.0
320.8
572.6
824.4
1076.2
1328.0
Mass (m/z)
887.3
B7
926.4
1002.3
B8
1023.4
850
890
930
970
1010
1050
Mass (m/z)

compound	Mass expected ($[M+H]^+$)	Mass found ($[M+H]^+$)
OBP1	1315.7	1315.8
OBP2	1247.7	1247.8
OBP3	1297.6	1297.7
OBP4	1240.5	1240.6
OBP5	1258.5	1258.6
OBP1-1	1258.6	1258.7
OBP1-2	1258.6	1258.7
OBP1-3	1258.6	1258.7
OBP1-4	1258.7	1285.8
OBP1-5	1225.7	1225.7
OBP1-6	1195.7	1195.8
OBP1-7	1285.7	1285.8
OBP1-8	1258.6	1258.7
OBP1-9	1258.6	1258.7
OBPt	370.1	370.2
OBPt-1	460.2	460.2
OBPt-2	474.2	496.4 ($[M+Na]^+$)
OBPt-3	403.1	403.2
OBPt-4	474.2	474.6
OBPt-5	417.2	417.7
OBPt-6	417.2	417.7
CON	336.2	336.3

Table 1. MALDI-TOF/MS data

References for experimental section

1. M. M. Reddy, T. Kodadek, *Proc. Natl. Acad. Sci.* **2005**, *102(36)*, 12672.
2. H. J. Olivos, P. G. Alluri, M. M. Reddy, D. Saloney, T. Kodadek, T. *Org. Lett*. **2002**, *4*, 4057.
3. N. M. Khan, V. Arumugam, S. Balaubramanian, *Tetradedron Lett*. **1996**, *37*, 4819.
4. D. Sikder, T. Kodadek, *Genes Dev*. **2007**, *21(22)*, 2995.
5. P. Alluri, B. Lui, P. Yu, X. Xiao, T. Kodadek, *Mol. Biosyst*. **2006**, *2(11)*, 568.

2.5. References

[1] A. L. Hopkins, C. R. Groom, *Nat Rev Drug Discov* **2002**, *1*, 727.

[2] Y. Fang, J. Lahiri, L. Picard, *Drug Discov Today* **2003**, *8*, 755.

[3] W. Thomsen, J. Frazer, D. Unett, *Curr Opin Biotechnol* **2005**, *16*, 655.

[4] S. Siehler, *Biotechnol J* **2008**, *3*, 471.

[5] O. H. Aina, T. C. Sroka, M. L. Chen, K. S. Lam, *Biopolymers* **2002**, *66*, 184.

[6] O. H. Aina, J. Marik, R. Liu, D. H. Lau, K. S. Lam, *Mol. Cancer Ther.* **2005**, *4*, 806.

[7] D. G. Udugamasooriya, S. P. Dineen, R. A. Brekken, T. Kodadek, *J. Amer. Chem. Soc.* **2008**, *130*, 5744.

[8] G. M. Figliozzi, R. Goldsmith, S. C. Ng, S. C. Banville, R. N. Zuckermann, *Methods Enzymol.* **1996**, *267*, 437.

[9] G. MacBeath, A. N. Koehler, S. L. Schreiber, *J. Amer. Chem. Soc.* **1999**, *121*, 7967.

[10] M. Uttamchandani, D. P. Walsh, S. Q. Yao, Y. T. Chang, *Curr Opin Chem Biol* **2005**, *9*, 4.

[11] M. M. Reddy, T. Kodadek, *Proc Natl Acad Sci U S A* **2005**, *102*, 12672.

[12] R. M. Chemelli, J. T. Willie, C. M. Sinton, J. K. Elmquist, T. Scammell, C. Lee, J. A. Richardson, S. C. Williams, Y. Xiong, Y. Kisanuki, T. E. Fitch, M. Nakazato, R. E. Hammer, C. B. Saper, M. Yanagisawa, *Cell* **1999**, *98*, 437.

[13] L. Lin, J. Faraco, R. Li, H. Kadotani, W. Rogers, X. Lin, X. Qiu, P. J. de Jong, S. Nishino, E. Mignot, *Cell* **1999**, *98*, 365.

[14] T. Sakurai, A. Amemiya, M. Ishii, I. Matsuzaki, R. M. Chemelli, H. Tanaka, S. C. Williams, J. A. Richardson, G. P. Kozlowski, S. Wilson, J. R. Arch, R. E. Buckingham, A. C. Haynes, S. A. Carr, R. S. Annan, D. E. McNulty, W. S. Liu, J. A. Terrett, N. A. Elshourbagy, D. J. Bergsma, M. Yanagisawa, *Cell* **1998**, *92*, 573.

[15] H. Funato, A. L. Tsai, J. T. Willie, Y. Kisanuki, S. C. Williams, T. Sakurai, M. Yanagisawa, *Cell Metab* **2009**, *9*, 64.

[16] J. A. Hollander, Q. Lu, M. D. Cameron, T. M. Kamenecka, P. J. Kenny, *Proc Natl Acad Sci U S A* **2008**, *105*, 19480.

[17] C. Brisbare-Roch, J. Dingemanse, R. Koberstein, P. Hoever, H. Aissaoui, S. Flores, C. Mueller, O. Nayler, J. van Gerven, S. L. de Haas, P. Hess, C. Qiu, S. Buchmann, M. Scherz, T. Weller, W. Fischli, M. Clozel, F. Jenck, *Nat Med* **2007**, *13*, 150.

[18] A. J. Roecker, P. J. Coleman, *Curr Top Med Chem* **2008**, *8*, 977.

[19] J. M. Bergman, A. J. Roecker, S. P. Mercer, R. A. Bednar, D. R. Reiss, R. W. Ransom, C. Meacham Harrell, D. J. Pettibone, W. Lemaire, K. L. Murphy, C. Li, T. Prueksaritanont, C. J. Winrow, J. J. Renger, K. S. Koblan, G. D. Hartman, P. J. Coleman, *Bioorg Med Chem Lett* **2008**, *18*, 1425.

[20] M. Mieda, J. T. Willie, J. Hara, C. M. Sinton, T. Sakurai, M. Yanagisawa, *Proc Natl Acad Sci U S A* **2004**, *101*, 4649.

[21] M. Hungs, E. Mignot, *Bioessays* **2001**, *23*, 397.

[22] T. Holmqvist, L. Johansson, M. Ostman, S. Ammoun, K. E. Akerman, J. P. Kukkonen, *J Biol Chem* **2005**, *280*, 6570.

[23] D. Sikder, T. Kodadek, *Genes Dev* **2007**, *21*, 2995.

[24] B. C. Cunningham, J. A. Wells, *Science* **1989**, *244*, 1081.

[25] S. Ammoun, L. Johansson, M. E. Ekholm, T. Holmqvist, A. S. Danis, L. Korhonen, O. A. Sergeeva, H. L. Haas, K. E. Akerman, J. P. Kukkonen, *Mol Endocrinol* **2006**, *20*, 80.

[26] K. B. Seamon, W. Padgett, J. W. Daly, *Proc Natl Acad Sci U S A* **1981**, *78*, 3363.

Chapter 3: A small molecule allosteric potentiator of orexin receptors

3.1. Introduction

When blood glucose levels in the brain fall, specific neurons in the brain produce orexin, which mediates wakefulness, at least in part through stimulation of energy-producing pathways in target neurons [1, 2, 3]. Most cases of human narcolepsy are caused by the loss of most orexin-producing neurons [4, 5], possibly due to an autoimmune response against these neurons in afflicted individuals. It has been shown that the symptoms of narcolepsy can be attenuated by injection of orexin peptide into the brains of orexin-deficient mice, suggesting that an orexin receptor agonist might be effective for the treatment of narcolepsy [6]. Orexin also has peripheral effects and recent studies have suggested that stimulation of orexin receptor function would have beneficial effects in the treatment of obesity and diabetes [7, 8]. In particular, overexpression of orexin or prolonged central administration with a peptidic orexin receptor agonist conferred resistance to obesity and insulin insensitivity to rodents fed a high fat diet [8]. However, while the biology of the orexin system makes clear that small molecules that stimulate receptor function would be useful pharmacological tools, none have been reported to date.

Two basic types of orexin receptor-stimulating molecules would be desirable, agonists or potentiators. Unlike agonists, allosteric potentiators bind to a site on the receptor distinct from that of the native ligand and accentuate the response of the receptor to that ligand, but cannot stimulate receptor function independently [9-14]. It has been suggested that allosteric potentiators might have advantages over classical orthosteric agonists from the therapeutic point of view. For example, allosteric potentiators would not drive chronic receptor activation, but rather accentuate natural cycles of activation of the receptor [15, 16]. In the case of the orexin receptors, one can imagine that potentiators might be particularly

interesting in the treatment of obesity and diabetes and might also have efficacy in narcolepsy if neuronal levels of orexin are merely low, but not zero. Here, we describe a first small-molecule allosteric potentiator of orexin receptor.

3.2. Results

In Chapter 2, we described the discovery of a novel OXR1/OXR2 antagonist (OBPt-1; Figure 12A). Several derivatives of OBPt-1 were made and tested as part of an effort to identify more potent antagonists. In the course of these studies, we fortuitously identified three compounds (Figure 22A) that did not antagonize the response of OXR1 to orexin A, but rather appeared to slightly enhance OXR1-mediated signaling as monitored in a cell culture assay using OXR1-expressing cells that also carried an orexin-responsive luciferase reporter gene. This was somewhat surprising, given the very modest structural alterations in OBPt-7-9 relative to OBPt-1. These original experiments employed concentrations of the orexin A peptide near the EC_{100}. Therefore, to determine if these compounds are indeed OXR1 potentiators, we carried out experiments at 16 nM orexin A, which drives OXR1-mediated reporter gene expression in this assay at only about 20% of the maximum possible level (i.e., $EC_{20} \approx 16$ nM). As shown in Figure 22B, all of the compounds stimulated OXR1 activity. The most potent compound, OBPt-9, was chosen for further characterization. As shown in Figure 22C, the maximal potentiation at this concentration of orexin A was about 2.5-fold, with an EC_{50} value for potentiation of approximately 120 nM. Note that a control peptoid (CON) did not show any activity. Importantly, OBPt-9 alone caused no activation of OXR1 (Figure 25), indicating that the compound did not act as an agonist, but as an allosteric potentiator.

We next determined the effect of OBPt-9 on the potency and efficacy of orexin A. Cells ware pre-incubated with OBPt-9 or DMSO (vehicle) and subsequently stimulated with increasing concentrations of orexin A. As shown in Figure 23, OBPt-9 induced a leftward and upward shift of the orexin A concentration- responsive curve. The EC_{50} value for orexin A in the presence of vehicle was 41.1 nM, whereas, the EC_{50} values were 27.6, 12.5 nM in the presence of 0.1 μM and 5 μM of OBPt-9, respectively, meaning that the potency of orexin A

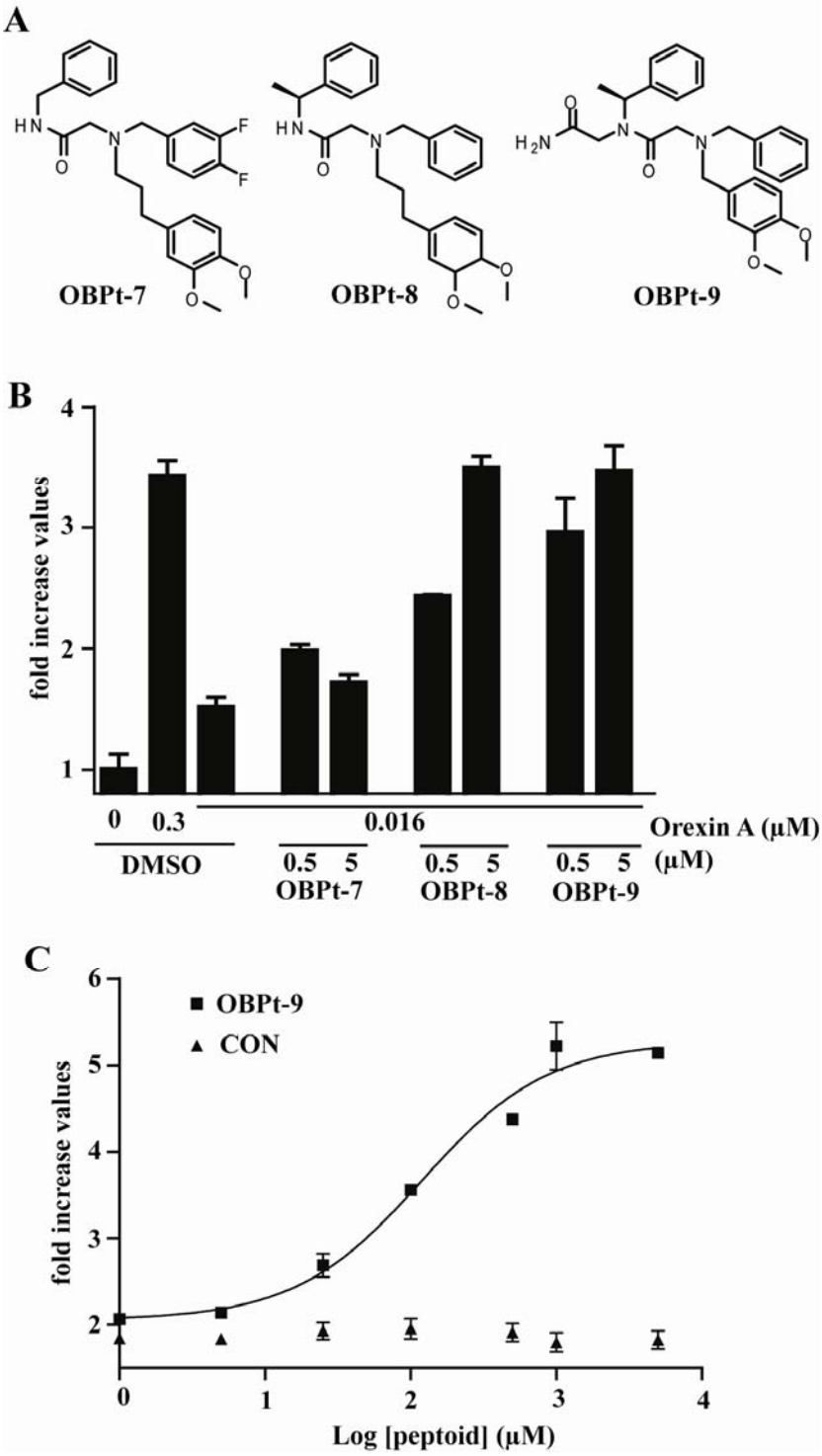

Figure 22. (A) Chemical structures of tested compounds (OBPt-7, OBPt-8, and OBPt-9). (B) Effects of the compounds on the response (cAMP elevation) of OX1R expressing cell to EC_{20} concentration of orexin A. Level of cAMP elevation by 0.3 μM orexin A (EC_{100} concentration) was also shown for comparison. (C) Concentration-responsive curves of OBPt-9 and CON (control peptoid) were performed in the presence of EC_{20} concentration of orexin A.

increases in the presence of OBPt-9. We also observed an increase in the efficacy of orexin A. The maximal response to orexin A was about 2-fold higher in the presence of OBPt-9 (5 μM) than with vehicle alone.

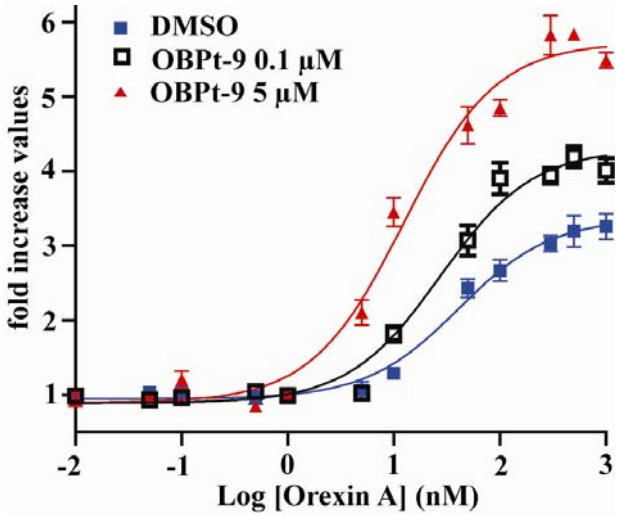

Figure 23. Concentration-response curves of orexin A on cAMP elevation of OXR1 expressing cells in the presence or absence of OBPt-9.

Finally, we examined if OBPt-9 can also potentiate the response of OXR2 to orexin A. Since OXR2, not OXR1, is thought to play the central role in metabolic syndromes[37], this is an important issue pharmacologically. After transient expression of OXR2, HEK293 cells also carrying a receptor-driven reporter gene were treated with OBPt-9 and then with increasing concentrations of orexin A. As depicted in Figure 24, OBPt-9 showed a similar potentiation pattern as was observed with the OXR1-containing cells. The Orexin A EC_{50} was 60 nM in the presence of vehicle and 22 nM in the presence of OBPt-9. Moreover, the maximum level of reporter gene activation in the presence of OBPt-9 was almost twice that observed in the presence of vehicle.

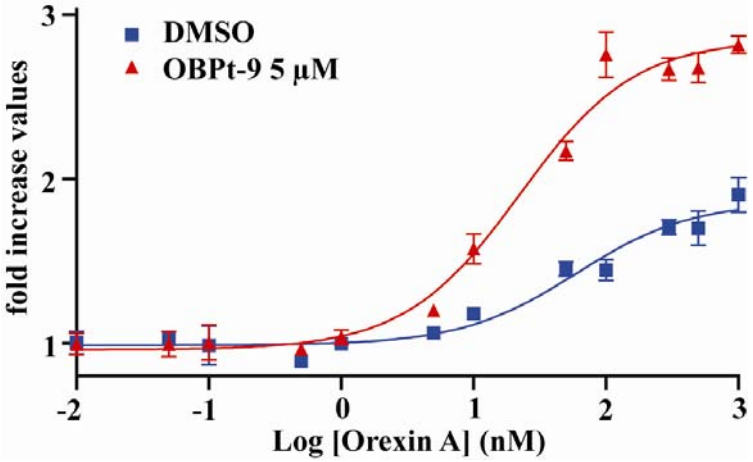

Figure 24. Concentration-response curves of orexin A on cAMP elevation of OXR2 expressing cells in the presence or absence of OBPt-9.

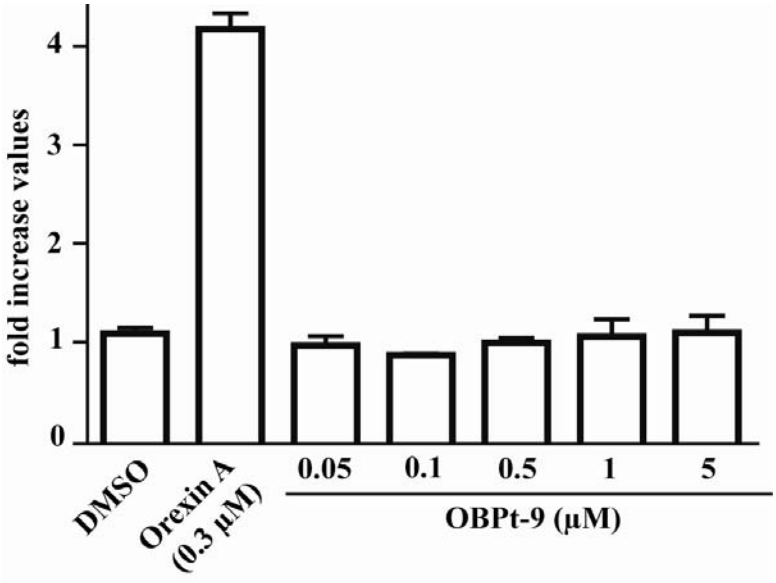

Figure 25. Effect of OBPt-9 in the absence of orexin A on cAMP level of OXR1 expressing cells. HEK293/hOX1R cells were transfected with pGL3-3xCRE-TATA and pRLuc for 24 hr. After starvation for 4 hr, DMSO, Orexin A, or increasing concentrations of OBPt-9 were added to cells. After 6 hr, cAMP elevation of cells was monitored by measuring luciferase activity of lysates.

3.3. Discussion

In conclusion, we have discovered, to the best of our knowledge, the first small-molecule allosteric potentiator of the orexin receptor. OBPt-9, which has a mass of less than 500 Daltons, may prove to be a useful pharmacological tool for probing orexin biology in vivo and perhaps may serve as a lead compound for drug development. Such studies are underway.

.

3.4. Experimental section

General remarks

All chemicals and solvents were purchased from commercial suppliers and used without further purification. Mass spectra were obtained with a Voyager-DE^{TM} PRO (Applied Biosystems) for MALDI-TOF with α-cyano-4-hydroxycinnamic acid matrix. MS/MS spectra were obtained on a 4700 Proteomics Analyser (Applied Biosystems).

Peptoid synthesis

OBPt-7 and OBPt-8: TentaGel Macrobeads NH_2 resin (RAPP Polymere) was reacted with 4-(bromomethyl)-3-nitrobenzoic acid (5 eq) in the presence of DIC (5 eq) and HOBt (5 eq) in DMF (3 mL) for 3 hr. After washing with DMF (3 mL x 10), the resin was reacted with benzylamine (for OBPt-7) or (R)-α-methylbenzylamine (for OBPt-8) in DMF (2 M) for 3 hr. The resin was washed with DMF (3 mL x 10) and then reacted with DIC (2 M) and bromoacetic acid (2 M) for 3 hr. After washing with DMF (3 mL x 10), the resin was reacted with 3,4-dimethoxyphenylpropylamine (for OBPt-7 and OBPt-8) in DMF (2M) for 3 hr to afford secondary amine. The resin was washed with DMF (3 mL x 10) and then reacted with 3,4-difluorobenzaldehyde (for OBPt-7) or benzaldehyde (for OBPt-8) (10 eq) and BAP (10 eq) in THF / DMF(v/v = 3:1, 2 mL) for reductive alkylation.[1] After washing with DMF (3 mL x 10) and MeOH (3 mL x 5), peptoids were cleaved from the resin by exposing to UV (365 nm, 6W) for 12 hr in 2% v/v TFA/MeOH and the crude cleavage product was purified by preparative RP-HPLC. **OBPt-7:** MALDI/TOF: $[M+H]^+$ calculated: 469.2, observed 469.5. **OBPt-8:** MALDI/TOF: $[M+H]^+$ calculated: 447.2, observed 447.6.

OBPt-9 and CON: Chemical structure of a control peptoid, CON is shown below. These

peptoids were synthesized by on Rink Amide AM resin (NovaBiochem) using the sub-monomer approach by a microwave-assisted protocol.[2] Briefly, bromoacetic acid was coupled to resin and then (R)-α-methylbenzylamine (for OBPt-9) or isobutylamine (for CON) was added for alkylation reaction. After coupling of second bromoacetic acid, 3,4-dimethoxybenzylbromide (for OBPt-9) or 2-metoxyethylamine (for CON) was added for second alkylation reaction. The secondary amine was then reacted with benzaldehyde (10 eq) and BAP (10 eq) for reductive alkylation. After washing, Peptoids were cleaved from resins with cleavage cocktail (95% TFA, 2.5% water, 2.5 % TIS) and purified by preparative RP-HPLC. **OBPt-9:** MALDI/TOF: $[M+H]^+$ calculated 476.2, observed 476.5. **CON:** MALDI/TOF: $[M+H]^+$ calculated 336.2, observed 336.5.

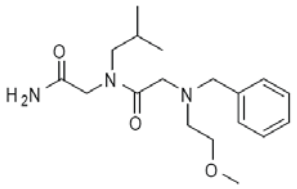

Cell culture

HEK293 cells were maintained in DMEM (Dulbecco's modified Eagle's medium, Invitrogen) supplemented with 110 mg/L sodium pyruvate, 2mM L-glutamine and 10% (v/v) fetal calf serum at 37˚C in a 5% CO_2 environment. For HEK293/hOX1R cells,[3] G418 (500μg/mL, Gibco) was included in the medium.

cAMP production assay

HEK293/hOX1R Cells were grown to ~60% confluency in 48-well plates and transfected with the luciferase reporter plasmid, pGL3-3xCRE-TATA (100 ng/well) [4] together with plasmid encoding constitutively active Renilla luciferase (pRLuc, 2 ng/well). 24 hr after

transfection, the cells were serum-starved for 4hr and treated with vehicle (DMSO) or compounds for 20 min. Orexin A (for potentiator test) or ddH_2O (for agonist test) were added as indicated conditions. After 6 hours, luciferase activity of the cell lysate was measured using the dual-luciferase assay kit (Promga) following the manufacture's protocol and normalized to Renilla luciferase activity. Fold increase values of the normalized luciferase activities were presented in data. When examining the effect of OBPt-9 on OX2R expressing cells, HEK293 cells were transfected with phOX2R (OriGene Technology Inc., 50 ng/well), pGL3-3xCRE-TATA (50 ng/well), and pRLuc (1 ng/well) for 24 hr before starvation.

References for experimental section

1 N. M. Khan, V. Arumugam, S. Balaubramanian, *Tetradedron Lett*. **1996**, *37*, 4819.

2 H. J. Olivos, P. G. Alluri, M. M. Reddy, D. Saloney, T. Kodadek, T. *Org. Lett*. **2002**, *4*, 4057.

3 D. Sikder, T. Kodadek, *Genes Dev*. **2007**, *21(22)*, 2995.

4 P. Alluri, B. Lui, P. Yu, X. Xiao, T. Kodadek, *Mol. Biosyst*. **2006**, *2(11)*, 568.

3.5. References

[1] T. Sakurai, *Curr Opin Clin Nutr Metab Care* **2003**, *6*, 353.

[2] J. T. Willie, R. M. Chemelli, C. M. Sinton, M. Yanagisawa, *Annu Rev Neurosci* **2001**, *24*, 429.

[3] T. E. Scammell, *Curr Biol* **2001**, *11*, R769.

[4] J. M. Siegel, *Cell* **1999**, *98*, 409.

[5] R. M. Chemelli, J. T. Willie, C. M. Sinton, J. K. Elmquist, T. Scammell, C. Lee, J. A. Richardson, S. C. Williams, Y. Xiong, Y. Kisanuki, T. E. Fitch, M. Nakazato, R. E. Hammer, C. B. Saper, M. Yanagisawa, *Cell* **1999**, *98*, 437.

[6] A. J. Roecker, P. J. Coleman, *Curr Top Med Chem* **2008**, *8*, 977.

[7] D. Sikder, T. Kodadek, *Genes Dev* **2007**, *21*, 2995.

[8] H. Funato, A. L. Tsai, J. T. Willie, Y. Kisanuki, S. C. Williams, T. Sakurai, M. Yanagisawa, *Cell Metab* **2009**, *9*, 64.

[9] S. Rees, D. Morrow, T. Kenakin, *Receptors Channels* **2002**, *8*, 261.

[10] L. T. May, A. Christopoulos, *Curr Opin Pharmacol* **2003**, *3*, 551.

[11] C. W. Lindsley, D. D. Wisnoski, W. H. Leister, A. O'Brien J, W. Lemaire, D. L. Williams, Jr., M. Burno, C. Sur, G. G. Kinney, D. J. Pettibone, P. R. Tiller, S. Smith, M. E. Duggan, G. D. Hartman, P. J. Conn, J. R. Huff, *J Med Chem* **2004**, *47*, 5825.

[12] J. A. O'Brien, W. Lemaire, T. B. Chen, R. S. Chang, M. A. Jacobson, S. N. Ha, C. W. Lindsley, H. J. Schaffhauser, C. Sur, D. J. Pettibone, P. J. Conn, D. L. Williams, Jr., *Mol Pharmacol* **2003**, *64*, 731.

[13] Z. G. Gao, K. Ye, A. Goblyos, A. P. Ijzerman, K. A. Jacobson, *BMC Pharmacol* **2008**, *8*, 20.

[14] J. K. Shirey, Z. Xiang, D. Orton, A. E. Brady, K. A. Johnson, R. Williams, J. E. Ayala,

A. L. Rodriguez, J. Wess, D. Weaver, C. M. Niswender, P. J. Conn, *Nat Chem Biol* **2008**, *4*, 42.

[15] T. W. Schwartz, B. Holst, *Trends Pharmacol Sci* **2007**, *28*, 366.

[16] P. J. Conn, A. Christopoulos, C. W. Lindsley, *Nat Rev Drug Discov* **2009**, *8*, 41.

Part II

Targeted inactivation of proteins triggered by visible light

Chapter 1: Introduction

1.1. Identification of protein function via 'loss of function' approaches

Identification of protein function inside living cells is important for target validation and drug discovery [1, 2]. Three are two different ways to do this. First, in 'gain of function' approach, genes of interest are overexpressed inside cells and phynotypical changes attributed to the overexpression are monitored. However, overexpression may not be capable of revealing some cellular functions for proteins due to toxicity or compensation. Alternatively, in 'loss of function' approaches, genes of interest or genes products (target proteins) will be knocked-out or knocked-down and phynotypical changes will be monitored (Figure 26).

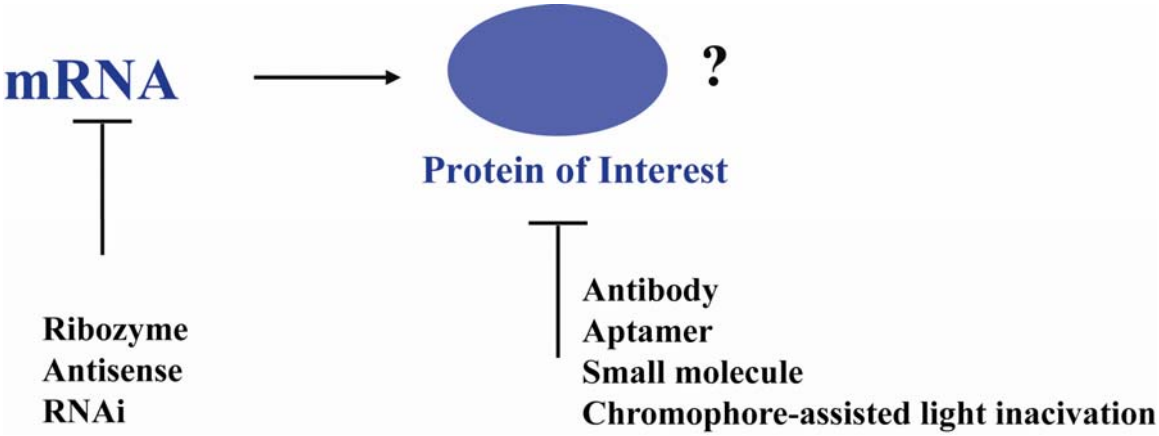

Figure 26. Identification of protein functions via 'loss of function' approaches

1.1.1. Genetic methods targeting mRNA

Gene knockouts

Gene knockouts are attractive tools for identification of protein functions because they involve whole animals and allow us to observe the behavior of the knockout animal and to elucidate the functional role of the gene product [3-5]. However, a major disadvantage of gene knockout is that they are labor-intensive and time-consuming. Other disadvantages that can complicate the interpretation of the phenotype resulted from gene knockouts are that gene products often have embryonic effects, which mask their actions in fully developed animals. Often, genetic knockouts fail to produce any effect at all. This is often caused by developmental compensation when a closely related protein is thought to take over the function of the deleted protein during development.

Antisense

Antisense agents are RNA-like chemically modified oligonucleotides, which are engineered for stability and are designed to bind to a target mRNA molecule through complementary base-pair hybridization. Binding of the antisense agent to the target mRNA prevents it from being translated and, therefore, blocks synthesis of the encoded protein. In some cases, cleavage of the bound mRNA occurs, catalyzed by a ribonuclease that is specific for double-stranded RNA (dsRNA). Unlike the gene knockout approach, which is irreversible, the continuous presence of the antisense agent is required for

inhibition of target gene expression [6-8]. The use of antisense agents in an *in vivo* can be problematic. For example, delivery of these large oligonucleotides can be difficult.

Ribozymes

Ribozymes are RNA molecules that can act as enzymes. They are designed to recognize, bind to and cleave a specific mRNA through complementary base-pair hybridization, thus preventing translation of the mRNA. The big challenges with ribozymes are specificity and delivery.

RNAi

dsRNA is introduced into the cell and is digested into short interfering RNAs (siRNAs) of ~20 nucleotides in length. These siRNAs are replicated by an RNA-dependent RNA polymerase (initiation step), and the siRNA duplexes then bind to a nuclease complex that forms an RNA-induced silencing complex (RISC). In the effector step, this complex binds to complementary mRNA by base-pairing interactions, and the mRNA is cleaved. RNA interference (RNAi) is broadly useful, but recent concerns have been raised about the specificity of RNAi. In addition, RNAi depends on the gradual degradation of the target protein, and can thus take hours or days to deplete the target protein from cells. Despite these challenges, RNAi remains one of the most favorite methods for identification of protein functions [9-11].

Limitations of genetic methods

Genetic methods including gene knock-out and knock-down, while powerful methods to understand gene function, are not able to discriminate between post-translationally modified proteins. Knockout or knockdown of a gene eliminates all post-translationally modified protein forms, which may complicate the analysis of the protein's function in its differently post-translationally modified states. Alternatively, loss of an essential gene might stimulate a compensation mechanism that could replace the missing gene product with a functional homolog. In addition, removal of a single gene can cause the roles of other proteins to be changed, which makes it difficult to evaluaate the missing protein as a drug target. In addition, these methods lack spatial control of the inactivation of the target protein. Subcellular actions of proteins remain an important topic of investigation. Thus, methods to inactivate proteins in a spatially controlled manner are an important goal.

1.1.2. Non-genetic methods targeting proteins directly.

Function-blocking antibody

Function-blocking antibodies are an alternative to genetic methods used to inactivate protein function in situ, but specific reagents are not available for much of the proteome. Typically less than one percent of binding antibodies that are raised against a specific protein can effectively block its function. Additionally, the big challenge with antibodies is delivery.

Aptamer

Initially, Tuerk and Gold established the in vitro screening process termed "systematic evolution of ligand by exponential enrichment" (SELEX), to identify the RNA ligands with affinity for T4 DNA polymerase[12]. Such nucleic acids were termed "aptamers". Aptamers are functional nucleic acids that bind cellular proteins or protein domains [6, 7, 13]. They can be generated against a wide variety of target proteins, and preferentially bind to sites of biological activity of target proteins. In addition, the chemical stability of aptamers can be enhanced by adding substituent to the 2′ position of the ribose sugar.

Small molecules

The classical protein inactivation tool is the small, bioactive molecule that inactivates target proteins directly or indirectly. Using small molecules remains the most powerful validation strategy. Recently, systematic application of this tool has been defined as 'chemical genomics' which aims to discover a small molecule regulator for every protein encoded by the genome. These molecules can be used as probes of cellular function and possible drug leads. The success of this technology is dependent on the quality of the chemical library and the ability to identify the affected target protein(s).

Chromophore-assisted light inactivation

Chromophore-assisted light inactivation (CALI) is a technique to inactivate proteins with high spatial and temporal resolution. This technology uses an antibody to deliver a suitable chromophore specifically to the protein of interest (Figure 27) [14, 15]. Irradiation

induces generation of reactive oxygen species (ROS, mainly singlet oxygen). Since these species have very short lifetimes, the antibody-targeted proteins are specifically inactivated. Because inactivation is mediated by light, CALI can be controlled spatially and temporally. Most CALI experiments are achieved by the laser excitation of malachite green-conjugated antibodies that are targeted to a protein of interest. More recently, it has been found that fluorescein can be used as a CALI reagent (this form of CALI is termed FALI) [1]. Although CALI is a powerful technique, its practical use has been limited by the complexity of the procedures, such as delivery of labeled antibody using invasive methods (such as microinjection) and accessibility of non-functional blocking antibodies. Genetically targeted CALI is developed as an alternative method, in which the target protein is tagged with a tetracysteine tag that is recognized by a cell-permeable biarsenical chromophore (FlAsH)[16]. However, this method also causes nonspecific damage, due to the nonspecific binding of the biarsenical chromophore to cysteine-rich proteins. EGFPs have also been used as chromophores to inactivate EGFP-fused target proteins[17]. However, EGFP are usually considered as non-efficient ROS photosensitizer.

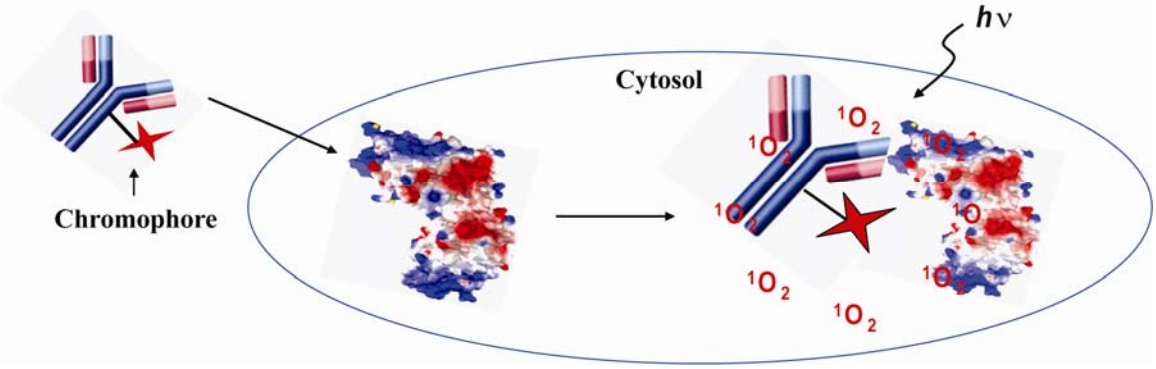

Figure 27. Illustration of chromophore-assisted light inactivation (CALI)

Limitation of CALI

Although CALI has been proved a very powerful method of target protein inactivation, it has limitations. First, organic chromophore or photosensitizer commonly used for CALI experiment can be photobleached. The chromophore itself reacts with singlet oxygen, is oxidatively modified, and loses its ability to absorb light and generate singlet oxygen. Other limitations are primarily attributable to the use of antibody for the protein-targeting reagent. It is difficult to label antibodies with chromophores at specific amino acid residues, so that the extent of the damage done on the target protein cannot easily be controlled. Also, since antibody is a macromolecule, attached chromophore may be placed far away from target protein to cause less efficiency in CALI. Moreover, since antibody itself is not cell-permeable, it is necessary to use an invasive method such as microinjection to introduce antibodies into cells, which may jeopardize the physiological functions and long-term viability of the cells. Therefore, these problems have to be solved before CALI can become a practical method of target protein inactivation.

1.2. Singlet oxygen-mediated protein inactivation

1.2.1. Singlet oxygen chemistry

The most abundant and stable form of oxygen that we are breathing in is triplet oxygen. On the other hand, singlet oxygen is an electronically excited form of molecular oxygen[18, 19]. Differences in the chemical properties of triplet and singlet oxygen are best illustrated by their molecular orbitals (Figure 28). The total spin quantum number (S) of triplet oxygen is 1. Triplet state oxygen has a spin multiplicity of 3 and is paramagnetic with diradical properties. Triplet

oxygen reacts readily with other radical compounds in nature. However, most compounds in nature are not radical and are in the singlet state. The molecular orbital of singlet oxygen differs from that of triplet oxygen whose electrons in the π antibonding orbital (π*) are paired, as shown in Figure 29. The energy of singlet oxygen is 22.5 kcal above the ground state of triplet oxygen and exists long enough to react with other singlet state molecules. Singlet oxygen, which is not a radical, reacts with nonradical, singlet state, and electron-rich compounds containing double bonds. It can react with all major classes of biomolecules, leading to protein oxidation, lipid peroxidation and DNA damage.

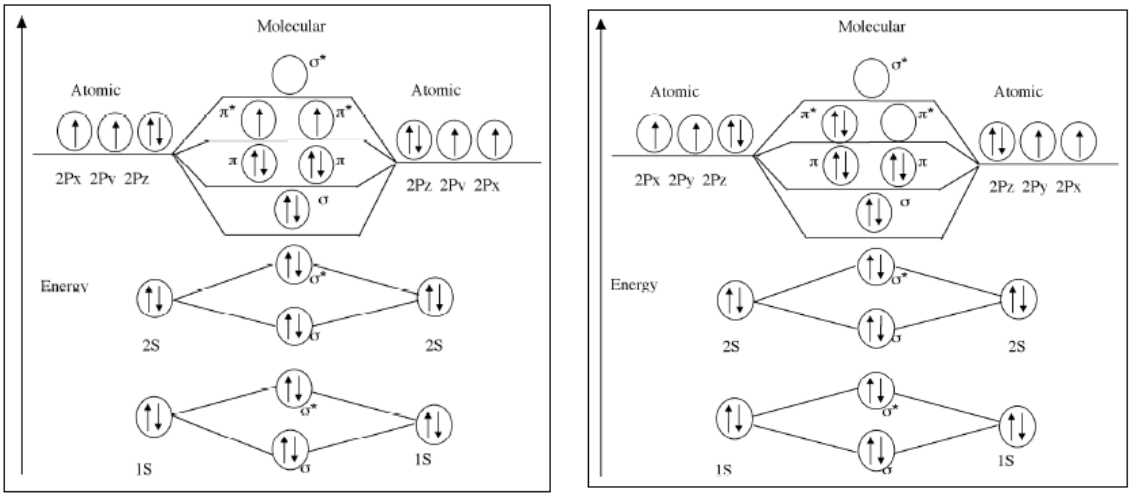

Figure 28. Molecular orbitals of Triplet (left) and Singlet oxygen (right)

1.2.2. Singlet oxygen generation

Singlet oxygen can be generated photochemically as shown in Figure 29. Photosensitizers such as chlorophyll, pheophytins, porphyrins, riboflavin, myoglobin, and synthetic chromophores can absorb energy from light and transfer it to triplet oxygen to form singlet oxygen. The photosensitizer absorbs light and becomes an unstable, excited, singlet state molecule (1Sen*). The excited singlet photosensitizer loses its energy by internal conversion, emission of light, or intersystem crossing (ISC) as shown in Figure 29.

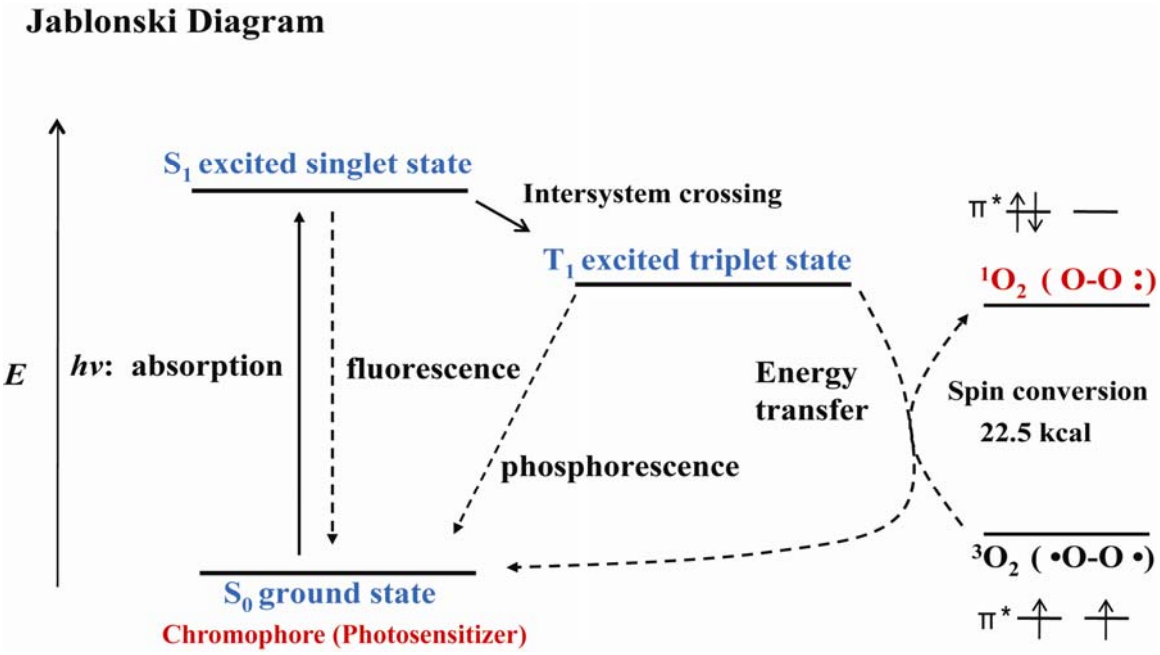

Figure 29. Photochemical generation of singlet oxygen. A photosensitizer in its singlet, ground state is elevated into an excited singlet state by the absorption of light of appropriate wavelength.

Emission of fluorescence converts the excited singlet sensitizer to ground-state singlet sensitizer. The excited sensitizer may also undergo an intersystem crossing (ISC) from the excited singlet-state molecule to an excited triplet-state molecule (3Sen*). The emission of phosphorescence converts the excited triplet sensitizer to ground-state singlet sensitizer. If the lifetime of the 3Sen* is greater than 1Sen*, the 3Sen* reacts with $^3O_2$ to form $^1O_2$ through triplet-triplet annihilation mechanism. The sensitizer returns to ground state (1Sen) and may repeat the cycle again to generate singlet oxygen. Usually, sensitizers may generate 103 to 105 molecules of singlet oxygen before becoming inactive. However continued generation of singlet oxygen is possible if the photosensitizer is photo-stable and thus can not be oxidatively damaged by singlet oxygen.

1.2.3. Singlet oxygen-mediated oxidative modification of proteins

Due to electrophilicity of singlet oxygen, it reacts primarily with amino acids that contain electron-rich side chains such as tryptophan, histidine, tyrosine, methionine, and cystein to form (endo)peroxide intermediates. The intermediates will be thermally fragmented to afford modified derivatives (see Figure 30 for histidine modification). Tryptophan, histidine, and tyrosine contain double bonds and can easily react with singlet oxygen. Methionine and cystein contain a sulfur atom with 4 nonbonding electrons, which react rapidly with singlet oxygen. As amino acids become oxidative modified by singlet oxygen, the protein or enzyme looses activity.

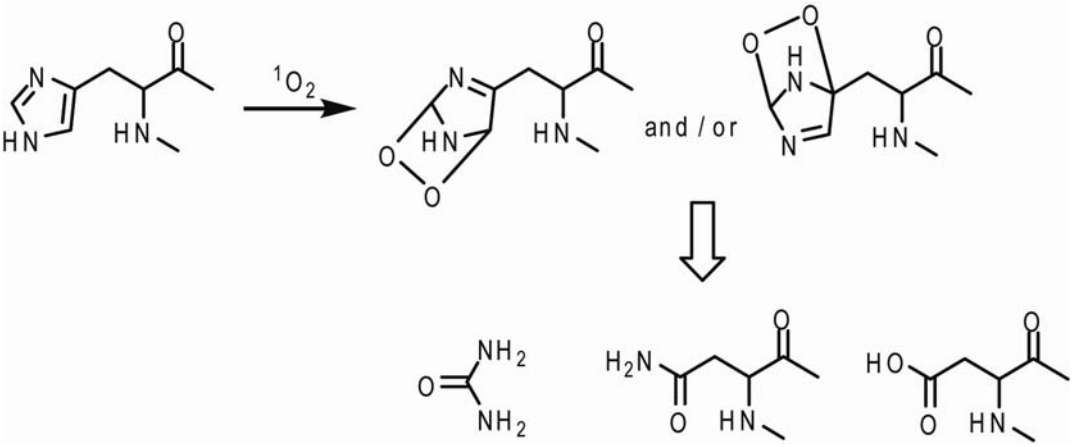

Figure 30. Singlet oxygen-mediated oxidative modification of histidine

1.3. References

[1] S. Beck, T. Sakurai, B. K. Eustace, G. Beste, R. Schier, F. Rudert, D. G. Jay, *Proteomics* **2002**, *2*, 247.

[2] M. Sioud, *Methods Mol Biol* **2007**, *360*, 1.

[3] H. Mashimo, R. K. Goyal, *Am J Physiol* **1999**, *277*, G745.

[4] M. Blank, M. Blind, *Curr Opin Chem Biol* **2005**, *9*, 336.

[5] A. Bartke, *Exp Gerontol* **2006**, *41*, 1217.

[6] D. R. Corey, *Nat Chem Biol* **2007**, *3*, 8.

[7] E. R. Rayburn, R. Zhang, *Drug Discov Today* **2008**, *13*, 513.

[8] C. Leonetti, G. Zupi, *Curr Pharm Des* **2007**, *13*, 463.

[9] A. Kourtidis, C. Eifert, D. S. Conklin, *Ernst Schering Res Found Workshop* **2007**, 1.

[10] D. Kim, J. Rossi, *Biotechniques* **2008**, *44*, 613.

[11] R. Sacher, L. Stergiou, L. Pelkmans, *Curr Opin Cell Biol* **2008**, *20*, 483.

[12] L. Gold, B. Singer, Y. Y. He, E. Brody, *Curr Opin Genet Dev* **1997**, *7*, 848.

[13] C. Borghouts, C. Kunz, B. Groner, *Comb Chem High Throughput Screen* **2008**, *11*, 135.

[14] J. C. Liao, J. Roider, D. G. Jay, *Proc Natl Acad Sci U S A* **1994**, *91*, 2659.

[15] K. Jacobson, Z. Rajfur, E. Vitriol, K. Hahn, *Trends Cell Biol* **2008**, *18*, 443.

[16] O. Tour, R. M. Meijer, D. A. Zacharias, S. R. Adams, R. Y. Tsien, *Nat Biotechnol* **2003**, *21*, 1505.

[17] M. A. McLean, Z. Rajfur, Z. Chen, D. Humphrey, B. Yang, S. G. Sligar, K. Jacobson, *Anal Chem* **2009**.

[18] M. J. Davies, *Biochem Biophys Res Commun* **2003**, *305*, 761.

[19] A. Wright, W. A. Bubb, C. L. Hawkins, M. J. Davies, *Photochem Photobiol* **2002**, *76*, 35.

Chapter 2: A general system for evaluating the efficiency of chromophore-assisted light inactivation (CALI) of proteins reveals Ru(II) tris-bipyridyl as an unusually efficient "warhead"

2.1. Introduction

There is great interest in the development of techniques for the selective inactivation of protein function as a tool for the study of biological systems. By far the most general and powerful method to do so in mammalian cells is RNA interference (RNAi) technology, which results in the destruction of the message that encodes the protein of interest.[1, 2] Another general and powerful approach is the construction of transgenic animals lacking the gene that encodes the protein of interest. However, all such genetic methods have significant limitations, one of which is that they do not allow for the possibility of carrying out time-resolved studies of the effects of protein knockouts.[3] Thus, there has been a great deal of interest in chemical approaches to protein inactivation.

Of the many strategies that have been explored, chromophore-assisted light inactivation (CALI) holds the promise of being a particularly useful tool.[4-7] In this technique, a chromophore capable of generating singlet oxygen when irradiated is somehow delivered to the target protein. Singlet oxygen is an extraordinarily reactive and short-lived molecule and thus will rapidly inactivate only proteins in the immediate vicinity of its point of origin. Thus, this technique provides high spatial and temporal control over protein inactivation.

Unfortunately, the practical utility of this technology is currently limited. There are two major barriers. The first is the paucity of high-affinity, high-specificity ligands for the protein of interest. In most cases, chromophore-conjugated antibodies are employed, but these molecules are cell-impermeable and the use of a macromolecular targeting agent may place the chromophore some distance away from the target protein when bound. Cell permeable small molecules hold great promise as targeting agents and will probably dominate this area in the future. However, while the selection of cell permeable protein-binding small molecules from combinatorial libraries is advancing rapidly, it remains challenging to obtain ligands with affinities in the low nM region, which would be ideal for this application. For this reason, various strategies have been reported by which engineered proteins can be inactivated by CALI.[8-10] One of the most effective of these is to tag the target protein with the sequence CCXXCC (where X can be several amino acids), which is a high affinity and relatively specific receptor for biarsenical fluorescein derivatives.[8, 9] Of course, this approach is most useful in cases where the native analogue of the tagged protein has also somehow been eliminated.

The second limitation of this technology is the efficiency of singlet oxygen generation exhibited by the chromophores used routinely in CALI. The most common "warheads" employed in CALI experiments are organic fluorophores with relatively long-lived triplet states.[4-7] While some cases of efficient protein inactivation using organic fluorophore-containing constructs have been reported, there remains a need for better singlet oxygen generators since these molecules are sensitive to self-bleaching.

Recently, we have become interested in developing a comprehensive approach for CALI of native proteins. In previous reports, we have demonstrated that protein-binding peptoids (oligo-N-alkylglycines) can be consistently and rapidly isolated from combinatorial libraries.[11-14] The screening conditions that we have developed routinely provide peptoids that bind their target with good specificity and equilibrium dissociation constants in the low μM range. Furthermore, these peptoids are generally cell permeable[15, 16] and thus peptoid libraries provide a promising source of specific binding agents required for CALI of native proteins (again however, the challenge of maturing these ligands to nM binders remains). At the same time, we have begun to turn our attention to the development of more efficient "warheads" for use in CALI reagents that overcome the current limitations of organic fluorophores. In this paper, we report our initial efforts towards this goal. First, we designed a convenient system that allows the efficiency of protein inactivation of any chromophore to be compared to any other (Figure 31). As is discussed below, this system allows CALI warheads to be evaluated both in crude extracts as well as in living cells. Using this system, we compared the efficacy of a Ru(II) tris(bipyridyl) dication ($Ru(bpy)_3^{2+}$) derivative with fluorescein, one of the most efficient and commonly used organic chromophores. A wealth of literature is available showing that $Ru(bpy)_3^{2+}$ is an efficient photocatalyst for singlet oxygen generation and thus might be an excellent CALI warhead.[17-22] We demonstrate that the ruthenium complex is indeed a more efficient CALI warhead than fluorescein and is capable of supporting essentially quantitative inactivation of the target protein. $Ru(bpy)_3^{2+}$ derivatives can be attached easily to synthetic protein-binding molecules and thus are likely to be of considerable utility in the next generation of CALI reagents.

2.2. Results

Covalent attachment of small molecules to the target protein in complex biological mixtures

In order to facilitate the comparison of different chromophores for their efficiency in singlet oxygen generation and subsequent protein inactivation, we sought to develop a system that would eliminate the need for complex biological antibody-based or synthetic targeting agents. To do so, we made use of the commercially available, mutant haloalkane dehalogenase, the HaloTag protein (HTP).[23] Wild-type haloalkane dehalogenases from *Xanthobacter autotrophicus GJ10* (*Xa*DHL)[24] and *Rhodococus rhodochrous* (*Rr*DHL)[25] hydrolyze halogen-containing alkane substrates to the corresponding alcohols via a mechanism that involves formation of a substrate-enzyme ester intermediate. This occurs through attack of an active site carboxylate (Asp106) anion on the primary alkyl chloride (Figure 31).[26, 27] In the wild-type protein, this ester

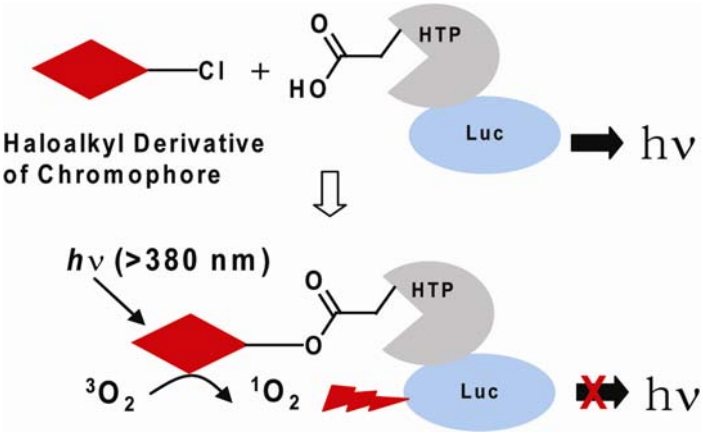

Figure 31. A system to evaluate CALI efficiencies of different chromophores. A haloalkyl derivative of the chromophore of interest is used to label a target protein, 3xFlag-Luc-HTP-Myc. The photoexcited chromophore converts triplet oxygen to singlet oxygen in the vicinity of the target protein, leading to inactivation. The efficiency of target protein inactivation is determined by measuring the remaining luciferase activity.

intermediate is subsequently hydrolyzed. However, mutation of a residue in the active site (His272 to Phe) provides a protein that cannot hydrolyze the covalent intermediate. This allows HTP fusion proteins to be labeled covalently with a variety of haloalkane-containing compounds (generically called HaloTags). The labeled product is known to be very stable. While a few other methods exist for the delivery of chimeric small molecules to protein tags, the ease of synthesis of chloroalkane derivatives makes this technique particularly convenient. Since HTP does not exhibit additional, easily assayed activities, we constructed an expression vector for an epitope-tagged Luciferase-HTP (3xFlag-Luc-HTP-Myc) fusion protein. Luciferase activity is easily monitored in cells and in crude extracts and is a convenient target for CALI experiments. Thus, this system should allow the efficient and covalent delivery of a primary haloalkane derivative of the chromophore to a luciferase fusion protein, whose activity is monitored before and after irradiation.

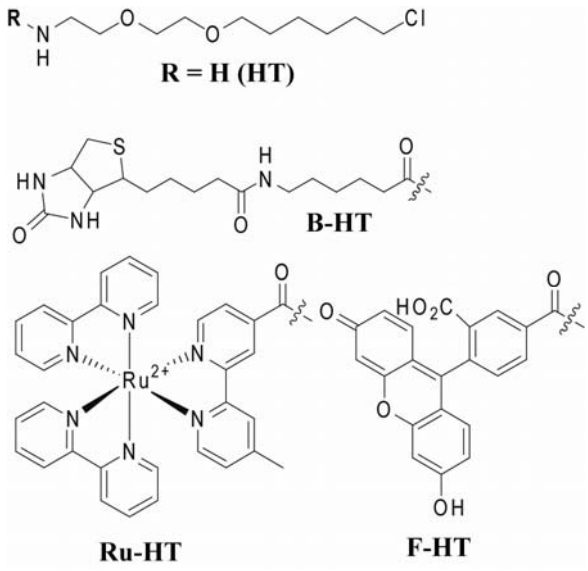

Figure 32. Chemical structures of the HaloTag reagents used in this study.

First, to test if the target protein 3xFlag-Luc-HTP-Myc can be efficiently labeled by HaloTag ligands (Figure 32), a lysate prepared from HeLa cells transfected with the 3xFlag-Luc-HTP-Myc expression vector was prepared and incubated with increasing concentrations of a primary haloalkane derivative of biotin (B-HT). After a brief incubation, streptavidin–agarose beads were employed to pull out biotinylated proteins. As shown in Figure 33A, the use of increasing amounts of B-HT followed by streptavidin-agarose pull-out resulted in the loss of luciferase activity in a dose-dependent fashion up to a concentration of 100 nM under the conditions employed. However, addition of higher concentrations of B-HT did not result in increased pull-out of luciferase activity. About 50% of the input was still observed in supernatant, indicating that the labeling reaction was incomplete. Pull-downs with anti-Myc agarose or anti-Flag agarose

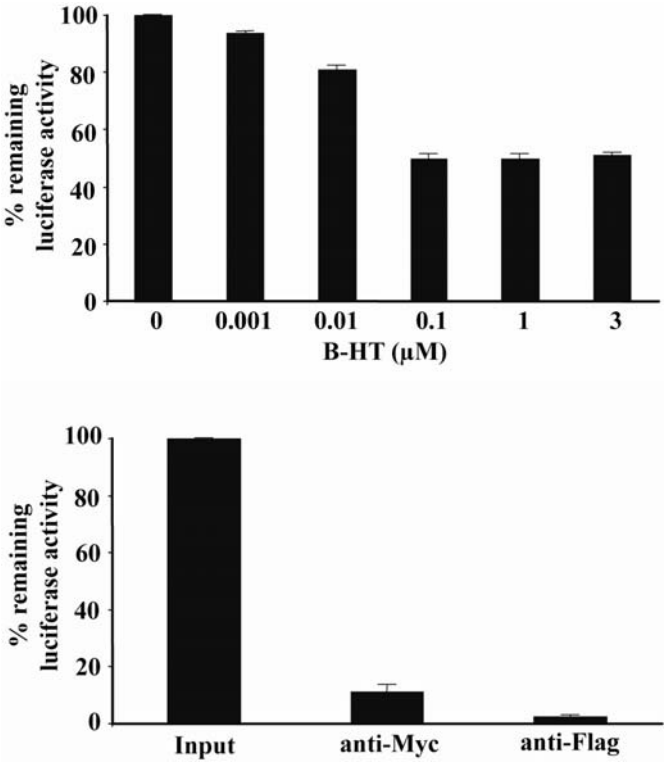

Figure 33. Labeling of target protein with the HaloTag reagent. (A) Extract from HeLa cells expressing the 3xFlag-Luc-HTP-Myc fusion protein was incubated with increasing concentrations of B-HT. Biotinylated protein was then precipitated with streptavidin-agarose. The relative level of luciferase activity remaining in the supernatant was then measured. (B) The same extract was incubated with immobilized anti-Myc or anti-Flag antibodies and the luciferase activity remaining in the supernatant was measured. The data represent the mean of triplicate experiments; error bars indicate standard deviations.

removed almost all luciferase activity from the cell lysate (Figure 33B), arguing that the inability of 50% of the protein to be biotinylated could not be ascribed to proteolysis of half of the fusion protein, a conclusion confirmed by Western blot (Figure 35B). Instead, these data suggest that while most of the fusion protein is intact, only about half of the molecules that display luciferase activity also have active HTP capable of being alkylated by a HaloTag ligand. This phenomenon of bifunctional fusion proteins expressed with only one of the activities intact is not uncommon.

Delivery of fluorescein and Ru(II) tris(bipyridyl) dication derivatives to the Luc-HTP fusion protein and comparison of their efficacy in CALI

We next tested whether primary haloalkyl derivatives of $Ru(bpy)_3^{2+}$ (Ru-HT; Figure 32) and fluorescein (F-HT; Figure 32) can label the target protein. Since we are comparing different chromophores for their CALI efficiencies, it is important for the ligands to have same efficiency in the labeling reaction and so this was tested first. Cell lysate prepared from HeLa cells expressing 3xFlag-Luc-HTP-Myc was first incubated with 100 nM of Ru-HT or F-HT and then treated with an excess of B-HT (1 μM). If any active protein fails to link to either Ru-HT or F-HT, it will be labeled by B-HT and will be removed from the solution by subsequent streptavidin–agarose pull-down. By measuring remaining luciferase activity of the solution, we can indirectly evaluate the labeling efficiencies of Ru-HT and F-HT. As shown in Figure 34, for both Ru-HT and F-HT, no significant decreases of luciferase activities were observed in the B-HT treated-solutions. This means that all of the active target proteins were already labeled during

pretreatment with Ru-HT or F-HT. More importantly, Ru-HT and F-HT showed the same efficiencies of protein labeling within experimental error.

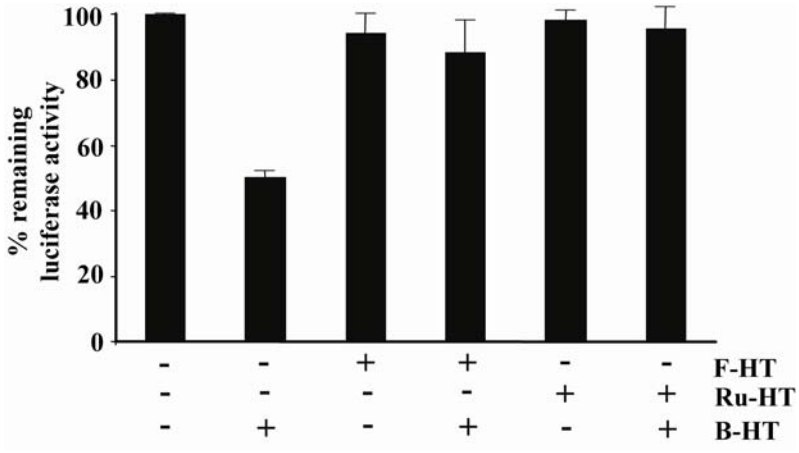

Figure 34. Comparison of the 3xFlag-Luc-HTP-Myc labeling efficiencies of Ru-HT and F-HT. Extract from HeLa cells expressing the 3xFlag-Luc-HTP-Myc fusion protein was incubated with either F-HT or Ru-HT. Subsequently, B-HT was added and the biotinylated material was precipitated with streptavidin-agarose. The amount of luciferase activity remaining in the supernatant, representing fusion protein that had reacted with F-HT or B-HT or contains an inactive HTP domain, was measured. The data represent the mean of triplicate experiments; error bars indicate standard deviations.

To evaluate the CALI efficiencies of the inorganic and organic chromophores, a HeLa cell lysate containing 3xFlag-Luc-HTP-Myc and Renilla luciferase was again incubated with Ru-HT or F-HT to allow alkylation of the active fusion protein. The sample was then irradiated with visible light using a Xenon arc lamp and a filter that blocks wavelengths below 380 nm. As shown in Figure 35A, the rate of protein inactivation was dependent on the concentration of the Ru-HT compound. In the case 100 nM of Ru-HT was used, maximal inactivation was achieved after 30 min irradiation. However, slower inactivation of the target protein could be achieved

with as little as 10 nM Ru-HT. Recall that since 50% of the protein is incapable of being alkylated, this represents essentially quantitative inactivation of the accessible target protein. Note that no proteolysis of the target protein was observed during labeling and irradiation (Figure 35B), excluding the possibility that residual luciferase activity can be from cleaved protein. In the absence of irradiation, but in the present of Ru-HT, there was no loss of

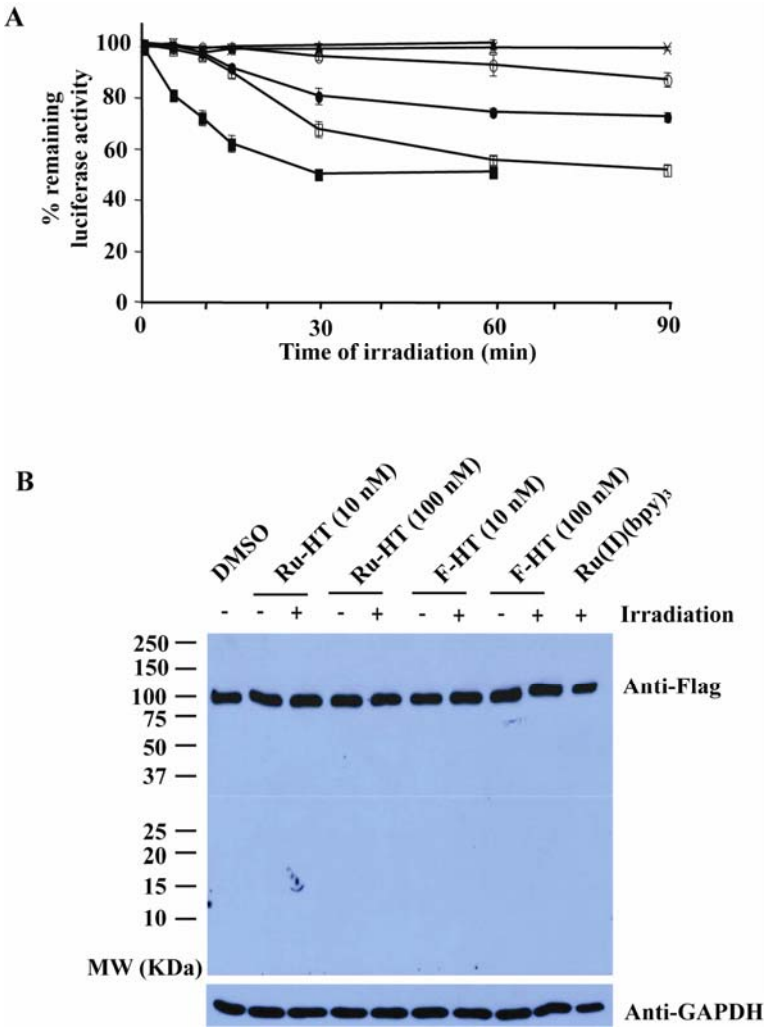

Figure 35. Comparison of Ru-HT and F-HT as CALI "warheads". (A) Extract from HeLa cells expressing the 3xFlag-Luc-HTP-Myc fusion protein was incubated with DMSO (✕), F-HT (10 nM: ○, 100 nM: ●), Ru-HT (10nM: □, 100 nM: ■), or $Ru(bpy)_3^{2+}$ (100 nM: ▲). After irradiation for the indicated times, the remaining luciferase activity was measured. Data represent mean of triplicate experiments; error bars indicate standard deviations. (B) Western blot showing no proteolysis during experimental procedures. 2 μL of HeLa cell extract in PBS (total volume: 50 μL, pH 7.4) was incubated with compounds as indicated for 30 min at room temperature and irradiated for 30 min at room temperature.

luciferase activity. Furthermore, $Ru(bpy)_3^{2+}$, i.e., the chromophore not incorporated into a HaloTag, also had no effect (Figure 35A). This shows that the ruthenium complex must be delivered to the fusion in order to be effective and that luciferase inactivation is triggered only after irradiation. Interestingly, under identical conditions, the sample treated with F-HT exhibited little loss of luciferase activity. Note the decrease of luciferase activity by 100 nM of F-HT is even smaller than that of 10 nM of Ru-HT. Since the labeling efficiencies of Ru-HT and F-HT are the same, these data indicate that Ru-HT is a more efficient CALI reagent than one of the best organic fluorescent dyes, fluorescein.

Evidence that singlet oxygen is the protein-damaging agent in Ru-HT-mediated CALI

The reactive oxygen species (ROS) involved in protein inactivation in CALI is mainly either singlet oxygen or hydroxyl radical. Since the half-maximal radius of inactivation of hydroxyl radical (15 Å) is shorter than that of singlet oxygen (40 Å),[6] CALI mediated by hydroxyl radical is generally considered to give higher specificity.[7] Laser excitation of Malachite Green, a commonly used CALI dye, was shown to generate hydroxyl radical,[4] while fluorescein-mediated protein inactivation occurs via singlet oxygen generation.[6] We assumed that this is also

the case for the ruthenium complex, since photo-excited $Ru(bpy)_3^{2+}$ (triplet state) is known to convert triplet oxygen to singlet oxygen by energy transfer.[18] To confirm that singlet oxygen is indeed the major vector for protein inactivation in Ru-HT mediated CALI, we tested inhibition of protein inactivation by ROS quenching molecules. As shown in Figure 36, sodium azide (NaN_3), a potent singlet oxygen quencher[28 29] inhibited Ru-HT mediated inactivation of target protein. On the other hand, D-mannitol, a hydroxyl radical or superoxide anion quencher,[30] had no effect. Imidazole, a less potent singlet oxygen quencher than sodium azide,[31] also showed some extent of inhibition. We conclude that, as expected, CALI mediated by Ru-HT indeed proceeds via a singlet oxygen intermediate.

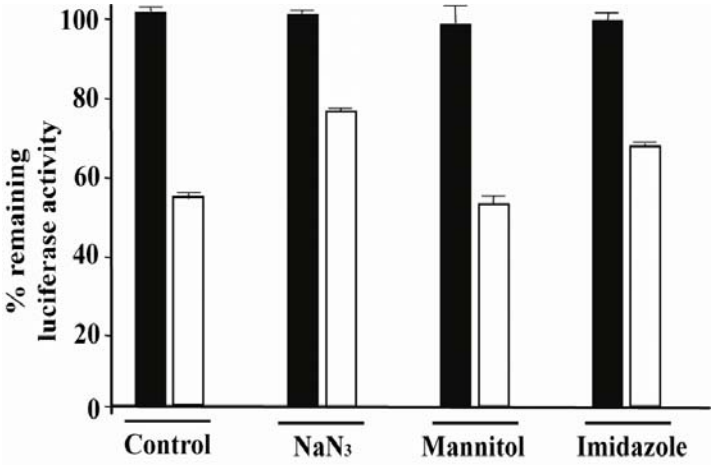

Figure 36. Ru-HT-mediated protein inactivation involves singlet oxygen. Extract from HeLa cells expressing the 3xFlag-Luc-HTP-Myc fusion protein was incubated with Ru-HT (100 nM) for 30 min at room temperature. NaN_3 (30 mM), D-mannitol (65 mM), or imidazole (30 mM) were added immediately before irradiation. Open bars: irradiated (30 min) sample, filled bars: non-irradiated sample. Data represent mean of triplicate experiments; error bars indicate standard deviations.

Ru-HT inactivates target protein inside living cells.

All of the experiments described above were carried out in cell extracts. However, CALI is most useful if it can be performed in living cells. Since $Ru(bpy)_3^{2+}$ is known to be cell

permeable,[32] we speculated that Ru-HT should be able to pass through the cell membrane and label HTP-containing target proteins. To test this, HeLa cells expressing 3xFLAG-Luc-HTP-Myc as well as Renilla luciferase were treated with Ru-HT and irradiated with visible light. As shown in Figure 37, cells treated with 1 μM Ru-HT and irradiated for 30 minutes exhibited a 40 % inactivation of luciferase activity relative to cells treated with DMSO only that were also irradiated. When the extracellular concentration of Ru-HT was increased to 10 μM, 63% of the target luciferase activity was lost. Note that the specific activity of the protein may well be higher in living cells relative to that observed in the crude extract, explaining the ability to knock out more than 50% of the activity. The Renilla luciferase activity was unaffected by Ru-HT and irradiation. Furthermore, incubation of the cells with 10 μM $Ru(bpy)_3^{2+}$ had no effect on the activity of the 3xFLAG-Luc-HTP-Myc protein. Taken together, these data argue that the Ru-HT can indeed permeate cells and that its ability to inactivate the target protein requires formation of the covalent intermediate and irradiation, as expected. Under the same conditions, irradiation of cells treated with F-HT also resulted in inactivation of the target protein, but less efficiently than was observed using the Ru-HT reagent. This suggests that, as was observed in vitro, the $Ru(bpy)_3^{2+}$ is a more efficient CALI warhead than fluorescein, although we cannot absolutely rule out the possibility that the fluorescein-containing reagent is somewhat less permeable. Finally, it is important to note that under all of the conditions employed in this experiment, neither the ruthenium complex nor irradiation affected cell viability (data not shown).

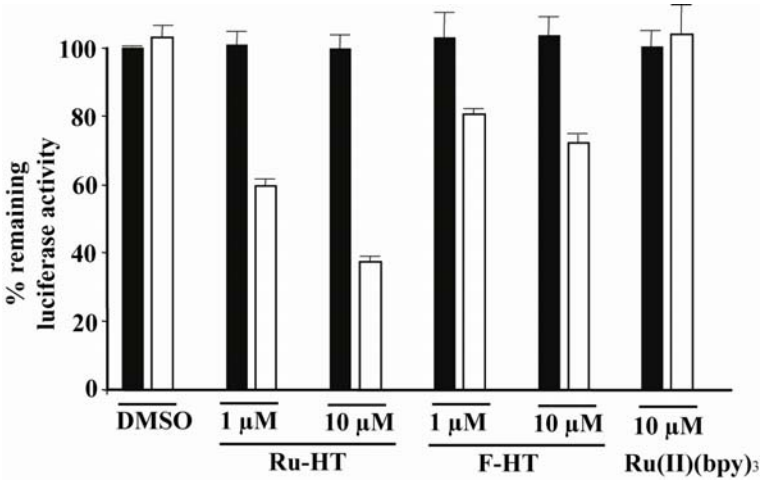

Figure 37. Ru-HT-mediated CALI in living cells. HeLa cells expressing 3xFlag-Luc-HTP-Myc were incubated with DMSO (control), Ru-HT, F-HT, or $Ru(bpy)_3^{2+}$ and irradiated. After lysis, the luciferase activities of lysates were measured and presented as described before. Open bars: irradiated sample, filled bars: non-irradiated sample. Data represent mean of triplicate experiments; error bars indicate standard deviations.

2.3. Discussion

We have developed a general system to compare the efficiencies of different chromophores as reagents for CALI. This is based on the delivery of a primary haloalkyl derivative of the chromophore to a fusion protein containing the target linked to HTP, which reacts irreversibly with the primary alkyl chloride. Since such derivatives are synthesized easily, this approach should be convenient for testing the efficiency, in a standardized fashion, of new potential CALI agents as they arise. Using this system, we found that a $Ru(bpy)_3^{2+}$ has much higher efficiencies in singlet oxygen generation and subsequent target protein inactivation than conventional organic fluorophore, fluorescein. Indeed, $Ru(bpy)_3^{2+}$ can mediate quantitative

protein inactivation in vitro. In addition, the $Ru(bpy)_3^{2+}$-based CALI reagent employed in this study was found to be cell permeable and thus capable of triggering target protein inactivation inside living cells.

There is no evidence that the Ru-HT molecule exhibits significant off-target effects at lower concentrations of the ruthenium complex. The experiments reported here all contained two luciferase reporter activities, one fused to HTP (firefly) and one that is not (Renilla). There was no indication that Ru-HT and photolysis affected the activity of the Renilla luciferase. However, for in vitro CALI, the use of high concentrations of untargeted $Ru(bpy)_3^{2+}$ at 1 μM or extended photolysis periods (≥ 1 hour) did show inactivation of both target protein and Renilla luciferase. Thus, these reagents are best employed at concentrations of <1 μM and irradiation times should be held to 30 min. or less, at least using the light source that we employed.

The greater efficiency of protein inactivation observed using the $Ru(bpy)_3^{2+}$ warhead as compared to fluorescein is consistent with the photophysical and photochemical properties of the two molecules. Singlet oxygen is generated from the reaction of ground state oxygen triplet with the triplet state of the excited fluorophore. The quantum yield for triplet formation of fluorescein is relatively low (0.1 in MeOH)[21] in comparison to $Ru(bpy)_3^{2+}$ (0.86 in MeOH) due to the latter's access to a metal to ligand charge transfer state (MLCT).[33]

Photochemical stability of fluorophores to singlet oxygen can be another factor affecting the efficiency of CALI reagent. In other words, the sensitivity of the CALI warhead to photobleaching limits the number of singlet oxygen generation events that can occur. While organic fluorophores, commonly used in CALI, are known to be very sensitive to

photobleaching, $Ru(bpy)_3^{2+}$ is stable to singlet oxygen as shown in previous studies of photo-oxidation of 1, 3-cyclopentadiene by $Ru(bpy)_3^{2+}$.[34, 35] Thus, it is likely that the $Ru(bpy)_3^{2+}$ warhead has a far greater turnover number for singlet oxygen generation in a CALI experiment than does fluorescein or most other organic fluorophores. Finally, it is worth mentioning that the Ru-HT/HTP-based system reported here may also be of practical utility for studies of protein function. If the HTP fusion protein is somehow made the only form of the target protein present in a cell (for example by gene replacement in yeast or using RNAi in mammalian cells), then most or all of its activity could be knocked out using the experiments reported here, though currently, the efficiency of this approach would appear to be limited by the specific activity of the HTP fusion protein.

In conclusion, we have reported a general and convenient system for the comparison of different chromophores for CALI efficiency. This technique has been used to identify the $Ru(bpy)_3^{2+}$ as an unusually efficient warhead for this purpose. We propose that appropriate small molecule-$Ru(bpy)_3^{2+}$ chimeras may well be useful tools for the rapid and specific inactivation of target protein activities, which are described in Chapter 3.

2.4. Experimental Section

Materials and Instruments.

All chemicals, unless stated, were purchased from Aldrich Chemical Co., and were used without further purification. ^{1}H NMR spectra were recorded on a *Varian Inova-400* spectrometer at operating frequency of 400 MHz. Chemical shift (δ) are given in ppm; downfield shifts are reported as positive values from tetramethylsilane (TMS) standard at 0.00 ppm. Mass spectra (MS) were measured with Voyager-DE™ PRO (Applied Biosystems) for MALDI-TOF. Irradiation was done using 150-W xenon arc lamp (Oriel, Stamford, CT). Light was filtered first through 10 cm of distilled water and then through a 380- to 2,500-nm cut-on filter (Oriel 49470). Samples were positioned at 25 cm distance from the light source and light intensity at the distance was 50 mW/cm^2.

Syntheses HaloTag reagents.

Ru-HT: To a stirred solution of **HT**[36](2.8 mg, 0.01 mmol) in DMF (200 μL) was added Bis-(2,2'-bipyridin)-4'-methyl-4-carboxy-bipyridin-ruthenium-N-succinimidylester-bis-(hexafluorophosphate) (5.0 mg, 0.005 mmol) and DIPEA (5 μL). After 4 hr at room temperature, the reaction mixture was diluted with dH_2O (0.1 % TFA, 3 mL) and directly purified by HPLC to afford Ru-HT as a red solid (75% yield). B-HT and previously reported F-HT [37] were prepared in same way using Sulfo-NHS-LC-Biotin (Pierce) and 5-carboxyfluorescein succinimide ester (Molecular Probe), respectively. **Ru-HT** ^{1}H NMR (DMSO-d_6): δ 9.14-9.11 (m, 2H), 8.84-8.82

(m, 4H), 8.77 (bs, 1H), 8.18-8.14 (m, 4H), 7.86 (d, 1H, J = 6.0), 7.80-7.79 (m, 1H), 7.76 (d, 1H, J = 5.6), 7.70-7.69 (m, 3H), 7.56 (d, 1H, J = 5.6), 7.53-7.49 (m, 4H), 7.39 (d, 1H, J = 6.0), 2.52 (S, 3H), 1.65-1.61 (m, 2H), 1.44-1.40 (m, 2H), 1.30-1.22 (m, 4H); MALDI/TOF: $[M]^+$ calculated 833.24, found 833.23. **B-HT** ^{1}H NMR (DMSO-d_6): 7.86 (t, 1H, J = 5.2), 7.72 (t, 1H, J =5.2), 4.30-4.27 (m, 1H), 4.12-4.09 (m, 1H), 3.62-3.59 (m, 2H), 3.46-3.45 (m, 4H), 3.38-3.33 (m, 4H), 3.17-3.13 (m, 2H), 3.08-3.06 (m, 1H), 2.97 (dd, 2H, J = 12.8, 4.8), 2.80 (dd, 1H, J = 12.4, 4.8), 2.57-2.52 (m, 2H), 2.04-2.00 (m, 4H), 1.70-1.67 (m, 2H), 1.60-1.54 (m, 1H), 1.50-1.43 (m, 8H), 1.38-1.26 (m, 10H), 1.22-1.18 (m, 2H); MALDI/TOF: $[M+H]^+$ calculated 563.30, found 563.47.

Plasmid.

The vector backbone of the host plasmid that is used to construct the 3xFlag-Luc-HTP-Myc plasmid was derived from the mammalian expression vector pEGFP-N3 with multiple convenient restriction sites after the CMV promoter. The DNA sequences encoding different parts of the fusion construct were ligated into the host vector sequentially. The sequence encoding the full length luciferase (Luc) was amplified through PCR using pGL3 basic (Promega) as template, along with forward primer (5'-GGACGCTAGCGAAGACGCCAAAAACATAAAG-3') and reverse primer (5'-GAAAGATCTCACGGCGATCTTTCCGCCCTTC-3'). The PCR product was digested with NheI / BglII and inserted into the digested host plasmid. The sequence encoding the full length haloalkane dehalogenase (HTP) was amplified through PCR using pHT2 (Promega) as template, along with forward primer (5'-GACCAGAGATCTG

CCACCATGGGATCCGAAATC-3') and reverse primer (5'-GAAAACAAGCTTGCCG GCCAGCCCGGGGAG-3'). The PCR product was digested with BglII / HindIII and inserted into the digested host plasmid. The sequence encoding the start codon followed by the 3x Flag tag was inserted into the BamHI / NheI sites, and the sequence encoding the Myc tag followed by the stop codon was inserted into the HindIII / NotI sites of the host plasmid.

Cell culture, transfection, and preparation of cell lysate.

HeLa cells (American Type Culture Collection, CCL-2) were grown in 10 cm plates at 37°C under 5% CO_2 in Dulbeco's modified Eagle medium (Invitrogen) supplemented with 10% (vol / vol) fetal calf serum (Invitrogen). Cells were allowed to reach 70% confluence before transfection. Cells were transfected by the Lipofectamine^{TM} Plus method (invitrogen) with 8 μg of plasmid for 3Flag-Luc-HTP-Myc and 80 ng of Renilla reniformis luciferase plasmid (pRL-SV40). After transfection, cell were maintained at 37°C under 5% CO_2. After 30 hr, cells were lysed with 1x passive lysis buffer (Promega) including protease inhibitor cocktail. Total protein concentration of cell extract was measured (1.59 mg / mL) using the BCA protein assay kit (Pierce).

Measurement of luciferase activities.

Luciferase activities were measured using dual-luciferase assay kit (Promega) following manufacture's protocol. The firefly luciferase activity in sample was measured and normalized

with the Renilla luciferase activity and then presented as the percentage of the activity normalized of input (control).

Labeling of target protein with HaloTag reagents.

1) Target protein labeling with B-HT: 2 μL of HeLa cell lysate in PBS (total volume: 50 μL, pH 7.4) including BSA (4 mg / ml final concentration) was incubated with increasing concentrations of B-HT. After incubation for 30 min at room temperature, samples were incubated with streptavidin-agarose (invitrogen) in PBS (40 μL, 1:1 vol / vol, pH 7.4) for 30 min at room temperature. After centrifugation, the luciferase activity of supernatant (20 μL) was measured as described above.

2) Target protein labeling with Ru-HT or Fl-HT: 2 μL of HeLa cell lysate in PBS (total volume: 50 μL, pH 7.4) including BSA (4 mg / ml) was incubated with DMSO, F-HT (100 nM), or Ru-HT (100 nM). After 30 min at room temperature, B-HT (1 μM) was added to label any remaining target protein. After incubation for 20 min at room temperature, streptavidin-agarose in PBS (40 μL, 1:1 vol / vol, pH 7.4) was added and incubated for 30 min at room temperature. After centrifugation, luciferase activities of supernatant (20 μL) were measured as described above.

Immunoprecipitation.

2 μL of HeLa cell lysate in PBS (total volume: 50 μL, pH 7.4) including BSA (4 mg/ml) was incubated with PBS (40 μL, pH 7.4), anti-Myc agarose affinity gel (Sigma) in PBS(40 μL, 1:1

vol / vol, pH 7.4), anti-Flag M2 agarose affinity gel (Sigma) in PBS(40 μL, 1:1 vol / vol, pH 7.4) for 30 min at room temperature. After centrifugation, the remaining luciferase activities of the solutions were measured as described above.

In vitro CALI.

1 μl of HeLa cell lysate in PBS (total volume: 20 μL, pH 7.4) including BSA (4 mg / ml total) in transparent 96 well plate was incubated with DMSO or compounds for 30 min at room temperature in the dark. Samples were irradiated (without lid) for different times at room temperature. Luciferase activities of the solution were measured as described above.

In vivo CALI.

HeLa cell were seeded in 96-well plate (2.5x 10^4 cells/well) and grown in DMEM (10% FBS) for 24 hr before transfection. Cells in each well were transfected as above with 100 ng of 3Flag-HTP-Luc-Myc plasmid and 1 ng of Renilla reniformis luciferase plasmid (pRL-SV40). After transfection, cells were maintained at 37°C under 5% CO_2 for 15 hr. Medium was replaced with fresh DMEM (w/o phenol red, 10% FBS) and cells were treated with compounds. After 3 hr at 37°C, media was replaced with fresh DMEM (w/o phenol red, 10% FBS) to remove excess compound in media. Cells were irradiated at room temperature for 30 min as described above. After dark incubation for 30 min at 37°C, cells were lysed with 1x passive lysis buffer (20 μL per well, Promega). Luciferase activities of the lysates were measured as described above.

2.5. References

1. S. M. Elbashir, J. Harborth, W. Lendeckel, A. Yalcin, K. Weber and T. Tuschl, *Nature*, 2001, **411**, 494-498.
2. J. Harborth, S. M. Elbashir, K. Bechert, T. Tuschl and K. Weber, *J Cell Sci*, 2001, **114**, 4557-4565.
3. J. A. Wilson and C. D. Richardson, *Curr Opin Mol Ther*, 2003, **5**, 389-396.
4. J. C. Liao, J. Roider and D. G. Jay, *Proc Natl Acad Sci U S A*, 1994, **91**, 2659-2663.
5. D. G. Jay and T. Sakurai, *Biochim Biophys Acta*, 1999, **1424**, M39-48.
6. S. Beck, T. Sakurai, B. K. Eustace, G. Beste, R. Schier, F. Rudert and D. G. Jay, *Proteomics*, 2002, **2**, 247-255.
7. B. K. Eustace, A. Buchstaller and D. G. Jay, *Brief Funct Genomic Proteomic*, 2002, **1**, 257-265.
8. K. W. Marek and G. W. Davis, *Neuron*, 2002, **36**, 805-813.
9. O. Tour, R. M. Meijer, D. A. Zacharias, S. R. Adams and R. Y. Tsien, *Nat Biotechnol*, 2003, **21**, 1505-1508.
10. K. M. Marks, P. D. Braun and G. P. Nolan, *Proc Natl Acad Sci U S A*, 2004, **101**, 9982-9987.
11. P. G. Alluri, M. M. Reddy, K. Bachhawat-Sikder, H. J. Olivos and T. Kodadek, *J Am Chem Soc*, 2003, **125**, 13995-14004.
12. P. Alluri, B. Liu, P. Yu, X. Xiao and T. Kodadek, *Mol Biosyst*, 2006, **2**, 568-579.

13. X. Xiao, P. Yu, H. S. Lim, D. Sikder and T. Kodadek, *Angew Chem Int Ed Engl*, 2007, **46**, 2865-2868.

14. H.-S. Lim, C. T. Archer and T. Kodadek, *J. Amer. Chem. Soc.*, 2007, **129**, 7750-7751.

15. P. Yu, B. Liu and T. Kodadek, *Nature Biotech.*, 2005, **23**, 746-751.

16. Y. U. Kwon and T. Kodadek, *J. Amer. Chem. Soc.*, 2007, **129**, 1508-1509.

17. J. S. Winterle, D. S. Kliger and G. S. Hammond, *J. Amer. Chem. Soc.*, 1976, **98**, 3719-3721.

18. J. N. Demas, E. W. Harris and R. P. McBride, *J Am Chem Soc*, 1977, **99**, 3547-3551.

19. S. S. Miller, K. Zahir and A. Haim, *Inorg. Chem.*, 1985, **24**, 3978-3980.

20. Q. G. Mulazzani, H. Sun, M. Z. Hoffmann, W. E. Ford and M. A. J. Rodgers, *J. Phys. Chem.*, 1994, **98**, 1145-1150.

21. M. C. DeRosa and R. J. Crutchley, *J Coord Chem Rev*, 2002, **233-234**, 352-371.

22. A. Abdel-shafi, D. R. Worrall and A. Y. Ershov, *Dalton Trans.*, 2004, 30-36.

23. G. V. Los and K. Wood, *Methods Mol Biol*, 2007, **356**, 195-208.

24. D. B. Janssen, A. Scheper, L. Dijkhuizen and B. Witholt, *App. Environ. Microbiol.*, 1985, **49**, 673-677.

25. A. N. Kulakova, T. M. Stafford, M. J. Larkin and L. A. Kulakov, *Plasmid*, 1995, **33**, 208-217.

26. F. Pries, J. Kingma, M. Pentenga, G. van Pouderoyen, C. M. Jeronimus-Stratingh, A. P. Bruins and D. B. Janssen, *Biochemistry*, 1994, **33**, 1242-1247.

27. F. Pries, J. Kingma, G. H. Krooshof, C. M. Jeronimus-Stratingh, A. P. Bruins and D. B. Janssen, *J Biol Chem*, 1995, **270**, 10405-10411.

28. C. S. Foote, T. T. Fujimoto and Y. C. Chang, *Tetrahedron Lett.*, 1972, **1**, 45-48.

29. N. Hasty, P. B. Merkel, P. Radlick and D. R. Kearns, *Tet. Lett.*, 1972, **1**, 49-52.

30. G. Ambrosio and J. T. Flaherty, *Cardiovasc. Drugs Ther.*, 1992, **6**, 623-632.

31. A. Grimmett, *Adv Heterocycl Chem*, 1970, **12**, 103-183.

32. J. R. Newcomb, B. Rivnay, C. M. Bastos, T. D. Ocain, K. Gordon, P. Gregory, S. M. Turci, K. A. Sterne, M. Jesson, J. Krieger, J. C. Jenson and B. Jones, *Inflammation Res.*, 2003, **52**, 263.

33. A. A. Abdel-Shafi, P. D. Beer, R. J. Mortimer and F. Wilkinson, *Helvetica Chimica Acta*, 2001, **84**, 2784-2795.

34. M. Suzuki, O. Bartels, R. Gerdes, G. Schneider, D. Wöhrle, G. Schulz-Ekloff, M. Kimura, K. Hanabusa and H. Shirai, *Chem Lett*, 1999, 579-580.

35. M. Suzuki, O. Bartels, R. Gerdes, G. Schneider, D. Wöhrle, G. Schulz-Ekloff, M. Kimura, K. Hanabusa and H. Shirai, *Phys Chem Chem Phys*, 2000, **2**, 109-114.

36. Y. Zhang, M. K. So, A. M. Loening, H. Yao, S. S. Gambhir and J. Rao, *Angew Chem Int Ed Engl*, 2006, **45**, 4936-4940.

37. K. V. Wood, G. V. Los, R. F. Bulleit, D. Klaubert, M. Mcdougall and C. Zimprich, *PCT Int Appl*, 2004, WO 2004072232.

Chapter 3: Facile transformation of low-potency small molecules into photochemical protein knock-out reagents

3.1. Introduction

Potent and specific agonists and antagonists of protein function are valuable tools in biomedical research, but are relatively rare. In an effort to enrich the chemical armamentarium available to cell and molecular biologists, large-scale efforts have been initiated to create and screen combinatorial libraries or compound collections for new agonists or antagonists [1-3]. While many such efforts have met with considerable success, it is becoming increasingly clear that a major issue in the further advancement of this field will be to improve upon the specificity and potency of the "hits" identified in such screens. With regard to specificity, it is critically important to minimize off target effects if a compound is intended as a tool for probing mechanism, yet high specificity for a single protein target is not usually a criterion in a primary screen. Instead, the degree of specificity is generally examined later by conducting assays with many individual proteins related to the protein target. With regard to potency, it is desirable to have compounds with IC_{50}s or EC_{50}s in the nanomolar range, but it is rare for primary hits from a screen to exhibit potencies better than the low micromolar region. The standard approach to improving the potency of a hit is to synthesize a large number of analogues and test each of them independently. These are labor-intensive efforts that are not amenable to high throughput, meaning that the current capacity to screen libraries far outstrips the capacity to mature them.

A potentially rapid and general approach to increasing the functional potency of a protein antagonist is to equip the molecule with a "warhead" capable of modifying the target protein irreversibly. In this way, even when the inhibitor diffuses away, the target protein remains inactive. An ideal warhead would generate a highly reactive, but short-lived, intermediate that would inactivate only proteins in the immediate vicinity. A singlet oxygen-generating moiety fulfills these requirements. Singlet oxygen modifies many different protein functional groups and it cannot diffuse more than ≈ 40 Å from its point of generation [4]. Finally, singlet oxygen generation is most easily triggered photochemically when a molecule excited into its triplet state relaxes back to the ground state with concomitant spin conversion of triplet to singlet oxygen. Indeed, efforts have been made to develop so-called CALI (chromophore-assisted light inactivation) reagents by linking organic chromophores such as fluorescein to protein-binding antibodies [5-8]. However, these reagents have not made a significant impact as pharmacological tools. First, the organic chromophores are themselves highly sensitive to singlet oxygen, resulting in a low efficiency of protein inactivation. Second, antibodies are difficult to tag with chromophores in a defined fashion and they are not cell permeable. In this report, we describe a general and practical route to simple synthetic, cell permeable CALI agents. This technology should provide rapid access to potent, photo-triggered knock-out reagents for almost any protein of interest.

3.2. Results

Ru(II)-conjugated VEGFR2 antagonist showed a significant increase in potency with visible light

It has long been known that Ru(II)(tris-bipyridyl)$^{2+}$ (Ru(II)(bpy)$_3^{2+}$) compounds are highly efficient photocatalytic sensitizers of singlet oxygen formation [9-12]. Moreover, the λ_{max} of Ru(II)(bpy)$_3^{2+}$ is approximately 450 nm, a wavelength outside the range of most cellular chromophores. Thus, it seemed reasonable to postulate that delivery of Ru(II)(bpy)$_3^{2+}$ to a target protein, followed by brief photolysis, would result in potent inactivation of the target. As described in Chapter 3, we demonstrated recently that this is the case when Ru(II)(bpy)$_3^{2+}$ is attached covalently to a Luciferase fusion protein [13]. To investigate the utility of this approach to photo-triggered protein inactivation with completely synthetic molecules, we employed a Vascular Endothelial Growth Factor Receptor 2 (VEGFR2)-binding peptoid, GU40C ($K_D \approx 2$ μM) [14]. GU40C is a weak antagonist of VEGF-induced VEGFR2 activation (75% inhibition at 500 μM) but is highly specific for this receptor. A Ru(II)(bpy)$_3^{2+}$-GU40C conjugate (RuGU40C, Figure 38A) was constructed via click chemistry and was shown to have an affinity for the VEGFR2 extracellular domain similar to that of the GU40C parent peptoid (Figure 39). The activity of this compound was then tested in an assay in which cultured endothelial cells were exposed to VEGF and the activation of VEGFR2 was monitored. As shown in Figure 38B, in the absence of irradiation, RuGU40C did not inhibit VEGF-induced autophosphorylation of

VEGFR2 even at the highest concentration examined (2 μM), as expected. However, with visible light (> 380 nm) irradiation (10 min), VEGFR2 autophosphorylation was inhibited

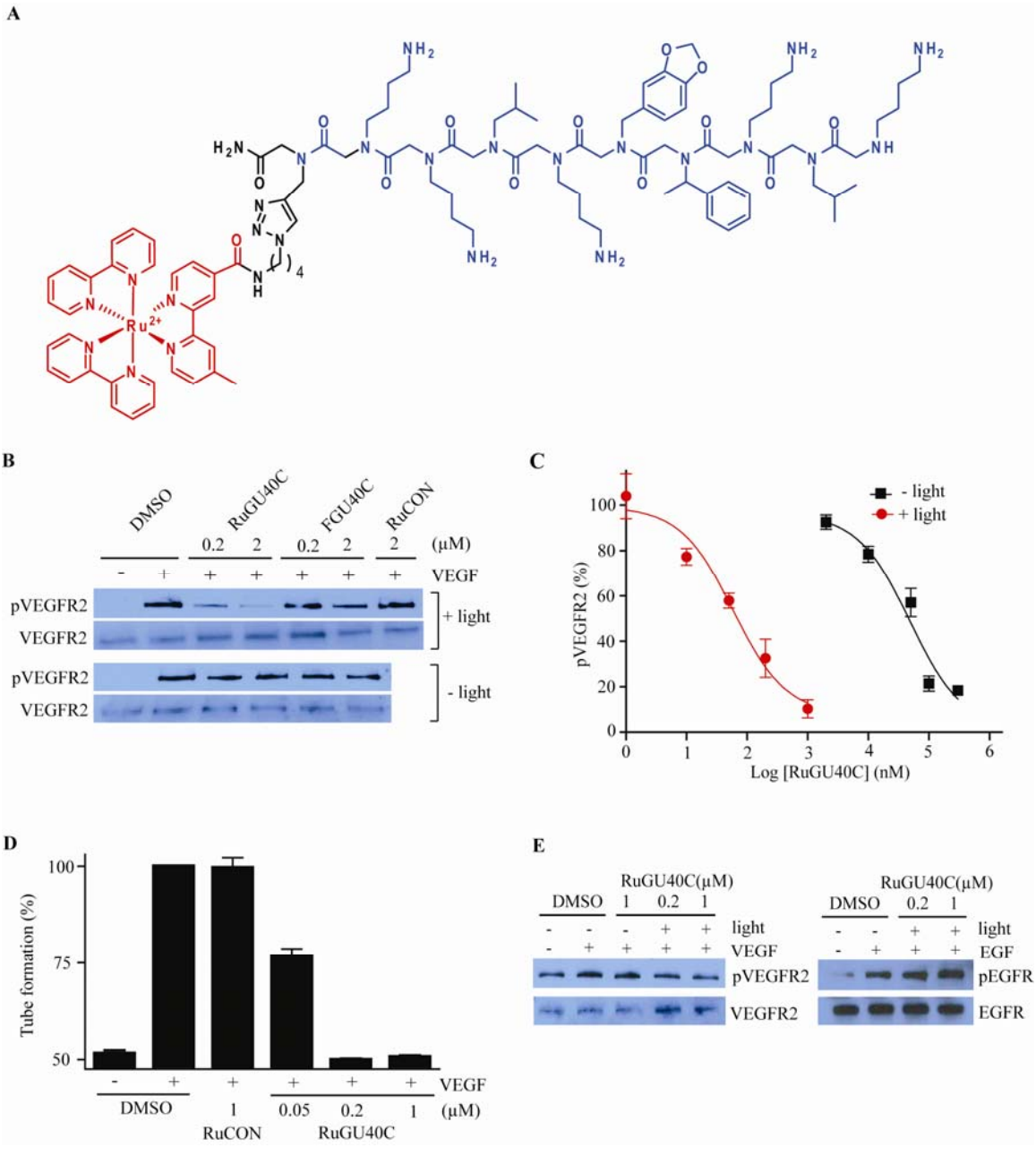

Figure 38. Visible light-triggered inactivation of the Vascular Endothelial Growth Factor Receptor 2 (VEGFR2) by a ruthenium-peptoid conjugate. (a) Chemical structure of RuGU40C. The modified $Ru(II)(bpy)_3^{2+}$ complex and the GU40C peptoid are shown in red and blue, respectively. (b) Western blots showing the level of phospho-VEGFR2 (the active form of the receptor) and total VEGFR2 after receptor-expressing cells (PAE/KDR) were incubated under the conditions indicated. The duration of irradiation was 10 minutes. FGU40C = fluorescein-conjugated GU40C (see Fig. S2). RuCON = a $Ru(II)(bpy)_3^{2+}$-conjugated control peptoid that does not bind VEGFR2 (see Fig. S2). (c) Dose-dependence of the inhibition of autophosphorylation of VEGFR2 by RuGU40C with or without irradiation. (d) Effect of ruthenium-peptoid conjugates on the VEGF-induced formation of tubes by human umbilical vascular endothelial cells (HUVECs). HUVECs on Matrigel-coated plates were incubated under the conditions indicated and irradiated (10 min). 16hr after the addition of VEGF, degree of tube formation was evaluated by quantitative analysis (AngioQuant software) of images obtained using a light microscope (see Fig S3 for representative images). (e) Analysis of the specificity of RuGU40C-mediated inhibition of VEGFR2. The effect of the ruthenium-peptoid conjugate on hormone-mediated activation of VEGFR2 or EGFR was examined in the presence or absence of irradiation (10 min) in cells that express both receptors (H441). A Western blot measuring the levels of the phosphorylated (activated) form of the receptor and total receptor is shown. Note that there is a basal level of phosph-VEGFR2 present even in the absence of VEGF treatment.

potently. A conjugate containing $Ru(II)(bpy)_3^{2+}$ tethered to a control peptoid that does not bind VEGFR2 (RuCON. Figure 40) did not show any inhibitory activity, demonstrating that the $Ru(II)(bpy)_3^{2+}$ warhead must be targeted to a protein in order for efficient inactivation to be observed. To obtain a more quantitative view of the increase in potency supported by the ruthenium photochemistry, a titration experiment was carried out, revealing that RuGU40C exhibited an IC_{50} of 49 μM in the absence of irradiation and 59 nM when irradiated. This represents a greater than 800-fold increase in potency (Figure 38C).

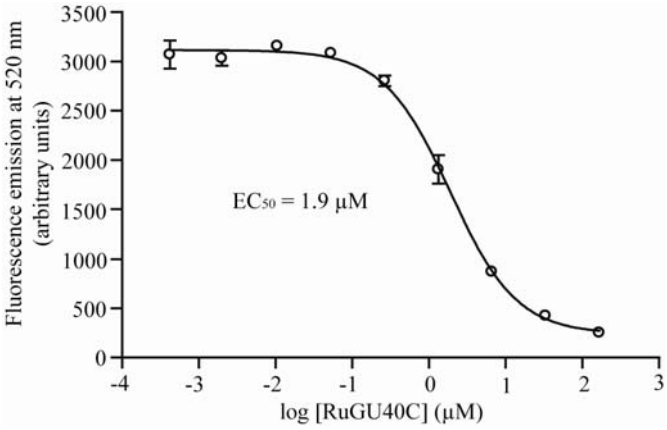

Figure 39. Competitive binding assay of RuGU40. Displacement of FGU40C (see Fig. S2) on immobilized VEGFR2 extracellular domain (ECD) by increased concentration of RuGU40C was assessed by measuring fluorescence emission at 520 nm

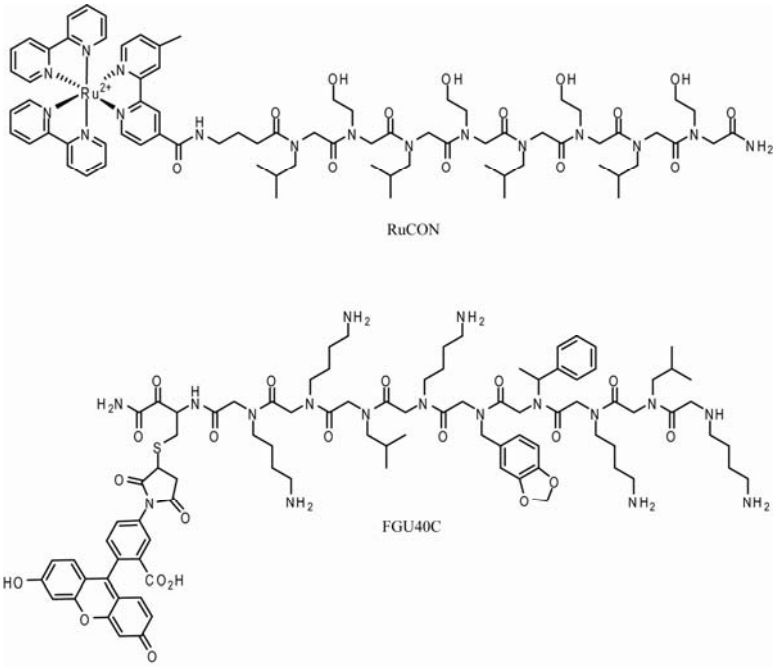

Figure 40. Structures of RuCON and FGU40C

To further validate that RuGU40C and light block VEGFR2 function, an in vitro angiogenesis assay was employed. Cultured endothelial cells form vessel-like tubular structures

when treated with VEGF, mimicking the process of vascular formation from preexisting blood vessels, which is a hallmark of cancer and various ischaemic and inflammatory diseases[15]. As shown in Figure 38D and Figure 41, upon irradiation, RuGU40C inhibited tube formation of HUVEC cells with an IC_{50} of about 50 nM while no inhibition was observed from cells that were treated with RuCON and irradiated.

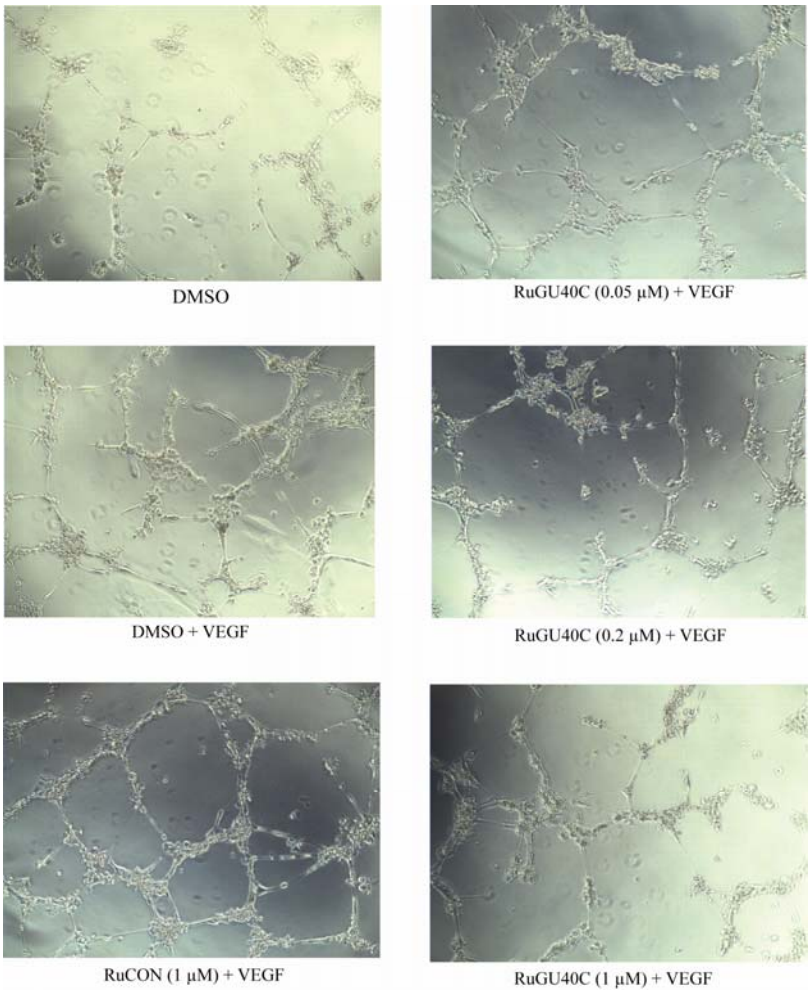

Figure 41. Effect of RuGU40C on VEGF-induced tube formation by HUVECs. HUVECs on Matrigel-coated 96-well plate were incubated under the conditions indicated and irradiated (10 min). 16 hr after VEGF addition, light microscopic images were taken.

A fluorescein conjugate of GU40C (Figure 40) also mediated the inhibition of VEGFR2 activation when irradiated, but much less efficiently than the ruthenium-peptoid conjugate (~50% at 2 μM, Figure 38B). Though fluorescein has often been used as a chromophore in classic CALI studies, this result is consistent with our previous finding that $Ru(II)(bpy)_3^{2+}$ is a far more efficient singlet oxygen generator than oxidatively sensitive organic fluorophores [13].

Specificity of VEGFR2 inactivation by RuGU40C

A critical issue is the degree of specificity of target protein inactivation. To examine this point, RuGU40C was mixed with recombinant Luciferase and the solution was irradiated. As shown in Figure 42, RuGU40C and light had no effect on Luciferase activity, which we have shown previously to be sensitive to targeted inactivation by singlet oxygen when the ruthenium complex is attached covalently to a Luciferase fusion protein [13]. This argues that non-specific damage by $^1O_2$ generated from unbound RuGU40C is negligible. More importantly, the effect of RuGU40C-mediated singlet oxygen production on a cellular receptor other than VEGFR2 was assessed in cultured cells. H441 cells, which express both EGFR (also a receptor tyrosine kinase) and VEGFR2 [16], were irradiated in the presence of RuGU40C and hormone induced autophosphorylation of each of the receptors was monitored.

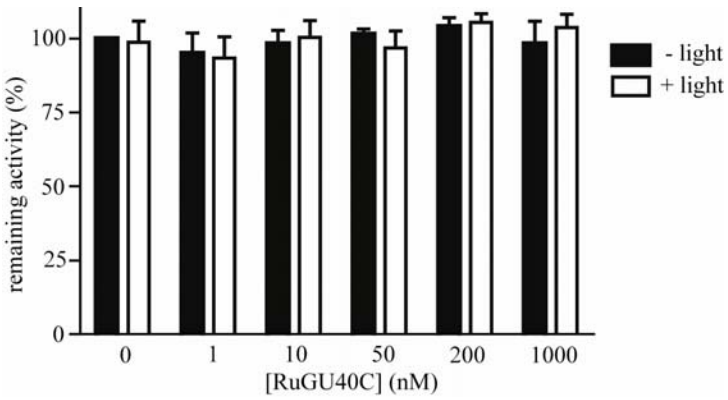

Figure 42. Effect of RuGU40C on recombinant Luciferase activity. Activity of recombinant Luciferase with indicated concentration of RuGU40C was measured after irradiation or dark incubation (10 min).

As shown in Figure 38E, at concentrations of RuGu40C that reduced VEGFR2 activation to basal levels, EGFR autophosphorylation was unaffected. Moreover, cell viability was unaffected by RuGU40C and light (Figure 43). Taken together, these data argue strongly that at these concentrations, protein inactivation is highly specific and that there is little or no "bystander damage" to other membrane receptors or the cells in general.

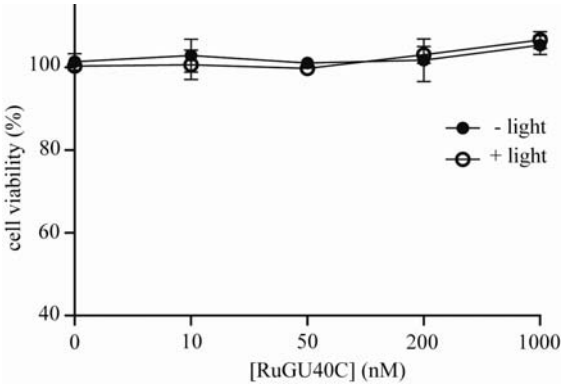

Figure 43. Effect of RuGU40C on the cell viability of PAE/KDR cells. Cells were incubated with indicated concentration of RuGU40C and irradiated or incubated in the dark (10 min). After 2 days, the cell viability was assessed by CellTiter 96® AQ_{ueous} One Solution Cell Proliferation Assay (Promega) and expressed as a percentage of DMSO (-light) control.

A Super-potent photo-antagonist of VEGFR2

The data shown in Figure 38 demonstrate that the $Ru(II)(bpy)_3^{2+}$ warhead can increase the potency of a poor inhibitor several hundred-fold. Would this type of result also be observed if one began with a more potent compound, or is a mid-nM potency for some reason the "speed limit" of singlet oxygen-mediated protein inactivation? To probe this point, a $Ru(II)(bpy)_3^{2+}$ conjugate of GU40C4 was created (Figure 44A). GU40C4, which contains two copies of GU40C joined by a linker, has increased binding affinity to dimeric VEGFR2 (K_D = 20~30 nM) and also showed increased potency in blocking VEGF-induced autophosphorylation of VEGFR2 in cultured cells (IC_{50} = 1 μM) [14]. After confirming that RuGU40C4 binds to the VEGFR2

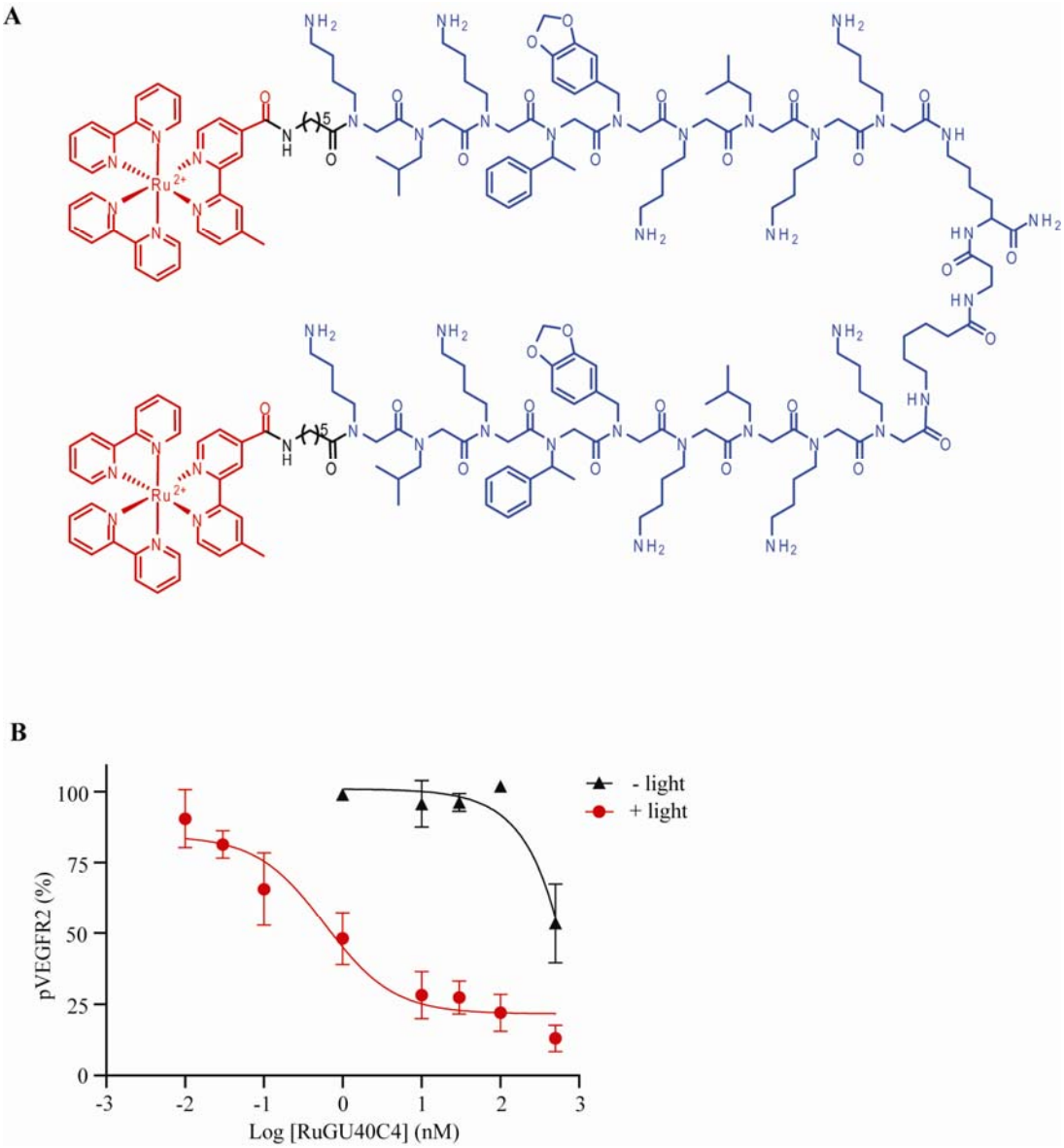

Figure 44. (a) Chemical structure of RuGU40C4. The modified Ru(II) $(bpy)_3^{2+}$ complex and GU40C4 peptoid are shown in red and blue, respectively. (b) Dose-dependent inhibition of VEGF-induced autophosphorylation of VEGFR2 on PAE/KDR cells by RuGU40C4 with irradiation (10 min).

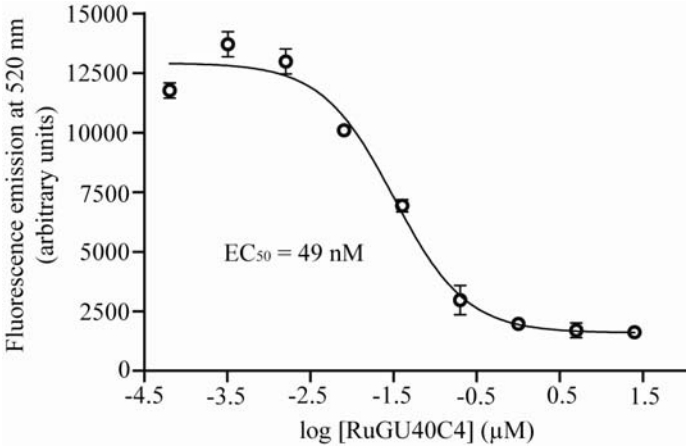

Figure 45. Competitive binding assay of RuGU40C4. Displacement of fluorescein conjugate of GU40C4 (GU40C4-FITC) on immobilized VEGFR2 extracellular domain (ECD) by increased concentration of RuGU40C4 was assessed by measuring fluorescence emission at 520 nm.

extracellular domain (Figure 45), autophosphorylation assays were performed to determine its potency in a cell culture assay. As shown in Figure 44B, in the absence of irradiation, RuGU40C4 showed about 50% inhibition of VEGFR2 at 500 nM, a potency similar to that of GU40C4 itself. However, with irradiation, RuGU40C4 inhibited VEGFR2 far more potently, with an IC_{50} of 590 pM. This represents a 1700-fold increase in potency compared to GU40C4, demonstrating that this strategy is capable of producing extremely effective inhibitors.

A photo-antagonist of the 26S proteasome

Next, we asked if this approach can be used for intracellular target proteins, requiring that the $Ru(II)(bpy)_3^{2+}$-synthetic molecule conjugate crosses the cell membrane and that the oxidation chemistry proceeds efficiently even in the reducing environment inside the cell. Rpt4, one of six AAA class ATPases in the 26S proteasome was chosen as a target. The proteasome is a large, multi-protein complex that is responsible for most non-lysosomal degradation of proteins in eukaryotic cells [17]. A ring of six ATPases (Rpts 1-6), which constitutes part of the 19S regulatory

particle (RP) of the proteasome, sits atop the barrel-like 20S catalytic core of the complex (Figure 47A). The ATPases act to unwind protein substrates and introduce the chains into the interior of the 20S where the catalytic sites reside [18]. They also stimulate peptidolysis by holding open a "flap" on the 20S core particle that otherwise restricts substrate access [19-21]. Previously, a peptoid called RIP1 was isolated in a screen for specific ligands to the yeast proteasome [22]. Cross-linking experiments demonstrated that RIP1 targets Rpt4 [23] and that it acts as an agonist of 26 proteasome-mediated peptidase activity (chymotrypsin-like; $EC_{50} \approx 3$ μM), presumably by locking the ATPase complex in the "flap open" conformation [24]. As shown in Figure 46, it also showed an enhancement of peptidase activity of the human 26S proteasome in living cells, but with lower potency ($EC_{50} \approx 50$μM).

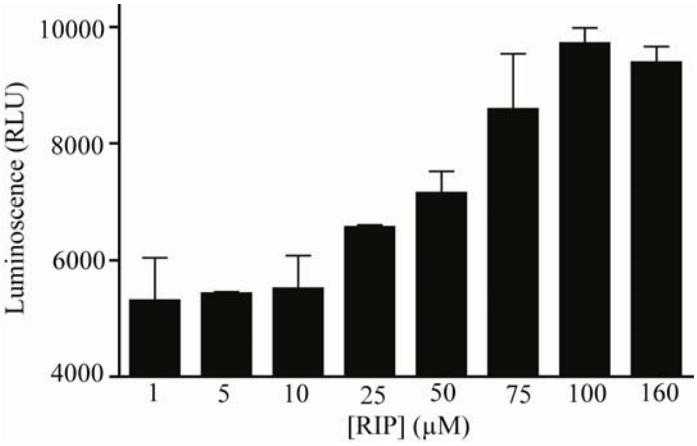

Figure 46. The Effect of RIP1 on chymotrypsin-like peptidase activity of the 26S proteasome in HeLa cells was assessed by measuring luminescence generated by substrate (Suc-LLVY-aminoluciferin) cleavage.

A $Ru(II)(bpy)_3^{2+}$ of RIP1 was created (RuRIP1, Figure 47B) and its effect on the yeast proteasome-mediated peptidolysis reaction in vitro was examined. In the absence of irradiation, Ru-RIP1, like RIP1, was an agonist of the chymotrypsin-like activity.

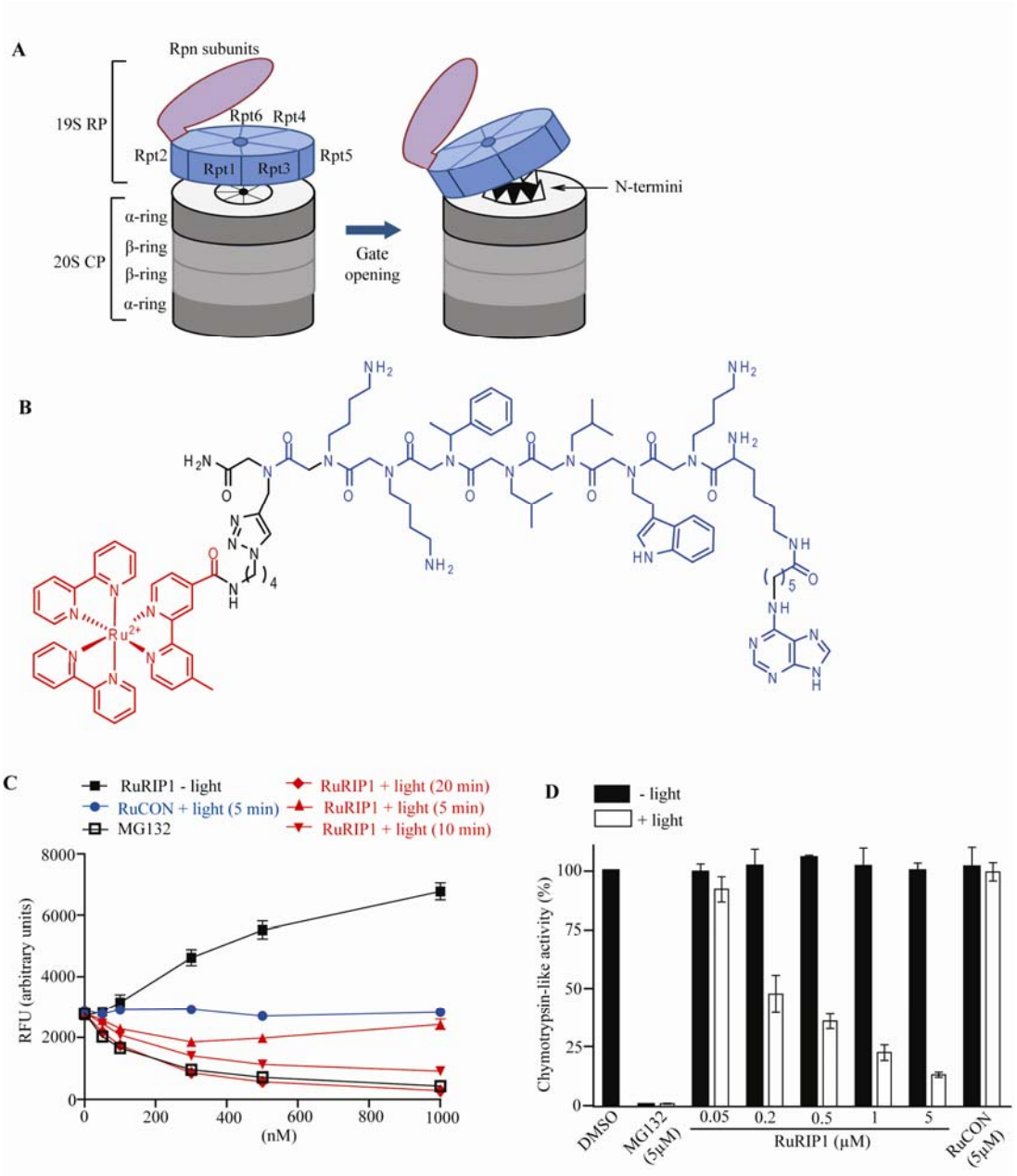

Figure 47. Visible light-triggered inactivation of the 26S proteasome by a ruthenium-peptoid conjugate. (a) Illustration of the 26S proteasome and gate opening of the 20S proteasome. (b) Chemical structure of RuRIP1. The modified Ru(II) $(bpy)_3^{2+}$ complex and RIP1 peptoid are shown in red and blue, respectively. (c) Chymotrypsin-like peptidase activity of purified, yeast 26S proteasome was measured in the presence of RuRIP1 with or without irradiation by monitoring the cleavage of fluorogenic substrate, Suc-LLVY-AMC. (d) The effect of RuRIP1 on chymotrypsin-like activity of the 26S proteasome in HeLa

cells with or without irradiation (30 min) was assessed by measuring luminescence generated by substrate (Suc-LLVY-aminoluciferin) cleavage.

However, irradiation resulted in an inversion of RuRIP1 activity and inhibition of peptidolysis was observed (Figure 47C). The potency of inhibition increased with the irradiation time (IC_{50} = 300 nM and 85 nM with 10 min and 20 min irradiation, respectively) suggesting that inhibition is dependent on the amount of $^1O_2$ generated. The potency of RuRIP1 when irradiated for 20 minutes was similar to that of MG132, a direct inhibitor of the chymotrypsin-like peptidase activity of the 26S proteasome. The two other peptidase activities of the 26S proteasome (caspase-like and trypsin-like) were also inhibited by RuRIP1 and light (Figure 48). Note that RuCON was neither an agonist nor a photo-antagonist of peptidolysis. Moreover, no inhibition of recombinant Luciferase was observed when this protein was irradiated in the presence of RuRIP1 (Figure 49). These data demonstrate that inactivation of the peptidolysis activity of the proteasome requires delivery of the oxidative warhead by the peptoid.

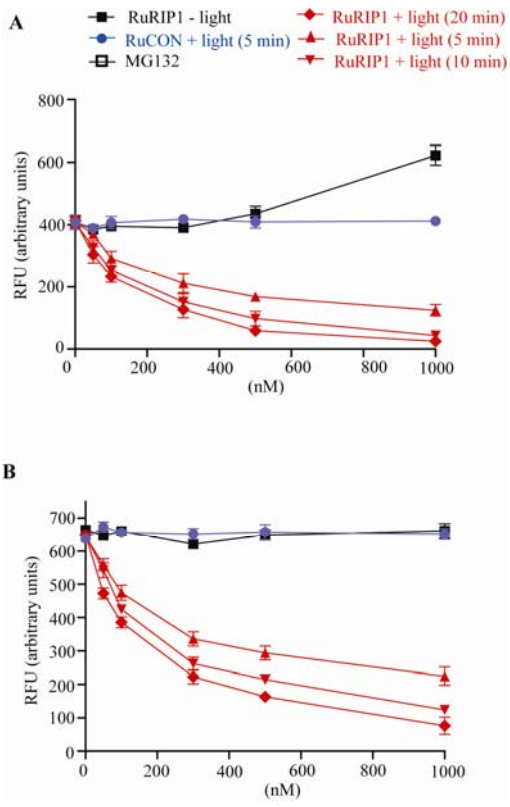

Figure 48. Trypsin-like (A) or caspase-like (B) peptidase activity of purified 26S proteasome was measured in the presence of RuRIP1 with or without irradiation by monitoring the cleavage of fluorogenic substrate Cbz-ARR-AMC and Cbz-LLE-AMC, respectively.

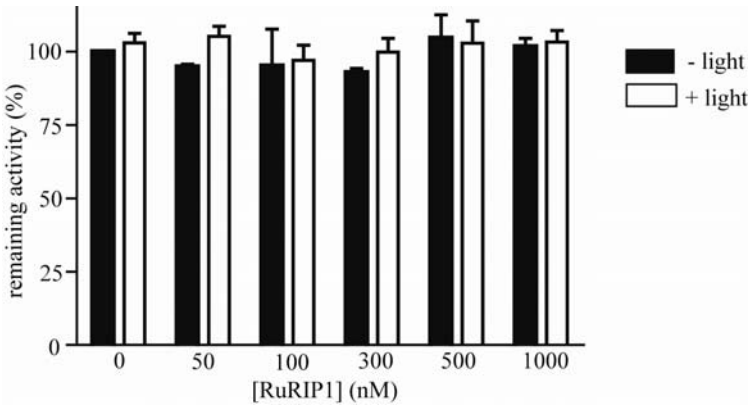

Figure 49. Effect of RuRIP1 on recombinant Luciferase activity. Activity of recombinant Luciferase with indicated concentration of RuRIP1 was measured after irradiation or dark incubation (20 min).

Inhibition of the 26S proteasome inside living cells

Given these in vitro data, we asked if RuRIP1 can inactivate the human 26S proteasome inside living cells upon irradiation. As shown in Figure 47D, a dose-dependent inhibition ($IC_{50} \approx$ 200 nM) of proteasome-mediated peptidolysis was observed when cells were incubated with RuRIP1 and irradiated for 30 minutes, whereas no effect was observed in the absence of light (note that the RuRIP1 concentration was well below that required for agonist activity). Note that complete inhibition of peptidase activity by RuRIP1 was not observed even at 5 μM peptoid. This may represent residual activity of the 20S core itself. Higher concentrations of RuRIP1 were not examined since some non-specific toxicity of this compound was observed at higher concentrations. To investigate whether RuRIP1 has off-target effects inside cells, the activity of *Renilla* Luciferase, which was expressed transiently in cells, was monitored. As shown in Figure 50, no inhibition was observed in cells irradiated in the presence of RuRIP1 showing that

proteasome inhibition is due to a targeted delivery of the singlet oxygen sensitizer by the peptoid. These experiments, which employed no special treatment to introduce the ruthenium-peptoid conjugate into the cells but simply relied on its inherent cell permeability, demonstrate that this technology can be used to target even intracellular proteins.

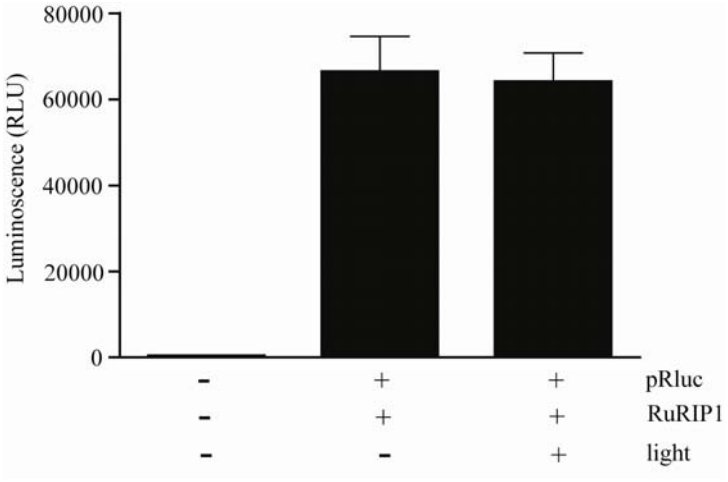

Figure 50. Effect of RuRIP1 on activity of *Renilla* Luciferase activity in HeLa cells. HeLa cells (1 x 10^4 cells / well) in 96-well plates were transfected with pRLuc which is a plasmid encoding *Renilla* Luciferase controlled by a constitutively active promoter. Cells were treated with RuRIP1 (1 μM) as indicated and irradiated or incubated in the dark (30 min). After lysis, *Renilla* Luciferase activity was measured.

Photo-stability of Ru(II)-conjugates

In order for efficient ruthenium-mediated photoinactivation to occur, the "delivery molecule" must be more resistant to singlet oxygen than the protein target. To examine this issue for the peptoids used in this study, solutions containing only RuGU40C or RuRIP1 were irradiated for different lengths of time and the degree of peptoid modification was assessed by mass spectrometry. Specifically, the rate of loss of the original molecular ion is shown in Figure

51. The proteasome-binding RuRIP1 peptoid was more labile than RuGU40C, probably because of the presence of the indole side chain and the adenine ring in this molecule, though no attempt has been made to characterize the photooxidation product. Importantly though, both ruthenium-peptoid conjugates were modified at a rate significantly slower than the observed rate of protein inactivation, as anticipated. This does raise the point however, that this approach to targeted protein inactivation will be most effective with molecules that lack oxidatively labile residues critical for binding.

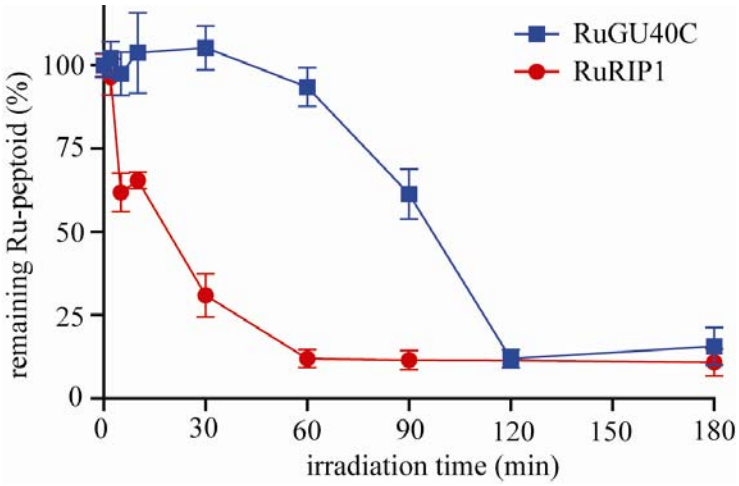

Figure 51. Relative amount of RuGU40C and RuRIP1 was monitored after irradiation with indicated times using MALDI-TOF MS.

3.3. Discussion

In summary, we have developed a practical method that allows modest potency hits from screening efforts to be transformed into much higher potency CALI reagents for the targeted, visible light photo-triggered inactivation of proteins. This approach was shown to be effective for the knock-out of VEGFR2, a transmembrane receptor, and the proteasome, an intracellular protein complex, in experiments using cultured mammalian cells. Little or no detectable inhibition of proteins not targeted by the delivery molecule was observed, though it is obviously impossible to rule out any off target effects completely. The high photocatalytic efficiency of singlet oxygen formation exhibited by the $Ru(II)(bpy)_3^{2+}$ complex and the ease with which derivatives can be tethered to protein-binding molecules makes it an ideal warhead for this type of application in vitro. However, the absorption maximum of this compound (≈450 nm) would restrict its use in animal systems. In the future it may be possible to develop protein-binding CALI agents with chromophores that absorb much farther towards the red in order to eliminate this limitation.

We have so far made no attempt to characterize the products of singlet oxygen-mediated photoinactivation, though it is clear that loss of protein activity is much faster than any detectable target protein cleavage (data not shown). This argues that oxidative side chain modifications are responsible for loss of target protein activity.

The experiments reported here employed peptoids as the protein targeting agents. Peptoids are nearly ideal for this application. We have developed methods to screen bead-displayed peptoid libraries that only register hits with low μM dissociation constants and, more

importantly, very high binding specificity, critical for the development of "tool compounds" [14, 22, 25]. Moreover, since the C-terminal end of the peptoid is linked to the bead, this provides a reliable site of attachment for the $Ru(II)(bpy)_3^{2+}$ warhead. Finally, peptoids are, in general, cell permeable [26, 27]. But this technology could be applied to other hit compounds from high-throughput screens so long as a site is available to which to tether the ruthenium complex without compromising the activity of the molecule. Thus, we believe that this technology will be of great utility in the development of pharmacological tools for the study of cell biology, in particular relieving the daunting roadblock of maturation of hits into more potent compounds by traditional medicinal chemistry methods.

The large, photo-triggered jumps in potency of the ruthenium-peptoid complexes (up to 1700-fold in this study) also provide opportunities for the manipulation of protein function that are not available with classical synthetic inhibitors. For example, it is possible to employ a concentration of the ruthenium-peptoid conjugate that is insufficient to inhibit the target protein in the dark, but then turn off protein function rapidly by photolysis, allowing one to carry out time-resolved studies of the effect of protein knock-out. In this study, a simple, high-intensity lamp was employed as the light source, requiring irradiation times of 5-20 minutes for complete protein knock-out. However, the use of more intense light sources, such as a laser, should reduce the required photolysis time drastically. It should also be feasible to carry out experiments under similar conditions in which only specific sub-cellular compartments of a cell are irradiated, thus achieving highly localized protein inactivation.

3.4. Experimental section

General remarks

All chemicals and solvents, unless stated, were purchased from Aldrich Chemical Co., and were used without further purification. Preparative HPLC was performed on a Waters Breeze HPLC system with a Vydac C18 preparative column (Flow rate = 10 ml/min.). Mass spectra were obtained with a Voyager-DE^{TM} PRO (Applied Biosystems) for MALDI-TOF with α-cyano-4-hydroxycinnamic acid matrix.

Cell culture

PAE/KDR cells (Sibtech, Inc.) and HeLa cells (ATCC, CCL-2) were maintained in DMEM (Invitrogen) supplemented with 110 mg/L sodium pyruvate, 2mM L-glutamine and 10% (v/v) fetal calf serum at 37˚C in a 5% CO_2 environment. H441 cells were maintained in RPMI-1640 (Invitrogen) supplemented as above. For irradiation experiments, phenol red-free DMEM or RPMI-1640 was used.

Peptoid synthesis

All peptoids were synthesized by on Rink Amide AM resin (Nova Biochem) using the sub-monomer approach (outline shown below) by a microwave-assisted protocol *(1).*

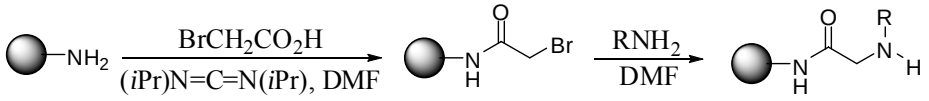

Peptoid synthesis outline: Coupling of bromoacetic acid followed by alkylation with amine completes addition of one residue in the sequence.

Preparation of Ruthenium-peptoids

Compound 1: To a stirred solution of Bis-(2,2'-bipyridin)-4'-methyl-4-carboxy-bipyridin-ruthenium-N-succinimidylester-bis-(hexafluorophosphate) (5.0 mg, 0.005 mmol) was added 4-azidobutylamine (0.025 mmol) *(2)* and DIPEA (0.025 mmol). After 3 hr at room temperature, the reaction mixture was diluted with dH_2O (0.1 % TFA, 3 mL) and directly purified by preparative HPLC and fractions containing product were lyophilized to afford compound 1 (0.004 mmol) as a red solid. MALDI/TOF: $[M]^+$ calculated 724.2, observed 723.4

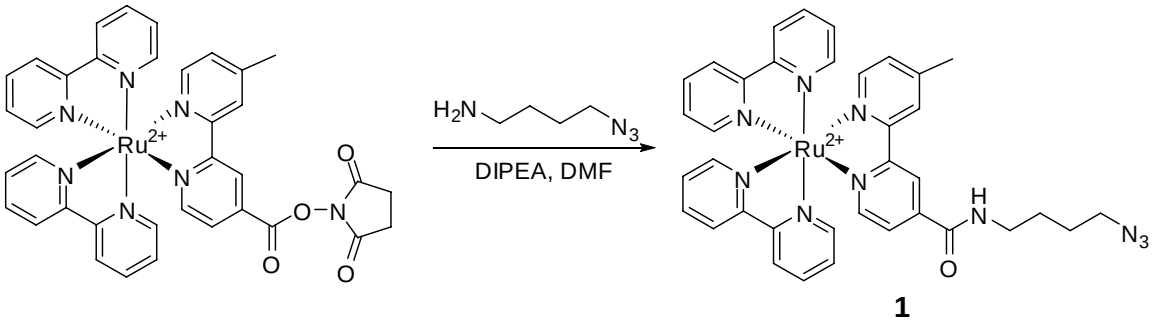

Scheme 1. Synthesis of azide-functionalized Ru(II) complex (1)

Compound 2. MALDI/TOF: $[M+Na]^+$ calculated 1465.9, observed 1466.7

Compound 3. MALDI/TOF: $[M+H]^+$ calculated 1331.8, observed 1332.1

RuRIP1: To a stirred solution of compound **1** (0.004 mmol) in MeOH (150 μL) was added compound **2**, CuI (0.012 mmol), and DIPEA (0.02 mmol). The reaction mixture was stirred overnight at room temperature and diluted with dH_2O (0.1 % TFA, 3 mL), and directly purified by preparative HPLC. MALDI/TOF: $[M]^+$ calculated 2167.1, observed 2167.1

RuGU40C: To a stirred solution of compound **1** (0.004 mmol) in DMSO (150 μL) was added compound **3** (0.004 mmol) and Tetrakis(acetonitrile)copper hexafluorophophate (0.0004 mmole, 10 mole %). The reaction mixture was microwaved (100 % power) for 45 sec, diluted with dH_2O (0.1 % TFA, 3 mL), and directly purified by preparative HPLC. MALDI/TOF: $[M]^+$ calculated 2055.0, observed 2054.0

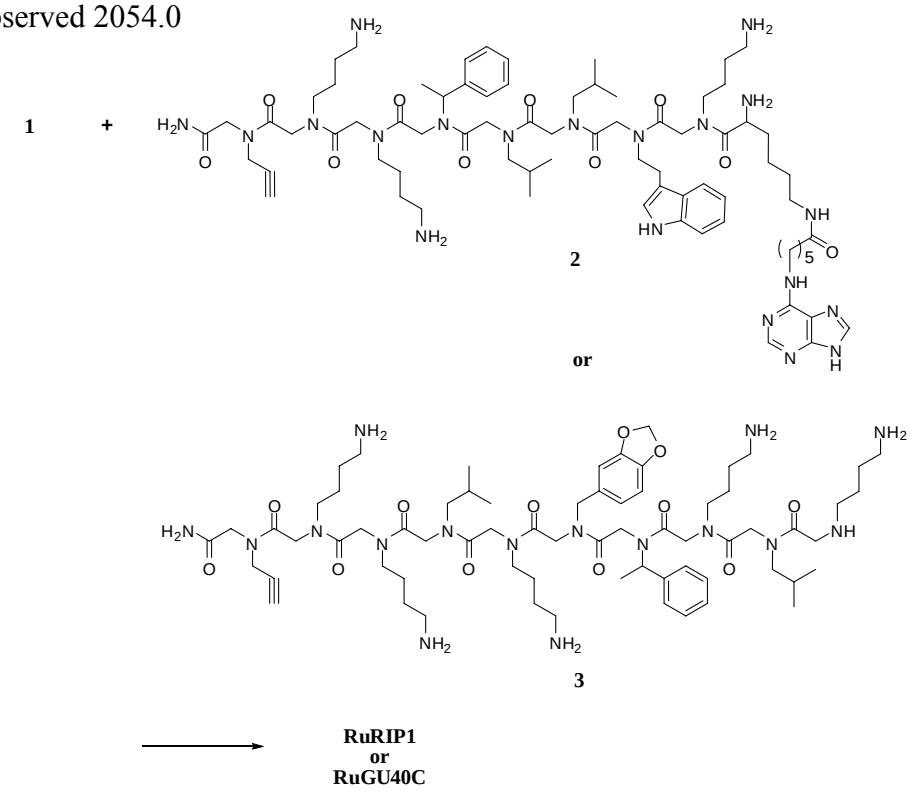

Scheme 2. Synthesis of RuRIP1 or RuGU40C via click chemistry

RuGU40C4: To a resin containing GU40C4 (0.0025 mmol) in DMF was added N-Fmoc-6-aminohexanoic acid (0.0075 mmol), HOBt (0.0075 mmol), HBTU (0.0075 mmol), and DIPEA (0.0075 mmol). The suspension was shaken overnight at room temperature. The resin was washed with DMF (2 mL x 8) and were treated with 20% piperidine in DMF for 1hr at room temperature. After washing with DMF (2 mL x 8), the resin was treated with Bis-(2,2'-bipyridin)-4'-methyl-4-carboxy-bipyridin-ruthenium-N-succinimidylester-bis-(hexafluorophosphate) (5.0 mg, 0.005 mmol) and DIPEA in DMF. After 2 hr, the resin was washed with DMF (2 mL x 8) and CH_2Cl_2 (2 mL x 8). The conjugate was cleaved from the resin by cleavage cocktail (1mL, 97.5% TFA, 2.5% water) at room temperature for 2hr. TFA was removed and the crude produce was purified by preparative HPLC. MALDI/TOF: $[M]^{4+}$ calculated 1053.5, observed 1054.5

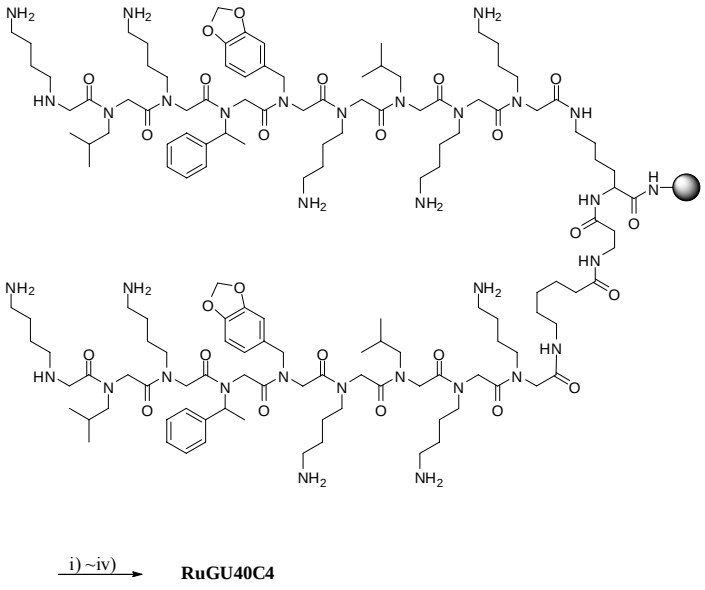

i) N-Fmoc-6-aminohexanoic acid, HOBT, HBTU, DIPEA, DMF ii) 20% piperidine in DMF
iii) Ru(bpy)2(mcbpy-OSu), DIPEA, DMF iv) TFA, H_2O

Scheme 3. Synthesis of RuGU40C.

RuCON: To a resin containing control peptoid (0.0025 mmol) in DMF was added N-Fmoc-γ-aminobutyric acid (0.0075 mmol), HOBt (0.0075 mmol), HBTU (0.0075 mmol), and DIPEA (0.0075 mmol). The suspension was shaken at room temperature for 2 hr. The resin was washed with DMF (2 mL x 8) and was treated with 20% piperidine in DMF for 2hr at room temperature. After washing with DMF (2 mL x 8), the resin was treated with Bis-(2,2'-bipyridin)-4'-methyl-4-carboxy-bipyridin-ruthenium-N-succinimidylester-bis-(hexafluorophosphate) (5.0 mg, 0.005 mmol) and DIPEA in DMF. After 2 hr, the resin was washed with DMF (2 mL x 8) and CH_2Cl_2 (2 mL x 8). The conjugate was cleaved from the resin by cleavage cocktail (1mL, 97.5% TFA, 2.5% water) at room temperature for 2hr. TFA was removed and the crude produce was purified by preparative HPLC. MALDI/TOF: $[M]^+$ calculated 1568.7, observed 1568.7

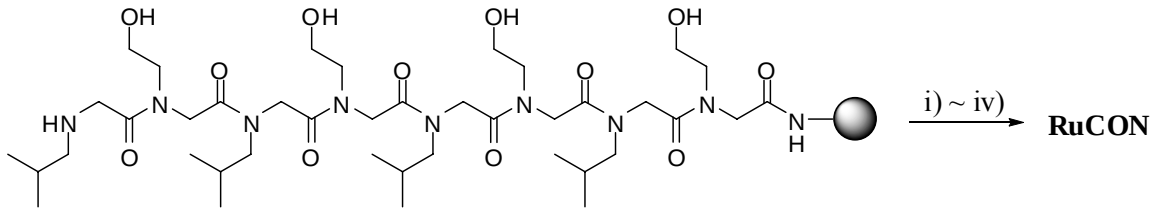

i) N-Fmoc-aminobutyricacid, HOBT, HBTU, DIPEA, DMF ii) 20% piperidine in DMF
iii) $Ru(bpy)_2$(mcbpy-OSu), DIPEA, DMF iv) TFA, H_2O

Scheme 4. Synthesis of RuCON.

Cell viability assay

Cell viability was determined by the CellTiter 96® AQ_{ueous} One Solution Cell Proliferation Assay (Promega). PAE/KDR cells (2 x 10^4 cells / well) in phenol red-free DMEM (10% FBS) in 96-well plate (white clear bottom) were incubated with DMSO, RuCON, or RuGU40 for 15 min and irradiated or incubated in the dark for 10 min. After 2 days incubation at 37˚C, CellTiter96® AQ_{ueous} One Solution Reagent (20 μL) was added to culture wells and incubated for 3 hr and then absorbance at 490nm was measured.

MS spectrometry for photostability measurement of Ruthenium-peptoids

RuGU40C (2.5 μM) or RuRIP1(2.5 μM) in 100 μL phenol red-free DMEM (0.1% FBS) containing 2.5 μM internal standard peptoid (structure shown below) were irradiated. At different time points, sample (3.5 μL) was taken and mixed with MALDI/TOF matrix solution (7 μL). 1 μL of the mixed solution was subjected to MALDI/TOF analysis and intensity of molecular ion peak of RuGU40C or RuRIP1 was normalized with that of internal standard peptoid (shown below) and expressed as percentage of initial value at 0 min irradiation.

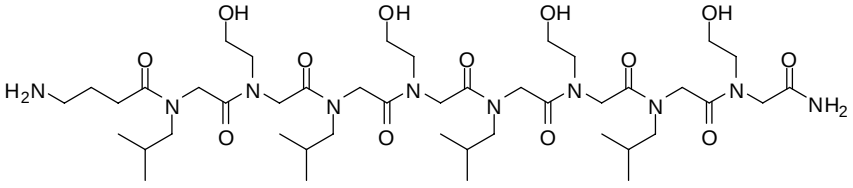

Visible light irradiation

Irradiation was done using 150-W xenon arc lamp (Oriel). Light was filtered first through distilled water (10 cm) and then through a 380- to 2,500-nm cut-on filter (Oriel). Samples were positioned at 25 cm distance from the light source and light intensity at the distance was 50 mW/cm^2.

Autophosphorylation assay

Cells were grown (~75% confluency) in 6-well plates, serum-starved overnight (0.1% FBS) and treated with compounds for 15 min. After irradiation or dark incubation for 10 min, cells were incubated for 37˚C for 10 min before addition of VEGF (37 ng/mL) or EGF (20 ng/mL). After 8 min, cells were lysed with nuclear lysis buffer (125 µL) for 10 min at 4˚C. The collected lysate was mixed with 2 x SDS sample buffer and was heated for 5min at 95˚C. The samples were separated by SDS-PAGE and transferred to PDVF membranes (Immobilon, Millipore). The membranes were probed with anti-phospho VEGFR2, anti-phospho-EGFR, anti-VEGFR2, or anti-EGFR primary antibodies (Cell signaling) and subsequently developed with appropriate HRP-conjugated secondary antibody (BioRad) followed by chemiluminescent detection using SuperSignal® West dura substrate (PIERCE). Quantifications of blot bands were performed using “Image J” software.

Tube-formation assay

HUVECs (2.5 x 10^4 cells/well) in phenol red-free Endothelial Cell Medium (ECM) basal media (ScienCell Research Lab.) containing 0.2% FBS were mixed with DMSO, RuCON, or

RuGU40C and then dispensed in growth-factor reduced Matrigel (BD biosciences)-coated 96-well plates and were incubated at 37˚C for 15 min. After irradiation or dark incubation for 10 min, cells were treated with VEGF (1.3 nM) and incubated for 16 hr. Images were taken under the light microscope and analyzed for quantitation of tube formation using software "AngioQuant".

26S proteasome peptidase assay

The proteasome peptidase activity was measured using fluorogenic substrates Suc-LLVY-AMC (Bachem), Cbz-ARR-AMC (Calbiochem), and Cbz-LLE-AMC (Calbiochem) to analyze the chymotrypsin-like, trypsin-like, and caspase-like activities of the 26S proteasome, respectively. 26S proteasome (2 nM) was incubated at 25^{o}C for 10 min with DMSO, MG132, RuCON, or RuRIP1 in the reaction buffer containing 50 mM Tris (pH 8.0) and 20 μM β-mercaptoethanol (100 μL of final reaction volume). Samples were irradiated or incubated in the dark for indicated time. 10 min after additional dark incubation, fluorogenic substrate (50 μM) was added and the peptidase activity was monitored after 30 min by measuring the fluorescence of the released 7-amido-4-methylcoumarin (Ex: 365 nm, Em: 460 nm).

Cell-based proteasomal peptidase assay

The Effect of RIP1 and RuRIP1 on the proteasomal chymotrypsin-like peptidase activity was determined using a chemiluminescent assay (Proteasome Glo Cell-based Assay, Promega). HeLa cells were dispensed into white, clear-bottom 96-well plate at a density of 1 x 10^4 cells in 100 μL

phenol red-free DMEM (10% FBS). After 6hr incubation, media was replaced with 100 μL serum-deficient, phenol red-free DMEM (0.1% FBS) and incubated for 4 hr. Cells were treated with compounds and incubated for 2 hr and then were irradiated or incubated in the dark for 30 min. After incubation at 37 ^{o}C for 2hr, cells were equilibrated to room temperature for 30 min and then assay buffer (100 μL) containing luminogenic substrate Suc-LLVT-aminoluciferin and a recombinant Luciferase were added. After 10 min incubation at room temperature, chemiluminescence was measured using plate reader and expressed as relative light units (RLU) after subtraction of background luminescence (100 μL media + 100 μL assay buffer).

References for experimental section

1. H. J. Olivos, P. G. Alluri, M. M. Reddy, D. Saloney, T. Kodadek, T. *Org. Lett*. ***4***, 4057 (2 002).

2. J. W. Lee, S. I. Jun, K. Kim. *Tetrahedron Lett*. ***42***, 2709 (2001).

3.5. References

1. Diller, D.J. The synergy between combinatorial chemistry and high-throughput screening. *Curr Opin Drug Discov Devel* **11**, 346-355 (2008).
2. Colas, P. High-throughput screening assays to discover small-molecule inhibitors of protein interactions. *Curr Drug Discov Technol* **5**, 190-199 (2008).
3. Snowden, M. & Green, D.V. The impact of diversity-based, high-throughput screening on drug discovery: "chance favours the prepared mind". *Curr Opin Drug Discov Devel* **11**, 553-558 (2008).
4. Davies, M.J. Singlet oxygen-mediated damage to proteins and its consequences. *Biochem Biophys Res Commun* **305**, 761-770 (2003).
5. Liao, J.C., Roider, J. & Jay, D.G. Chromophore-assisted laser inactivation of proteins is mediated by the photogeneration of free radicals. *Proc Natl Acad Sci U S A* **91**, 2659-2663 (1994).
6. Beck, S. et al. Fluorophore-assisted light inactivation: a high-throughput tool for direct target validation of proteins. *Proteomics* **2**, 247-255 (2002).
7. Hoffman-Kim, D., Diefenbach, T.J., Eustace, B.K. & Jay, D.G. Chromophore-assisted laser inactivation. *Methods Cell Biol* **82**, 335-354 (2007).
8. Jacobson, K., Rajfur, Z., Vitriol, E. & Hahn, K. Chromophore-assisted laser inactivation in cell biology. *Trends Cell Biol* **18**, 443-450 (2008).

9. Winterle, J.S., Kliger, D.S. & Hammond, G.S. Mechanisms of photochemical reactions in solution. 80. Photochemical oxidation of tri(2,2'-bipyridyl)ruthenium(II) by molecular oxygen. *J. Amer. Chem. Soc.* **98**, 3719-3721 (1976).

10. Mulazzani, Q.G., Sun, H., Hoffmann, M.Z., Ford, W.E. & Rodgers, M.A.J. Quenching of the excited states of ruthenium(II)-diimine complexes by oxygen. *J. Phys. Chem.* **98**, 1145-1150 (1994).

11. Zhang, X. & Rodgers, M.A.J. Energy and electron transfer reactions of the MLCT state of ruthenium Tris(bipyridyl) with molecular oxygen: A laser flash photolysis study. *J. Phys. Chem.* **99**, 12797-12803 (1995).

12. Fuller, Z.J. et al. Photostability of luminescent ruthenium(II) complexes in polymers and in solution. *Anal Chem* **75**, 2670-2677 (2003).

13. Lee, J., Yu, P., Xiao, X. & Kodadek, T. A general system for evaluating the efficiency of chromophore-assisted light inactivation (CALI) of proteins reveals Ru(II) tris-bipyridyl as an unusually efficient "warhead". *Mol Biosyst* **4**, 59-65 (2008).

14. Udugamasooriya, D.G., Dineen, S.P., Brekken, R.A. & Kodadek, T. A peptoid "antibody surrogate" that antagonizes VEGF receptor 2 activity. *J Am Chem Soc* **130**, 5744-5752 (2008).

15. Ito, Y., Iwamoto, Y., Tanaka, K., Okuyama, K. & Sugioka, Y. A quantitative assay using basement membrane extracts to study tumor angiogenesis in vivo. *Int J Cancer* **67**, 148-152 (1996).

16. Sini, P. et al. The antitumor and antiangiogenic activity of vascular endothelial growth factor receptor inhibition is potentiated by ErbB1 blockade. *Clin Cancer Res* **11**, 4521-4532 (2005).

17. Baumeister, W., Walz, J., Zuhl, F. & Seemuller, E. The proteasome: paradigm of a self-compartmentalizing protease. *Cell* **92**, 367-380 (1998).

18. DeMartino, G.N. et al. PA700, an ATP-dependent activator of the 20 S proteasome, is an ATPase containing multiple members of a nucleotide-binding protein family. *J Biol Chem* **269**, 20878-20884 (1994).

19. Smith, D.M. et al. ATP binding to PAN or the 26S ATPases causes association with the 20S proteasome, gate opening, and translocation of unfolded proteins. *Mol Cell* **20**, 687-698 (2005).

20. Smith, D.M. et al. Docking of the proteasomal ATPases' carboxyl termini in the 20S proteasome's alpha ring opens the gate for substrate entry. *Mol Cell* **27**, 731-744 (2007).

21. Rabl, J. et al. Mechanism of gate opening in the 20S proteasome by the proteasomal ATPases. *Mol Cell* **30**, 360-368 (2008).

22. Lim, H.S., Archer, C.T. & Kodadek, T. Identification of a peptoid inhibitor of the proteasome 19S regulatory particle. *J Am Chem Soc* **129**, 7750-7751 (2007).

23. Lim, H.S., Cai, D., Archer, C.T. & Kodadek, T. Periodate-triggered cross-linking reveals Sug2/Rpt4 as the molecular target of a peptoid inhibitor of the 19S proteasome regulatory particle. *J Am Chem Soc* **129**, 12936-12937 (2007).

24. Lim, H.S., Archer, C.T., Kim, Y.C., Hutchens, T. & Kodadek, T. Rapid identification of the pharmacophore in a peptoid inhibitor of the proteasome regulatory particle. *Chem Commun (Camb)*, 1064-1066 (2008).

25. Xiao, X., Yu, P., Lim, H.S., Sikder, D. & Kodadek, T. Design and synthesis of a cell-permeable synthetic transcription factor mimic. *J Comb Chem* **9**, 592-600 (2007).

26. Yu, P., Liu, B. & Kodadek, T. A high-throughput assay for assessing the cell permeability of combinatorial libraries. *Nat Biotechnol* **23**, 746-751 (2005).

27. Kwon, Y.U. & Kodadek, T. Quantitative evaluation of the relative cell permeability of peptoids and peptides. *J. Amer. Chem. Soc.* **129**, 1508-1509 (2007).